Optical Antennas Control Light Emission

Alberto González Curto

ICFO – Institut de Ciències Fotòniques
Universitat Politècnica de Catalunya
Barcelona, 11 April 2013

Optical Antennas Control Light Emission

Alberto González Curto

under the supervision of

Professor Niek F. van Hulst

submitted this thesis in partial fulfillment

of the requirements for the degree of

Doctor

by the

Universitat Politècnica de Catalunya
Barcelona, 11 April 2013

To my wife and parents.

Abstract

The emission of light is at the heart of both fundamental science and technological applications. At its origin lie electronic transitions in nanoscale materials such as molecules, atoms and semiconductors. The interaction of light with such single quantum emitters is inefficient because of their point-like character. Efficient interfaces between light and nanoscale matter are therefore necessary.

Inspired by the effective communication between small electronic circuits enabled by radio-frequency antenna technology, an emitter can be addressed efficiently with a nanoantenna, an optical element that converts localized energy into propagating radiation.

The control of light emission with such optical antennas is the topic of this Thesis. By coupling an emitter to a metal antenna, the emission properties are determined by the antenna mode in direction, transition rates, polarization, and spectrum. In Chapter 1, we set out the basic concepts of optical antenna theory.

To couple an emitter to an antenna, it must be within its near field. In Chapter 2, we introduce a nanofabrication method to place quantum dots on metal nanostructures with high spatial accuracy. The resulting emitter-antenna systems are imaged by confocal microscopy and their angular radiation patterns directly recorded. This combination of experimental methods allows us to study any optical antenna.

A metal wire is the canonical antenna design and the basis to understand and construct other optical antennas. Through selective coupling of a quantum dot to the resonant modes of a nanowire, we demonstrate in Chapter 3 that the emission of a dipolar source can be converted controllably into higher multipolar radiation. We describe the antenna as a standing-wave resonator for plasmons and reproduce its emission with a multipolar expansion.

An aperture in a metal film can be regarded as the complementary structure of a wire. In Chapter 4, we address the emission of light through a rectangular nanoaperture as an antenna problem. We demonstrate, explicitly, that resonant nanoslot antennas display a magnetic dipole response. Such antennas offer an efficient interface between emitters and surface plasmons.

The excitation or detection of a dipolar emitter from the far field involves large solid angles. To address quantum emitters efficiently, a low divergence of their radiation patterns is needed. To this end, in Chapter 5 we develop and realize unidirectional optical antennas. We show how the emission of a quantum emitter is directed by multi-element Yagi-Uda and log-periodic optical antennas and demonstrate directional operation of a single-element design based on a split-ring resonator.

Light emission usually occurs through electric dipole transitions because multipolar emission rates are orders of magnitude slower. In some materials, however, multipolar optical transitions do occur. In Chapter 6, we assess through simulations the feasibility of enhancing magnetic dipole and electric quadrupole transitions with several realistic nanoantenna designs.

The results in this Thesis demonstrate the potential of optical antennas as elements to control light on the nanoscale, based on radio and microwave antenna engineering. Within this powerful paradigm, the interaction of light with nanoscale matter can be tailored with complete flexibility.

Such a degree of control over light emission and absorption may have a practical impact in spectroscopy, sensing, display technologies, lighting, photovoltaics, and general optical and optoelectronic devices.

Resumen

La emisión de luz radica en el corazón tanto de la ciencia fundamental como de varias aplicaciones tecnológicas. En su origen están las transiciones electrónicas en nanomateriales como moléculas, átomos y semiconductores. La interacción de la luz con uno de estos emisores cuánticos es ineficiente debido a su carácter puntual. Es necesario, por tanto, desarrollar interfaces más eficientes entre la luz y la materia de tamaño nanoscópico.

Inspirándonos en la comunicación entre pequeños circuitos electrónicos que permiten las antenas de radio, se puede interactuar más eficientemente con un emisor utilizando una nanoantena como elemento óptico que convierte la energía localizada en radiación propagante.

Esta Tesis trata sobre el control de la emisión de luz con tales antenas ópticas. Acoplando un emisor a una antena metálica, las propiedades de la emisión pasan a estar determinadas por el modo de la antena en dirección, tasas de transición, polarización y espectro. En el Capítulo 1, establecemos las nociones básicas de la teoría de antenas ópticas.

Para acoplar un emisor a una antena, éste debe encontrarse en su campo cercano. En el Capítulo 2, presentamos un método de nanofabricación para posicionar puntos cuánticos sobre nanoestructuras metálicas con alta resolución espacial. Para caracterizar los sistemas emisor-antena resultantes, adquirimos imágenes mediante microscopía confocal y medimos sus patrones angulares de radiación. Esta combinación de métodos experimentales nos permite el estudio de cualquier antena óptica.

El diseño canónico de una antena es un cable metálico. Es la base para entender y construir otras antenas ópticas. Mediante acoplamiento selectivo de un punto cuántico a los modos resonantes de un nanocable, en el Capítulo 3 demostramos que la emisión de una fuente dipolar puede ser convertida en radiación multipolar controladamente. Describimos la antena como un resonador de onda estacionario para plasmones y reproducimos su emisión con una expansión multipolar.

Se puede considerar una apertura en una película metálica como la estructura complementaria de un cable. En el Capítulo 4, tratamos la emisión de luz a través de una apertura rectangular como un problema de antenas. Demostramos, explícitamente, que una nano-ranura resonante posee respuesta dipolar magnética. Estas antenas permiten una conversión eficiente entre emisores de fotones y plasmones superficiales.

La excitación o detección de un emisor dipolar conlleva ángulos sólidos grandes. Para abordar un emisor cuántico individual eficientemente desde el campo lejano, se requieren patrones angulares con una baja divergencia. Con estre fin, en el Capítulo 5 desarrollamos e implementamos antenas ópticas unidireccionales. Demostramos cómo la emisión de un emisor cuántico puede ser dirigida por antenas multi-elemento de Yagi-Uda y logarítmicas periódicas y observamos direccionalidad en una antena compuesta por un único elemento con forma de diapasón.

La emisión de luz ocurre normalmente a través de transiciones de dipolo eléctrico porque las tasas de emisión multipolares son, por lo general, mucho más lentas. Sin embargo, en algunos materiales se pueden observar transiciones multipolares. En el Capítulo 6, evaluamos la posibilidad de mejorar la emisión de transiciones dipolares magnéticas y cuadrupolares eléctricas mediante distintos diseños realistas de antenas ópticas.

Los resultados de esta Tesis demuestran el potencial de las antenas ópticas como elementos para el control de la luz a escalas nanométricas, basadas en la ingeniería de antenas de radio y microondas. Dentro de este paradigma, se puede manipular la interacción de la luz con la materia con total flexibilidad.

Tal grado de control sobre la emisión y la absorción de la luz podría tener un gran impacto práctico en espectroscopía, sensores, pantallas, iluminación, energía fotovoltaica y todo tipo de dispositivos ópticos y optoelectrónicos.

Acknowledgments

No man is an island, particularly in research. ICFO provided the perfect atmosphere to "take the most" out of the institute, its people, and its science.

First and foremost, I feel very fortunate for having had Niek van Hulst as advisor. He gave me plenty of opportunities for development, the freedom to be right and to be wrong, sincere advice on any topic. A PhD with Niek imprints a character: I am taking that with me.

This Thesis is the fruits of the collaboration with very bright people: Tim, Giorgio, Martin, Mark, Marta, Ion, Radostin. Romain was almost like a second mentor to me, a true luxury. I got so much from all of you!

Daan, Martin and Florian: this thesis would have been very different without bouncing ideas off of you. Thanks to Richard, Riccardo, Pablo, Jana, Jan, Emilie, Jean-Christophe, Lars, Anshuman, Gaëtan, Nicolò, Dominique, Lukasz, Klaas and Koen for helping me always, and never without a smile.

Tremendous was the support of the ICFO units. Too many people to be thanked individually (NanoLab, Purchasing, Mechanical Workshop, Human Resources, Projects, Frontdesk, …).

My visit to the Brongersma group in Stanford was a truly stimulating experience. I thank particularly Mark, Farzaneh, and Kevin. Discussions with Rashid Zia, Javier Aizpurúa, Javier García de Abajo, Alejandro, and Ana also enriched this Thesis.

I really enjoyed the time and the conversations with Rafa, Ramaiah, Armand, Petru and other great people at ICFO like Sudhir, Clara or Osamu.

Finally, my family: my sisters, my parents, my wife. They made this possible. They are my motivation to be better every passing day.

¡Gracias a todos!

Contents

1.

Optical Antennas

Molecules, ions, atoms and semiconductors are emitters of light behind core technological applications. In general, interaction with nanoscale materials, at the single quantum emitter level is inefficient. Thus, one of the main tasks of modern Optics is the development of more effective optical interfaces between light and the nanoscale. In this Chapter, we introduce the concept of a nanoantenna as an optical element to control light on the nanoscale based on radio and microwave antenna engineering. We describe the main physical mechanisms that allow antennas to control light, explaining the basic elements of optical antenna theory. Finally, we explore the applications that can potentially benefit from the design paradigm of optical antennas.

1.1. Nanoscale light-matter interaction

Light is ultimately emitted by single quantum oscillators. Electrons in single atoms and single molecules are confined to very small volumes, to dimensions on the order of the nanometer. Transitions between different energy states result in the emission of photons, one by one. Both from the quantum and classical electrodynamics perspectives, light emission can be fully described by a multipolar expansion [1]. The electric dipole moment is usually the dominant term, as a result of the point-like character of such quantum emitters compared to the wavelength of light.

This simple observation has profound implications for both fundamental and technological applications because it determines to a great extent how light interacts with matter. First, the probability that a photon in a beam is absorbed by a single quantum emitter is low because of the size mismatch between the nanoscale material and the light beam. A lens can reduce the interaction volume to the scale of the wavelength, but the diffraction limit prevents a perfect spatial overlap. Second, the emission and absorption of a dipolar emitter follows an angular pattern that involves fields within a wide solid angle range, isotropic on the plane perpendicular to the dipole orientation. The electromagnetic modes of the emitter and the propagating light beam are clearly different. Therefore, the task of making a single photon interact with a single dipolar emitter with unity certainty proves to be challenging.

Inside a resonator, light travels back and forth multiple times thus enhancing the probability that a photon meets a quantum emitter. For example, macroscopic mirror cavities are commonly used for the manipulation of atomic gases. Two mechanisms can contribute towards enhanced light-matter interaction: a long lifetime of the photon inside the cavity and a reduction of the mode volume. The lifetime of a photon inside a good resonator is inversely proportional to the spectral width of the resonance, also quantified in terms of the quality or Q factor $Q = f_{\text{resonance}}/\Delta f$. The interaction strength of an emitter with an optical field is thus proportional to the ratio Q/V, where V is the modal volume.

To find an optimal combination of both contributions (Purcell effect), novel optical elements have been developed in the past decades Single quantum emitters have been coupled to dielectric microcavities, based on Bragg mirrors or on the whispering gallery modes of spheres and toroids, and to cavities in photonic crystals [2].Dielectric microcavities can attain Q values as high as 10^6 but they can only focus light to the scale of the wavelength. Furthermore, their angular radiation patterns are complex, usually with multiple lobes. Consequently, addressing a quantum emitter coupled to these resonators is difficult from the far

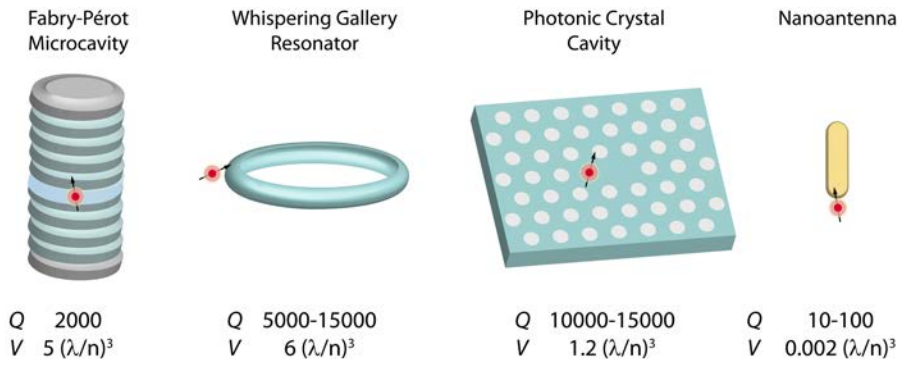

Figure 1.1 **Cavities for enhanced light-matter interaction.** Different dielectric microcavities compared to a metallic nanoantenna, showing typical quality factors (Q) and mode volumes (V). The strength of the interaction with a quantum emitter is approximately proportional to the ratio Q/V. For a nanoantenna, the strong field confinement compensates the quality factor of the resonator. Adapted from [2].

field, with low divergence fields such as plane waves or Gaussian beams. More efficient interfaces between light and nanoscale matter are thus required.

Antennas as optical elements

Electrical engineers commonly find similar problems to interact efficiently with electronic circuits through radiation, because a deeply sub-wavelength electronic circuit radiates very poorly by itself. The solution, at radio and microwave frequencies, is to couple the circuit to an emitting or receiving antenna [3]. Antenna engineers have developed a myriad of designs to link electromagnetic waves and matter; Optics can certainly tap on this vast knowledge.

Optical antennas are the counterparts of conventional radio and microwave antennas for frequencies in the visible regime (hundreds of THz) [4, 5]. By scaling down geometry and wavelength around a million times, the analogy with longer wavelength antennas becomes a useful paradigm for nanoscale light-matter interactions. The definition of an optical antenna that we will use in this Thesis is:

> *An optical element that converts efficiently localized energy (near field) into propagating radiation (far field), and vice versa.*

Antennas provide an effective route to couple photons in and out of nanoscale objects. They are generally resonant cavities that maximize the loss of the contained energy through radiation instead of ohmic dissipation.

A critical part of this definition is the presence of a localized light source. As such, the history of optical antennas is closely related to near-field optical microscopy. A hole in a metal film can concentrate optical fields to sub-diffraction-limited volumes, surpassing the capabilities of bulk optical components. Equally, a metal nanosphere can also be regarded as a primitive dipole optical antenna.

Miniaturization brought antennas first to the infrared regime, where they were used to improve photodetection. Further miniaturization, requiring fabrication accuracies of a few nanometers, enabled the use of antenna technology concepts and designs for shorter wavelengths in the visible regime. Top-down nanofabrication techniques, such as focused ion beam milling or electron-beam lithography, offer control on the geometry and position of individual nanoparticles with 10-20 nm resolution. Alternatively, bottom-up colloidal chemistry methods provide simpler mono-crystalline structures with higher quality optical properties.

Because of their ability to strongly confine electromagnetic fields and their efficient radiation into the far field, antennas overcome some of the drawbacks of dielectric microcavities to address single quantum emitters. In comparison, nanoantennas are relatively poor resonators with Q-factors lower than 100. Yet, antennas do exhibit a sub-wavelength mode volume V. As an approximation, the coupling strength between a quantum emitter and light is proportional to Q/V, known as the Purcell factor. For antennas, this combination results in a high enhancement of transition rates, competitive with microcavities with superior Q but also larger V (Fig. 2.1).

Optical nanoantennas offer intrinsic additional advantages. A much smaller footprint favors their integration in larger photonic devices. Importantly, the broadband response of these resonators is an advantage for most practical room-temperature applications, which often involve spectrally broad emitters such as fluorescent molecules or quantum dots.

1.2. Controlling light with optical antennas

Conventional radio-frequency antennas serve a wide variety of purposes by adopting very different shapes. To name a few, there are antennas that receive linearly or circularly polarized waves, antennas sensitive to electric fields or to magnetic fields, electrically small antennas or large-scale phased antenna arrays, omnidirectional and unidirectional antennas, ultra broadband or frequency-selective antennas. Each different goal requires a dedicated antenna design. Similarly, one can gain control over different properties of light with an optical antenna. The specific optimal design will depend on the desired functionality.

Such a degree of control is possible because the emission is directly controlled in the near field. By coupling an emitter to an antenna, the emitter interacts with radiation through the antenna mode. The properties of the emission are thus determined by the antenna mode. The design flexibility allows a tailored light-matter interaction. In this Section we give a brief overview of the main physical effects that optical antennas can use to manipulate, enhance, or modify light emission (Fig. 2.2).

Enhancement of emission and excitation rates

A basic parameter of light emission is its intensity. The amount of photons per second limits, for example, the detection of single molecules or the possibility to carry out certain spectroscopies on single emitters. Both excitation and emission transition rates can be enhanced by coupling to an optical antenna, which will have a direct effect on the observed intensity [6-8].

For an emitter based on a dipolar transition $\boldsymbol{d}$, if the excitation power of the local field $\boldsymbol{E}$ is far from saturation, the collected photon rate in an experiment is given by:

$$I \propto \eta_c \, \eta \, \Gamma_{exc}$$

where η_c is the collection efficiency of the detecting optical system, *i.e.* the fraction of the angular radiation pattern contained within the numerical aperture; $\Gamma_{exc} \propto |\boldsymbol{d} \cdot \boldsymbol{E}|^2$ is the excitation rate; $\eta = \Gamma_{rad}/(\Gamma_{rad} + \Gamma_{non\text{-}rad})$ is the quantum efficiency, *i.e.* the fraction of photons that are actually radiated instead of lost through non-radiative mechanisms. The enhancement of the local field $\boldsymbol{E}$ by an optical antenna results in a higher excitation rate and, consequently, a higher number of emitted photons.

On the other hand, at saturation of the excitation transition, the collected intensity does not depend any more on the excitation rate Γ_{exc} but it is proportional to the radiative rate Γ_{rad}. The radiative lifetime of the transition then limits the amount of photons per second that can be obtained from the emitter. The control of Γ_{rad} becomes important, for example, to obtain single-photon sources with maximum brightness.

Finally, a gain in intensity may be also obtained through changes in the quantum efficiency (η), particularly for poor emitters with low intrinsic quantum efficiency (η_0, in the absence of an antenna) [9]. The antenna can increase the quantum efficiency (external quantum efficiency, or radiation efficiency in antenna theory) by increasing the radiative rate over both the loss rate of the intrinsic non-radiative decay channels of the emitter and the loss rate as heat dissipation in the antenna.

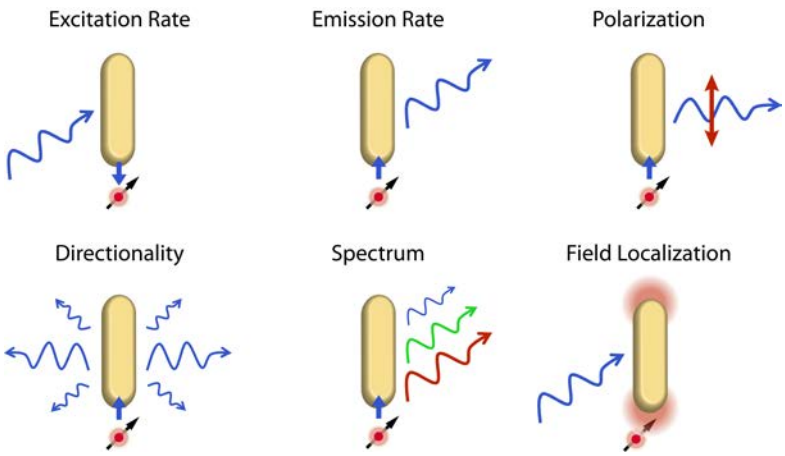

Figure 1.2 **Control of light-matter interaction with optical antennas.** The interaction of a quantum emitter with an optical antenna leads to the enhancement of excitation and emission rates, the control of the polarization, directions and spectrum of emission and excitation, and a confinement of the electromagnetic fields to sub-wavelength volumes.

The opposite is also possible, and the external quantum efficiency with an antenna may be lower than the intrinsic one, a situation known as quenching. Due to the rapid increase in the non-radiative rate at close proximity to a metal surface, the distance of emitter to antenna must be controlled to be within the optimal range of 5-12 nm [6, 7].

Control of directionality

The angular radiation pattern of an object determines how easily it can be addressed from the far field. The radiation pattern of a quantum emitter is typically dipolar, with angular emission covering a wide range of solid angles. Interaction with an emitter can be made more efficient by coupling it to an antenna with an angular pattern matching the detection or illumination angles, directing the emission or excitation into the optical system. An increase in the collection efficiency η_c results in a higher observed intensity.

Furthermore, emission can be converted to another, well-defined electromagnetic mode in the far field, with properties different to the original source. Examples include the conversion of an electric dipole emitter into a quadrupolar source or a mode in an optical fiber.

The directionality of a radiation pattern $P(\theta,\varphi)$, where θ is the inclination angle (latitude) and φ is the azimuth angle (longitude) in spherical coordinates, can be quantified by several metrics, including:

Directivity

Power density at a given angle compared to the total integrated power distributed isotropically over all directions:

$$D(\theta,\varphi)=4\pi P(\theta,\varphi)/\int P(\theta,\varphi)\mathrm{d}\Omega$$

An isotropic source would have a directivity of 1, a dipole has a directivity of 1.5, and directional antennas typically achieve values of 10-25.

Gain

To take into account not only the shape of the radiation pattern but also the radiation efficiency, the directivity is multiplied by the quantum efficiency:

$$G=\eta D$$

Front-to-Back Ratio

Power emitted in the direction of maximum emission $P(\theta_{max}, \varphi_{max})$ divided by the power radiated in the diametrically opposite direction:

$$F/B= 10\ log(P(\theta_{max},\varphi_{max})/P(\theta_{max}+\pi,\varphi_{max})),$$
$$\text{or } F/B=10\ log(P(\theta_{max},\varphi_{max})/P(\theta_{max},\varphi_{max}+\pi))$$

if the emission is contained only in one half-space.

Beam-Width at Half-Maximum

Angular width of the main radiation lobe.

The control of the directionality and of the electromagnetic modes of optical nanoantennas is a central topic in this Thesis.

Local field enhancement

Optical antennas allow a strong confinement of fields to sub-diffraction-limited volumes. This spatial localization can be used to improve spatial resolution in near-field imaging methods [10]. A higher local field results in higher excitation and emission rates and in a more efficient coupling of emitter to antenna.

Polarization control

An optical antenna can control the polarization of the interaction, both in the far and near fields. In the far field, the antenna mode can determine the emission or excitation polarization [11, 12]. In the near field, it can convert an external polarization into another local polarization of the evanescent fields. This local conversion between polarizations also enables their use as nanoscale interfaces between freely-propagating and guided waves of a specific polarization (*e. g.*, surface plasmons or waveguide modes). In- and out-couplers to such modes can be devised, with control of the local phase distribution.

Spectral control

Excitation or emission through a resonant antenna can shape the wavelength spectrum of the interaction [13]. This interaction usually occurs in the weak-coupling regime and the spectral response of the coupled emitter-antenna system is given by the product of the individual spectral responses of emitter and antenna [14]. In contrast, if the interaction strength reaches the strong-coupling regime, emitter and antenna cannot be separated as independent entities and the linear relation of spectral enhancement breaks down.

1.3. Fundamentals of optical antennas

Scaling down radio and microwave antenna designs for operation at shorter wavelengths is possible in Maxwell's equations. Material properties, however, are not scalable, and the frequency-dependent complex dielectric function of optical antenna materials needs to be considered. Whereas metals behave as perfect electrical conductors at lower frequencies, they are non-perfect conductors in the visible regime.

Importantly, noble metals support surface plasmon polaritons at optical frequencies. Surface plasmons are collective oscillations of the free electron gas with a concomitant electromagnetic wave bound to the material. Most optical antennas are based on metal nanoparticles exhibiting localized surface plasmon resonances in the visible and near infrared. Semiconductors and other materials display plasmonic resonances at infrared and terahertz frequencies. Dielectric optical antennas are also possible, as in conventional antenna engineering (*e.g.*, dielectric resonators), but they will generally lead to less confined near fields suitable only for specific applications.

Half-wave dipole nanoantenna

Being the canonical antenna, we introduce first the simplest resonant optical antenna: the half-wave dipole nanowire. Metal nanowires act as one-dimensional resonators for plasmons. They exhibit Fabry-Pérot resonances with a simple linear relation with length. Modes of increasing resonance order are characterized by an increasing number of longitudinal oscillations in the near field of the structure [15]. Consecutive modes are roughly separated by one half of the effective wavelength of the plasmon in the nanowire. Hence, the first resonance can be named half-wave dipolar mode. It possesses a standing-wave distribution of charges and currents, sketched in Fig. 1.3a and simulated in Fig. 1.3d.

The resonant lengths can be sensitively shorter than the free-space wavelength due to the finite skin depth of metals in the visible regime. The reduced effective wavelength of the plasmon along the metal nanowire is typically between 2 and 4

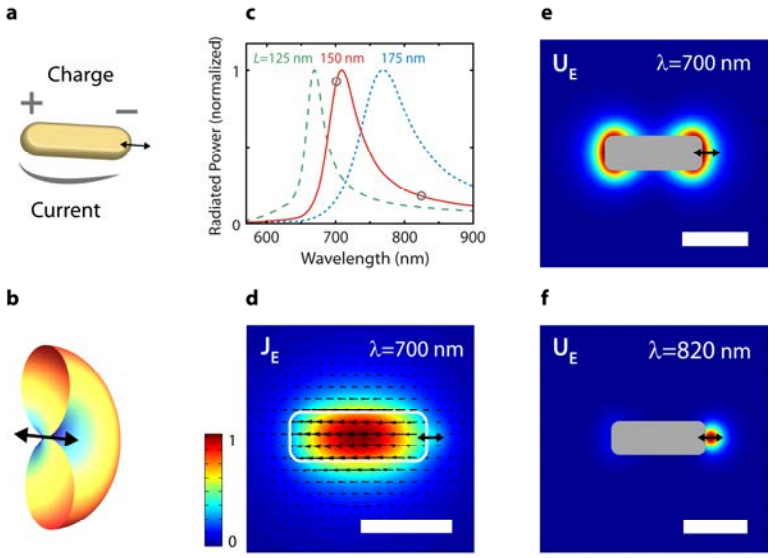

Figure 1.3 **Dipole nanoantenna excited by an emitter. (a)**A half-wave dipole antenna driven by an electric dipole source at one of its ends. The electric charges and currents depict a half a sinusoidal oscillation. **(b)** Section of the angular radiation pattern of an electric dipole in free space. **(c)** Radiated power spectrum for gold antennas of increasing length L (height 37 nm, width 55 nm) surrounded by air. The resonant wavelength shifts to the red for longer antennas. **(d)** Electric current on the surface of a 150-nm antenna at resonance, equivalent to the sinusoidal current sketched in **a**. Arrows represent Re ($\boldsymbol{J}_{\mathrm{E}}$). **(e, f)** Electric energy density $\mathrm{U_E}$, proportional to $|\mathbf{E}|^2$, at resonant and non-resonant wavelengths for the same antenna. Antennas in air were simulated with the FDTD method.

times shorter than the vacuum wavelength. The slope of the linear scaling of the resonances with length depends on material (metal dispersion and surrounding medium) and geometrical (width and height) parameters [16, 17]. For an Au nanowire of 55 nm of width and 37 nm of height surrounded by air, the spectrum of emission of a dipolar emitter coupled to the nanoantenna is presented in Fig. 1.3c. For example, a 150-nm long antenna is resonant around a wavelength of 700 nm. In our experiments, antennas will be lying on a glass substrate, resulting in an additional shortening of the resonant lengths, around 1.5 times less.

The angular radiation pattern of such an antenna is very similar to a point electric dipole oriented along the long axis of the nanowire (Fig. 1.3b), which draws a parallel with the resemblance of a radio-frequency $\lambda/2$ dipole antenna to a point Hertz electric dipole [3]. The angular pattern contains then two lobes with

a $\sin(\theta)^2$ angular dependence and rotational symmetry around the axis of the dipole.

The electric field is concentrated at the ends of the nanowire. At resonance, an emitter excites the antenna mode efficiently from one side of the antenna; both ends light up with comparable strength (Fig. 1.3e). Off resonance, however, the emitter couples inefficiently to the antenna mode; the original point dipole dominates the field distribution with a maximum at the source position (Fig. 1.3f).

The half-wave electric dipole antenna is a basic building block for other antenna designs. For example, two laterally shifted antennas can form a resonant gap antenna, further increasing the local field enhancement. An array of detuned dipole antennas is the basis for multi-element directional antennas, such as the popular Yagi-Uda design used in television reception. Finally, the understanding of the fundamental resonance of a nanowire is necessary to investigate higher order resonances in nanowires, with contributions to the emission from other multipoles. It proves also helpful in understanding the fundamental magnetic resonance of a nanoslot antenna, the complementary structure of a nanowire. Consequently, the $\lambda/2$ dipole antenna will prominently feature as the starting point of the discussion of all the Chapters in this Thesis.

1.4. Potential applications

Light is a universal tool to probe matter, to convert energy, and to transfer information. In particular, single quantum emitters are key elements in quantum optics as single-photon sources for quantum information technologies and also in sensing as the ultimate limit of detection. Optical antennas enable a richer control over light on the nanoscale in absorption, emission and scattering processes, opening new opportunities for developing applications in a broad range of fields.

Biochemical Sensing

Fluorescence-based sensors can directly benefit from enhancements of local fields, collection efficiency or transition rates. For example, the engineering of the external quantum efficiency may result in the detection of intrinsically poor emitters or labels [9]. Beaming of fluorescence can result in lower numerical-aperture requirements for detection optics. Fluorescence correlation spectroscopy, based on the diffusion of emitters through a focal volume, can expand its capabilities thanks to the very small volumes achieved with nanoantennas [18]. Single-molecule techniques could be boosted by the integration of microfluidic platforms with optical antennas. Antennas might also find use in photochemistry.

Spectroscopy

Due to their broad spectral response, metal nanoantennas are particularly suitable for room-temperature single-molecule studies. In the tradition of metal-enhanced spectroscopies, they can improve fluorescence, Raman, infrared vibrational and non-linear spectroscopies.

Single-Photon Sources

Photons are quantum information carriers and nanophotonic devices could offer a route for scalable quantum information technologies. By enhancing transition rates and directing the emission into specific electromagnetic modes, antennas can increase the maximum repetition rate and brightness of single photon sources [19].

Near-Field Optics

Field localization can contribute towards optimized scanning near-field microscopy probes for nanometer-resolution imaging and spectroscopy [10]. Furthermore, the antennas can be tailored to interact with specific polarizations of the electric and magnetic fields.

Photodetectors and Photovoltaics

Light-harvesting and emission devices based on thin films can be improved through the integration of optical antennas. For example, local field enhancement can focus the incident field to weakly-absorbing materials such as thin-film photovoltaics or graphene. In a photodetector, reducing the active material volume [20] allows for faster speeds thanks to improved carrier collection. Electro-optical devices in general can employ metallic antennas also as electrodes, combining electrical and optical functionalities [21].

Nonlinear Optics

In nonlinear optical processes, the signal scales at least quadratically with the local field. Resonant antennas, especially gap antennas, are particularly suited due to their field enhancement [22]. The non-linear response of external materials can be improved. The metal itself has a strong nonlinear susceptibility, resulting in two-photon luminescence, and second or third harmonic generation. They might be used as localized sources of coherent radiation.

Other Nanophotonic Components

Photonic and plasmonic circuitry can benefit from the interfacing to free-space radiation offered by antennas. A network of optical antennas might be more efficient for nanoscale point-to-point links than plasmonic

waveguides for distances beyond tens of micrometers. Other applications of the sub-wavelength local fields around metal nanoantennas are local heating and optical trapping of small dielectric objects.

In conclusion, optical antennas are attractive optical elements to control light-matter interaction at the single-emitter level with nanoscale resolution in a variety of innovative ways. In view of the possibilities and applications offered by optical antennas, in this Thesis we develop the Optical Physics of these novel nanophotonic components inspired by conventional Antenna Engineering.

2.

Experimental Methods for Nanoantennas

We introduce the experimental methods used in this Thesis for the characterization of light emission by optical nanoantennas. Firstly, we describe a technique to attach quantum dots to nanoantennas at predefined positions, a very flexible approach to couple light sources in the near field. The resulting emitter-antenna systems are characterized by confocal photoluminescence microscopy with polarization resolution, which allows a first quantification of the coupling of emitter and antenna. Importantly, we describe the angular measurement technique of back focal plane imaging for recording angular radiation patterns of nanoscale objects. In combination, these experimental methods are a powerful tool for the study of any nanoantenna design, regardless of the nature of its electromagnetic mode.

2.1. Characterizing optical antennas

The study of the optical properties of a single nanoscale object requires the effective interaction of light and matter, and therefore it can be considered an antenna problem in itself. Because of the diffraction limit to focusing, methods based purely on far-field sources and detectors are generally inefficient. Scattering methods include transmission and extinction spectroscopies, dark-field scattering spectroscopy or angular scattering measurements. Strategies can be devised to discriminate the incident and scattered fields (*e.g.*, in polarization or in angles) to achieve nearly background-free measurements in the far field.

Near-field characterization methods provide more information about antennas, including spatial mode maps. There exists a plethora of techniques that use at least one step of light-matter interaction in the near field as a contrast mechanism. Near-field scanning microscopies image the field distribution through localization of the detection or excitation volumes. Absorption and field enhancement can also be mapped in the near field by the modification of a photoactive material or by integration on a photodetector substrate. The strong non-linear optical response of metal nanoparticles, with origin in the near field too, can characterize antenna resonances. On the other hand, cathodoluminescence and electron energy-loss spectroscopy use electron beams as local probes of the density of optical states.

The purpose of an optical antenna is the efficient interfacing between the near field and the far field (evanescent and propagating waves). Therefore, the excitation of a nanoantenna by local light emitters is a particularly suitable characterization method; the emitter probes the antenna and the antenna controls the emission. The antenna dominates the interaction because of its substantially larger cross-section and moment strength.

The general experimental procedure that we will follow in this Thesis is to couple emitters to antennas, to locate individual antennas through confocal microscopy and to measure the angular radiation pattern of their emission.

2.2. Coupling an emitter to a nanoantenna

Feeding photons into an optical antenna is a task that can be best accomplished from its near field. Coupling of an emitter allows local excitation at a designated position, as opposed to driving the entire nanostructure simultaneously from the far field. The antenna modes that can be accessed are consequently different, with modal symmetries that cannot be excited by plane waves.

The emitter can be any local light source of nanometric dimensions: a single organic dye molecule, a fluorescent nanosphere, a quantum dot or well, an ion or

atom, a color-center in a diamond nanocrystal, etc. We employ quantum dots because of their brightness, broad excitation spectrum, and lower photo-bleaching compared to organic fluorescent molecules.

Dynamic and static emitter positioning methods

In order to couple efficiently, the emitter and the antenna need to be closer than 30 nm. Therefore, the probability of finding an efficiently coupled system fabricated by random deposition is limited and deterministic methods to position the emitters are needed. There are two main approaches for driving antenna modes with emitters from its near field: either by controlled deposition of the emitters (static), or by scanning the antenna over the emitter or vice versa (dynamic).

Dynamic methods

Requiring the spatial alignment of emitter and antenna with nanometric resolution, they generally rely on the scanning probes of near-field optical microscopy or atomic force microscopy [6-8, 10, 19, 23, 24]. The antenna (or the emitter) is mounted in the probe, while the other object is static on a substrate. They offer real-time control but have a low throughput. Alternative methods with a higher positioning uncertainty use a liquid environment to exploit microfluidic flow control, random diffusion of emitters, or optical trapping.

Static methods

The emitters can be permanently deposited or attached close to the antennas, ideally at predetermined positions. In order to collocate antenna and emitter, different methods may be used: attachment by chemical functionalization; site-selective attachment through DNA-linking; attachment by electrostatic forces [25-27]; positioning by vertical templating [28]; patterning in a polymer matrix [29, 30]. These methods can be assisted by conventional nanostructuring techniques (lithographies or focused ion beam milling) to achieve positioning at a specific location.

In this Thesis, we use primarily surface chemistry to attach semiconductor nanocrystals to gold nanoantennas. In some cases, it is assisted by a lithography-defined mask for more accurate positioning. We describe next this combined approach.

Positioning by two-step lithography and functionalization

We locally deposit quantum dots (QDs) on nanoantennas. We employ commercially available QDs (Qdot 800 ITK amino (PEG), Invitrogen). They are water-soluble core/shell nanocrystals (CdSeTe/ZnS) with a polyethylene glycol

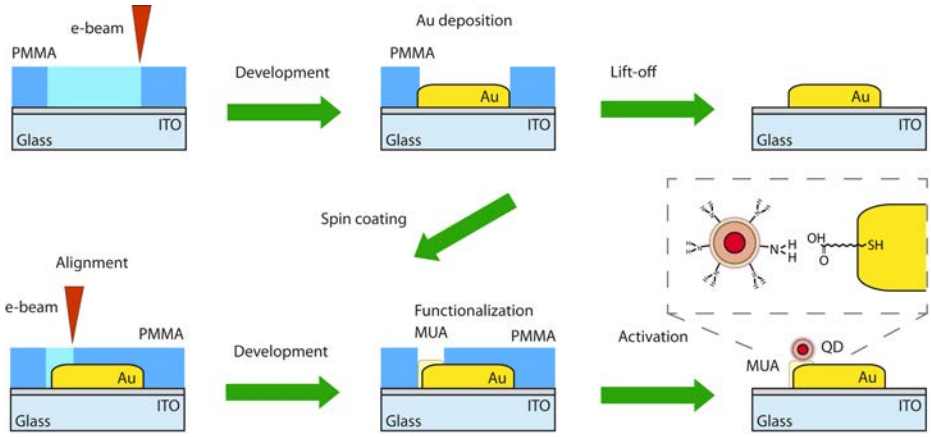

Figure 2.1 **Fabrication technique to position emitters on nanoantennas.** A combination of two steps of electron-beam lithography plus chemical functionalization provides spatial accuracy to position quantum dots, limited only by the resolution of the lithography.

coating. This polymer is functionalized; an amino group caps the QD surface. The total QD diameter is expected to be below 15 nm. The QD emission is centered around 790 nm with a full width at half maximum of 80 nm. Such long wavelengths are attainable thanks to the use of the alloyed ternary compound CdSeTe instead of the more usual CdSe core.

For the two lithographic steps, we employ polymethyl methacrylate (PMMA) as a positive electronic resist, spun-cast onto a glass substrate with a 10-nm layer of indium tin oxide (ITO). The first e-beam lithography defines the Au antennas and alignment markers, formed by thermal evaporation of a 30-40 nm Au layer and subsequent lift-off. The markers are used as a reference to accurately overlap the second lithographic layer, which sets the boundaries for the formation of a self-assembled monolayer of mercapto-undecanoic acid (MUA).

Specificity to gold is provided by the thiol groups of MUA, which physically adsorb on the Au surface. Next, a carbodiimide (EDC) activates the carboxylic acid terminations of MUA, so that the amino groups of the QDs can bind to them covalently. Finally, once the QDs are deposited and immobilized, the remaining PMMA is lifted off by rinsing in acetone with the sample in vertical orientation to avoid sticking of undesired QDs. The process flow is summarized in Figure 2.1. As a final result, we attain an accuracy of around 40 nm in positioning a QD patch relative to a metal structure, given by the resolution of the lithography.

To conclude, this fabrication technique will allow us to position a few emitters at designated positions on an arbitrary metal nanostructure. Using close to ideal

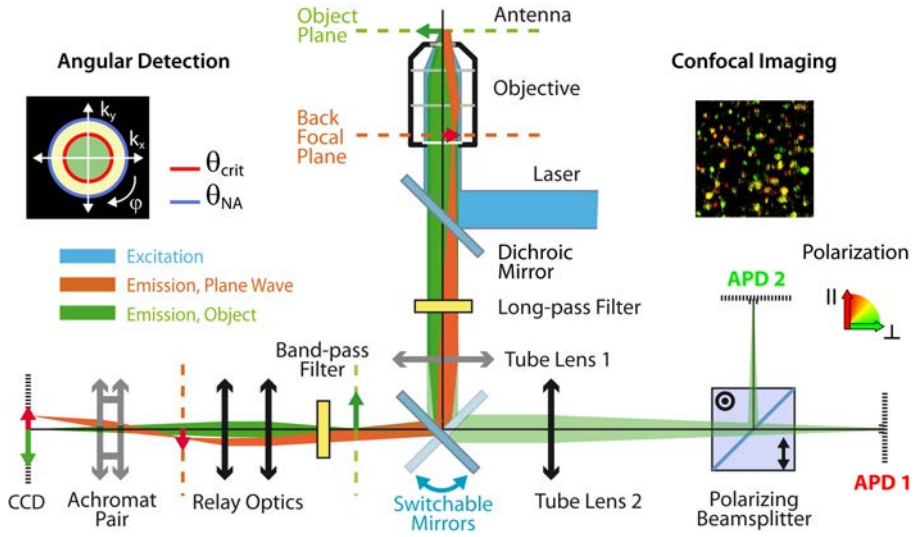

Figure 2.2 **Set-up for imaging and angular measurements.** Confocal photoluminescence microscope with avalanche photodiode detectors for real-space imaging and with a CCD camera for Fourier-space imaging. Different configurations depend on the position of Tube Lens 1 (in: conoscope to the left; out: confocal to the right) and the Achromat Pair (in: Fourier image in red; out: wide-field image in green). The left inset shows the structure of a back focal plane image, indicating critical and numerical aperture angles. The right inset shows a typical confocal image of single emitters with random polarizations (colors).

point sources, this method is a very powerful tool for the study of optical nanoantennas.

2.3. Imaging a nanoantenna

The first step to study the characteristics of a single antenna and to assess the reliability of the positioning method is to image the fabricated samples. Confocal photoluminescence microscopy with single-photon counters lets us locate individual antennas within an array and analyze their polarization and time-dependent signal, also with the possibility of studying photon statistics (anti-bunching and lifetime). The set-up is based on a Zeiss Axiovert 200 microscope with piezoelectric scanning of the sample with respect to the confocal volume.

This confocal microscope has three detection branches for luminescence imaging, angular detection and spectroscopy, respectively, all with single-emitter detection capability. A high-NA oil immersion objective (Zeiss, α Plan-Apochromat 100x/1.46 NA) is essential for efficient emission collection and as the

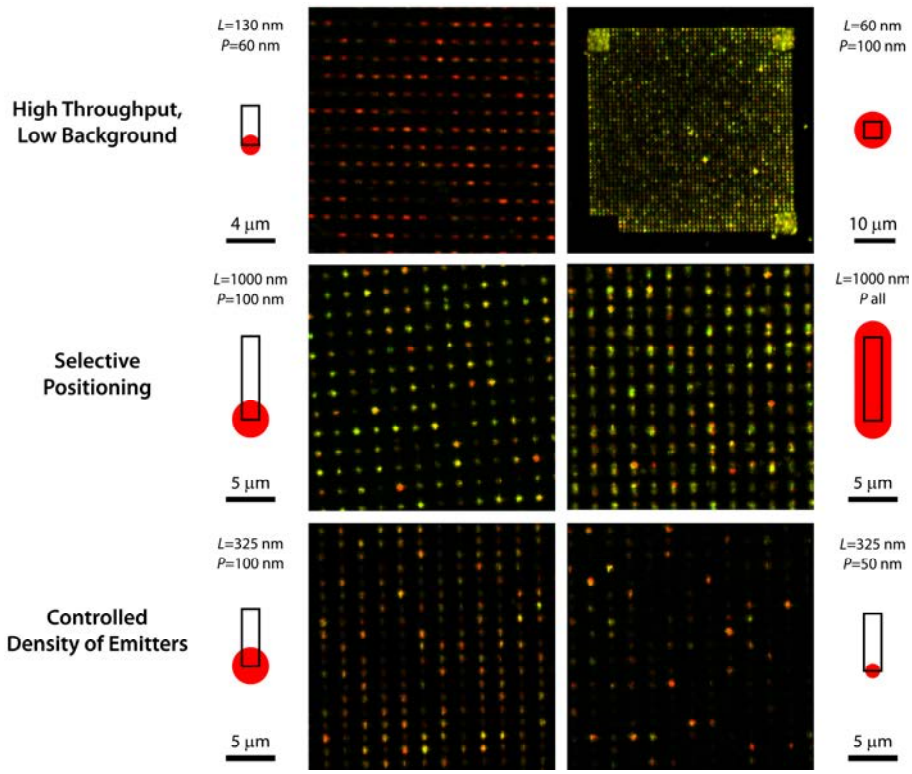

Figure 2.3 **Reliability and reproducibility of the fabrication technique.** Confocal photoluminescence microscopy images of arrays of antennas demonstrate that QDs can be selectively coupled at designated positions. Wire-shaped antennas (length L) with emitters positioned inside the red patches (size P) were fabricated using the two-step lithography method. In the upper right image, the areas of the three alignment markers for the second lithographic step are clearly visible at the corners. Images are color-coded for polarization (see Fig. 2.2).

basis for angular detection. The sample is excited by a circularly polarized He-Ne laser beam (λ=633 nm), with a power of a few µW after reflection on a long-pass dichroic mirror. The laser is focused to the diffraction limit in order to address one antenna at a time. The resulting luminescence is separated from the excitation wavelength with a long-pass filter. For alignment of the optical system, we use small clusters of quantum dots or dye-loaded fluorescent nanospheres.

Polarization analysis

The confocal signal is split by a polarizing beam-splitter cube onto two detection channels with avalanche photodiodes (Perkin Elmer, SPCM-AQR-14 and 16). The

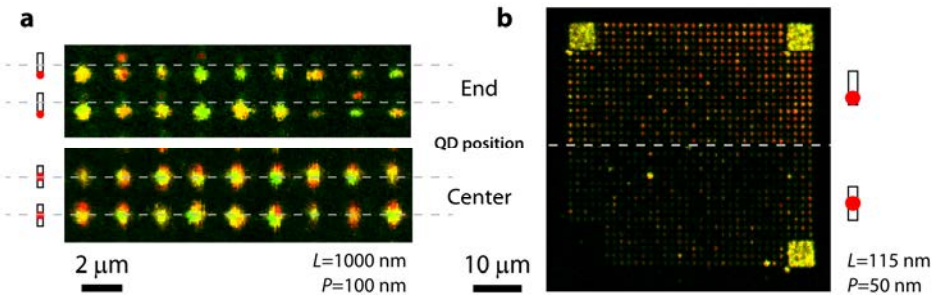

Figure 2.4 **Further direct evidence of the accuracy of the quantum-dot positioning technique. (a)** Nanowire antennas longer than the diffraction limit confirm by direct visualization that the emitters can be positioned at the end (top image) or at the center (bottom image) of the antenna. The images are saturated in intensity to better appreciate the spatial features of the polarization. Notice the dimmer polarized emission at the distal end of some antennas. When the emitter is placed one end, indirect excitation through the wire results in more polarized emission at the other end due to a lower uncoupled emission contribution. When the emitter is placed at the center, the image is symmetric. **(b)** Nanowire antennas smaller than the diffraction limit. A direct comparison of intensities for QDs at the end or at the center of a dipolar antenna, for which local fields and coupling are higher at the ends, demonstrates that the emitters can be positioned with the accuracy of the electron beam resolution. The length of the antennas (L) and the size of the predefined QD patch (P) are indicated below each image.

confocal aperture size is given by the area of the detectors. The two polarization channels enable polarization-resolved imaging; by calculating the degree of linear polarization $DOLP=(I_{\parallel}-I_{\perp})/(I_{\parallel}+I_{\perp})$, we represent the polarization anisotropy of the emission, where $I_{\parallel}$ is the counts detected in the vertical polarization (parallel to the long axis of a linear antenna). The $DOLP$ is one of the Stokes parameters that parameterize the polarization of light.

The images can be color-coded for degree of linear polarization, with brightness for each pixel proportional to the number of counts. Red (green) color represents vertical (horizontal) linear polarization, whereas yellow may be unpolarized emission or any polarization with a 45° degree projection on the image plane. The two APD signals are calibrated to account for differences in the quantum efficiencies of both detectors and for polarization by the optical elements (*e. g.,* induced by the dichroic mirror upon oblique reflection/transmission).

Coupling of an emitter to an antenna can lead to a complete modification of the polarization. The change in polarization (color) is evident in Figures 2.3, 2.4

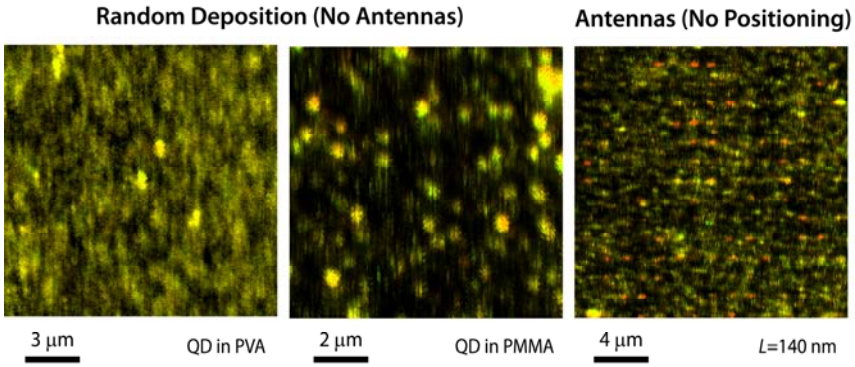

Figure 2.5 **Deposition of emitters without using the positioning technique.** If the double lithography technique is not used, a sizeable background signal arising from QDs not coupled to the antennas is detected, making it difficult to study the nanoantenna emission.

and 2.5. These images are conclusive proof of the ability of our double lithography technique to attach emitters to the antennas deterministically.

On the other hand, for a quantitative comparison of simulations with experimental polarization measurements, the calculated emitted fields must be also propagated through the confocal imaging system using the angular spectrum representation [31] [32]. The use of a high numerical aperture objective (non-paraxial imaging) for a linearly polarized nanoscale source (dipole) results in additional polarization components in the image plane. As a consequence, the highest value of *DOLP* that can be measured with our system is 0.9, even for a linearly polarized point source with nominal *DOLP*=1.

Number of emitters per antenna

The number of emitters attached to an antenna using the double lithography technique depends both on the area opened by the second lithography and the concentration of the QD solution, as shown in Fig. 2.3 (bottom right). For the antennas in Chapters 3 and 5, where this technique is employed, we opt for a size of the QD patch of 60 nm as a trade-off between low number of emitters and homogeneity of the sample. Based on the confocal imaging of individual antennas, time-resolved single-photon counting techniques allow an estimation of the number of QDs per antenna.

Intensity time traces show blinking behavior characteristic of single quantum emitters (Fig. 2.6); a telegraphic on/off signal due to the temporary passage of the exciton to a non-emitting state [33, 34]. Jumps in the number of detected counts are also manifest in scanning confocal images, as dark lines inside some antennas

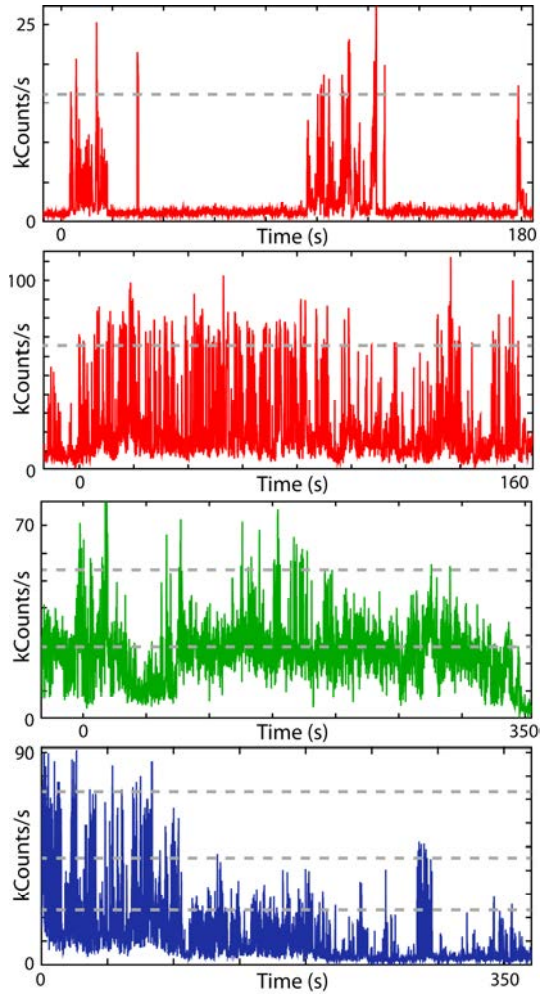

Figure 2.6 **Blinking in the emission of emitter-antenna systems.** Examples of luminescence time traces of antennas fabricated with the double lithography method with possibly one QD (red), two QDs (green), and three QDs (blue). Gray horizontal lines are guides to the eye for possible intensity levels. The timebin is 25 ms.

along the scanning direction (*e.g.*, in Figures 3.2 and 5.1). The non-radiative mechanisms that have been suggested to produce intermittency in emission [33] are based on the ionization of the QD or the existence of surface trap states. In our experiments, several factors might influence blinking simultaneously: the metal nanoparticle [35, 36]; the ITO substrate [37]; excitation power, rapid aging

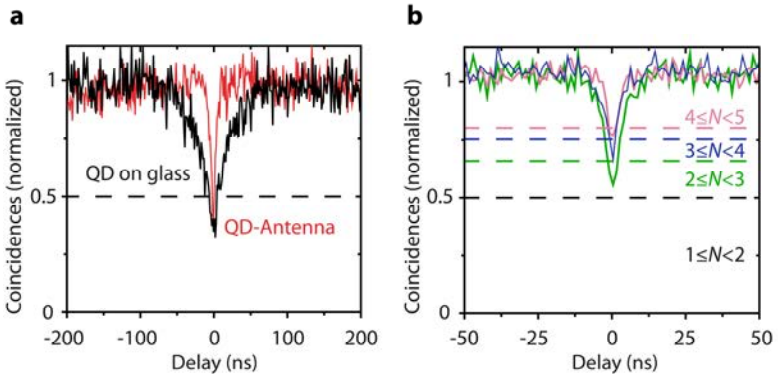

Figure 2.7 **Non-classical photon statistics of emitter-antenna systems.** **(a)** Photon anti-bunching measurements comparing the inter-photon delay of single photons emitted mostly by a single quantum dot on glass (black) and coupled to a dipolar antenna (red). Single photon emission is evidenced by a dip below 0.5 in coincidences. The total accumulation time was 50 minutes. Higher transition rates (narrower anti-bunching dip) are due to resonant coupling to the antenna. **(b)** Examples of antennas with more than one QD. The levels in coincidences indicate ranges of numbers of ideal single emitters. The time resolution was 1.184 ns. Background contributions to the coincidences were not subtracted.

under ambient conditions, and functionalization involving thiol groups [38] and solvents.

Photon anti-bunching measurements directly reveal non-classical light emission by the antennas. By using a non-polarizing beam-splitter instead of a polarizing cube, we turn our microscope into a Hanbury Brown and Twiss set-up to record the correlated arrival times of pairs of photons. The dip in photon coincidences around zero inter-photon delay time (Fig. 2.7a) is characteristic of single photon emission [39-41], confirming that as few as a single quantum dot can be attached to an antenna.

For N perfect single-photon emitters, the normalized coincidence rate at zero delay follows the dependence $1 - 1/N$. As seen in the case of a QD without antenna, our QDs are not ideal single-photon sources because bi-excitons provide a non-negligible probability of emitting two photons simultaneously. Furthermore, luminescence of the antennas themselves also contributes background photons. The finite temporal resolution around zero delay also increases the observed coincidences above zero.

Yet, the coincidences remain under 0.5, demonstrating that most photons come from a single quantum emitter. For a better contrast in single-photon emission, other emitters with lower bi-exciton rates or other antenna materials with lower autoluminescence might be used. Other examples of antennas with photons arising mostly from 2, 3 and 4 QDs are shown in Fig. 2.7b. In all cases, coupling to the antenna increases transition rates (radiative, non-radiative and excitation rates) resulting in a narrower dip than for a single QD on bare glass (black line).

To conclude, we find thanks to these photon-counting measurements that the number of QDs coupled to each antenna is usually between 1 and 3, with a most frequent value of 2 or 3, when the combination of two steps of lithography and chemical functionalization is used.

2.4. Measuring the angular radiation pattern of a nanoantenna

Polarization-resolved imaging of nanoantennas allows us to point to individual antennas for further characterization. In general, polarization measurements alone do not give access to all the available information in the emission of an antenna (*e.g.,* asymmetric radiation patterns or multipolar nature of the emission). Therefore, angular detection complements and expands the study of optical antennas. Several methods exist for the angular characterization of nanoscale objects. For example, defocused imaging provides mixed information between real and reciprocal spaces by imaging an object through an optical system slightly out of focus. Scanning-angle detection (a point-like photodetector mounted on a goniometer) is suitable for intense signals.

In this Thesis, we employ the technique of back focal plane imaging, also known as conoscopy, to record directly in one shot the angular radiation patterns of dim nanoscale emitters (Fig. 2.2). This technique is used, amongst others, in the display industry to quantify the brightness at different viewing angles. In nano-optics, it has been used to determine the orientation of single molecules [42] and to observe surface plasmons in leakage radiation microscopy [43-45]. We will image the intensity distribution on the back focal plane (BFP) of an oil-immersion high numerical aperture objective (Zeiss α Plan-Apochromat 100x, 1.46) onto an electron-multiplying CCD camera (Andor, iXon^{EM}+ 897). This plane contains the Fourier-space image of the object plane, namely the directions of emission. The signal is typically distributed over 120x120 pixels and accumulated for more than 20 s.

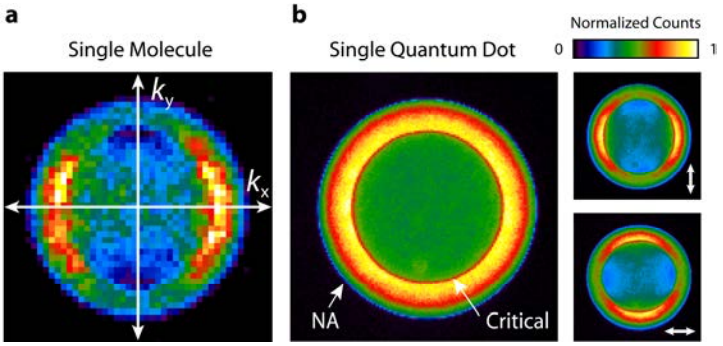

Figure 2.8 **Angular emission of single emitters without antennas.** Radiation patterns as recorded in the back focal plane of an oil-immersion microscope objective with a glass substrate. **(a)** A single molecule in a thin PMMA film. **(b)** A single quantum dot in PMMA. The inset shows an analysis of the polarization of the BFP image with a linear polarizer along the arrow direction. In all BFP images, individual pixels are shown directly as measured without any interpolation. The single-molecule image was binned 4 times during acquisition to compensate for a weaker signal.

The coordinates and power density of the emission as recorded on the BFP are related to the angular radiation pattern (power density per unit solid angle) by a projection given by the design of the microscope objective [46]. To assess the particular relation followed by our objective, we used several diffraction gratings to calibrate the k-space images with the known angles of the diffraction grating orders. We found that our objective satisfies the sine condition [46], that is to say, the coordinates on a BFP image (radius R) are related to the inclination angle (θ) between the optical axis and the wave vector by the relation $R(\text{pixel})=K\ \sin\theta$, where K is a calibration constant related to the magnification of the imaging system. The intensity on the back focal plane of the objective (k-space) is related to the angular pattern by $I(\theta,\varphi)=I_{\text{BFP}}(k_x,\ k_y)\ \cos(\theta)$, where $k_x=K\ R\ \sin(\theta)\ \cos(\varphi)$ and $k_y=K\ R\ \sin(\theta)\ \sin(\varphi)$. The cosine factor is an apodization factor introduced for conservation of energy, to account for the different solid angles covered by the area of a pixel at different BFP positions. When comparing our experimental results to simulations, we discard the last few pixels of the BFP image because transmission goes down gradually near the numerical aperture.

Emitters without nanoantennas

We excite and detect emitters on a substrate, one at a time, with a focused beam. As a reference for the antennas in the rest of this Thesis, we assess first the characteristics of emitters in the absence of antenna structures.

The radiation patterns as obtained in the BFP for a single molecule (DNQDI) in a thin PMMA film and a single QD embedded in a thin PMMA film are shown in Fig. 2.8. In all *k*-space images, we observe two distinct circles: the maximum collection angle of our objective (θ_{NA}=72.8°) and the critical angle of a glass-air interface (θ_{crit}=41.1°). Most of the radiation is emitted towards the substrate and it is contained between the critical angle and the numerical aperture angle. In the case of a single molecule (Fig. 2.8a), the anisotropic pattern of a single electric dipole with two lobes can be clearly identified [42].

Our QDs exhibit a degenerate transition dipole moment oriented almost isotropically on a "bright" plane [47-51], originating in the crystalline structure and shape of the semiconductor nanocrystals. As a result, the radiation pattern of even a single QD is nearly isotropic in the azimuthal angle φ, and its emission is approximately unpolarized (Fig. 2.5). We find only minor differences between the patterns of different QDs, and their emission can be described by a superposition of in-plane electric dipoles. This observation is confirmed when a linear polarizer is used to analyze the QD angular pattern (insets in Fig. 2.8b); the patterns then resemble two single, linear electric dipoles, as for the single molecule case.

Finally, to understand intuitively why the radiation pattern of a dipolar source peaks at the critical angle, we note that the fields of a point source contain evanescent components. Emission at angles beyond the critical angle arises from these fields [52]. Snell's law must be used to propagate the fields of a dipole from air into the dielectric; a plane wave is refracted at the critical angle for an incidence angle of 90°, and higher angles of refraction can only be obtained with imaginary angles out of the plane-wave angular spectrum. By bringing the source close to a dielectric interface, the evanescent fields can be funneled to the far field. This situation is reciprocal to the excitation of evanescent fields under total internal reflection.

3.

Nanowire Antennas for Multipolar Radiation

We demonstrate controlled emission of a quantum emitter into multipolar radiation through selective coupling to a linear nanowire antenna. In general, multipolar transitions other than electric dipoles are too weak to be observed at optical frequencies in single emitters such as fluorescent molecules and quantum dots, because they have dimensions much smaller than the wavelength of light. Therefore, they emit predominantly as point electric dipoles. In this Chapter, an antenna resonance tailors the interaction of a quantum dot with light, effectively creating a hybrid nanoscale source beyond the simple Hertz dipole. Our findings establish a basis for the controlled driving of fundamental modes in nanoantennas and metamaterials, for the understanding of the coupling of quantum emitters to nanophotonic devices such as waveguides and nanolasers, and for the development of innovative quantum nano-optics components.

3.1. Introduction to nanowire antennas

Optical antennas offer new possibilities to tailor the interaction of light with nanoscale matter [4, 53]. Emission and absorption can be controlled by near-field coupling to a properly designed antenna, with the properties of the interaction determined by the antenna mode instead of the original emitter. Nanoantennas based on dipolar resonances have been exploited to improve single-molecule detection [6], brighten single-photon sources [9, 19] or direct fluorescence [54].

Ultimately, having access to all possible multipolar terms in the field expansion, beyond the dipole, provides complete control over optical fields to exploit all the degrees of freedom of the three-dimensional, vectorial, electromagnetic field. Such control will allow engineering electromagnetic parameters like the phase, the polarization state, the directions of radiation and the orbital angular momentum of light. Additionally, the efficient coupling of an emitter to an arbitrary nanophotonic mode with subradiant or superradiant character can be desirable for applications in sensing or plasmon-based nanolasers.

In this Chapter, we demonstrate multipolar radiation of single quantum dots by coupling to multipolar resonances of nanowire antennas of increasing length, with alternating symmetry and multipole parity. The measured angular patterns and polarization states are reproduced by a one-dimensional model, and the underlying nature of the resonances is revealed by a multipolar expansion, showing controlled dipolar, quadrupolar, octupolar and higher multipolar character in the photon emission.

These results provide a first deterministic realization of the resonant interaction of quantum emitters with a variety of nanowire antenna modes of even and odd symmetries, which are fundamental building blocks in nano and quantum optics.

3.2. Resonant nanowires as optical antennas

Most optical antenna designs are based on short metal nanowires. Longer nanowires act as waveguides for surface plasmons [55] and coupling of quantum emitters to them results in confined transport of the emitted photons [56, 57]. In contrast, the aim of an optical antenna is to maximize the power radiated by emitters to the far field into well-defined modes of the light field.

Nanowire antennas are an ideal platform to explore photon emission beyond usual electric dipole radiation thanks to the higher-order resonances that they support. These resonances have been studied using various techniques, mainly capitalizing on spatial mapping through different near-field contrast mechanisms

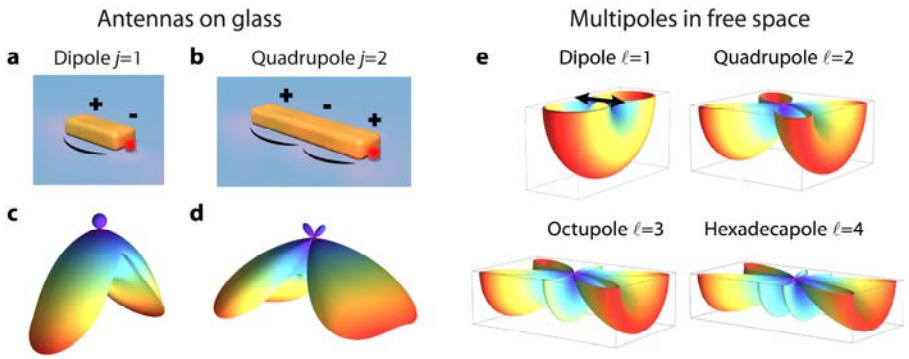

Figure 3.1 **Single quantum dots coupled to multipolar nanowire antenna modes. a-b,** A quantum dot is positioned at the end of a metal nanowire. The first two resonant modes have opposite symmetries in surface charge distribution and current along the antenna. Charge signs and current magnitudes are sketched. **c-d,** Angular radiation patterns of point electric dipole and quadrupole oriented parallel to the antenna above a glass substrate. Both patterns differ in direction and width of the lobes, with most radiation emitted into the substrate. The emission wavelength is 800 nm and the emitters are 15 nm above the substrate. **e,** Section of the angular patterns in free space of longitudinal multipoles oriented along the direction of the antennas.

such as near-field scanning probe microscopy, cathodoluminescence, electron energy-loss spectroscopy, and photocurrent imaging [58-68].

Nanowires as surface plasmon resonators

Intuitively, nanowires can be regarded as cavities for surface plasmons; at resonance, the oscillating surface charge and current distributions along the nanowire display stationary nodes of a standing-wave [15, 16, 69-71].

We model a nanowire as a one-dimensional resonator. We label the order of the different resonances with j, indicating the approximate number of half-wavelengths contained in the resonator or, equivalently, the current maxima along the antenna (Figures 3.1a and b). A nanowire can then be parameterized with the following values [70]:

- the **wavelength** of the plasmon propagating along the wire, λ_{SP}, related for a given mode to the effective refractive index;
- the **losses** on propagation, k_i;
- the **reflectivity** at the ends of the wire, r;
- the **phase** picked up on reflection at the ends of the wire, ϕ.

In other words, plasmons travel along the antenna (length L) with complex wave vector k and are reflected at the antenna ends with complex reflection coefficient $r=|r|e^{i\phi}$. The plasmon propagating along the antenna has a wavelength λ_{SP} ($Re(k)=2\pi/\lambda_{SP}$) and losses determined by $Im(k)=k_i$.

Resonances are found at lengths that satisfy the condition $L_n = \lambda_{SP}/2\ (n-\phi/\pi)$, where n is a positive integer. These parameters are retrieved by fitting to experimental results in polarization and angular measurements. This model describes the emission of the antenna mode alone, regardless of the number of emitters coupled to it, and does not include possible contributions of emission that is not coupled to the antenna mode. Note that the presence of the semiconductor nanocrystals will slightly perturb the antenna parameters.

The emission properties of these modes and their near-field interaction with quantum emitters are governed by the symmetry and spatial distribution of the characteristic currents for each mode. For example, the lowest order mode, j=1, has odd charge symmetry (Figure 3.1a) and its current distribution creates a dipole source. The j=2 mode has even symmetry, with a zero net dipole moment, and resembles a longitudinal quadrupole. Hence, j=1 corresponds to a half-wave dipole antenna, whereas j=2 is a full-wave, end-fed quadrupole antenna. As a first approximation, we expect that the angular radiation patterns of these two lowest order antenna modes are point dipoles and point quadrupoles (Figures 3.1c and d for an antenna on a glass substrate and Figure 3.1e for free space).

Coupling a quantum dot to a nanowire antenna

Each resonance can be locally driven at points where the coupling between quantum emitter and antenna is efficient. The electric mode density is high at the ends of a nanowire regardless of the symmetry of the resonant mode. Therefore, a point source (electric dipole) at the end of a nanowire couples to all possible resonant modes, breaking the symmetry that might prevent access by far-field illumination, and encompassing both sub- and super-radiant modes irrespective of symmetry [70, 72]. Our approach to drive antennas locally relies on positioning colloidal quantum dots (QDs) with nanometer accuracy at the end of each nanowire through a combination of two steps of electron beam lithography and chemical functionalization, as explained in Section 2.2. With our method, we obtain arrays of antennas with typically one to three QDs per antenna at a predefined position.

Polarization of nanowire antenna emission

First, we identify the resonant antenna lengths from the change of polarization of the emission [12] of QDs when coupled to nanowires of increasing length. To this

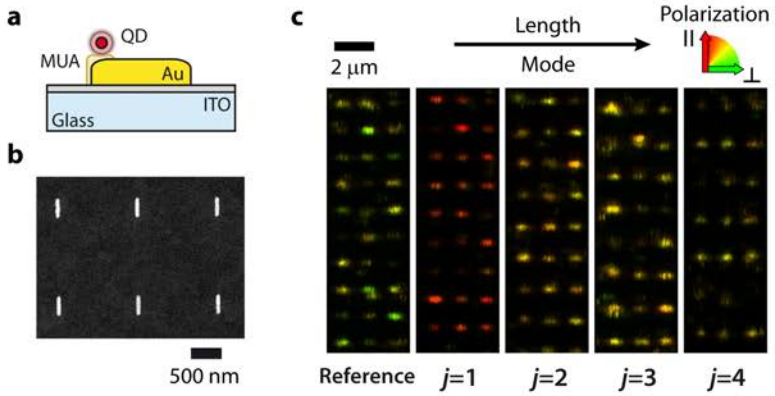

Figure 3.2 **The emission becomes polarized by coupling to different nanowire antenna modes. a,** Geometric configuration of the sample. **b,** Scanning electron microscopy image of an array of antennas. **c,** Scanning confocal luminescence microscopy image of arrays of identical antennas with increasing length, demonstrating a decreasing degree of linear polarization along the antennas. The polarization is colour-coded into the image, with red being the polarization along the antenna.

end, we record confocal photoluminescence images of arrays of identical antennas with lengths from 60 to 900 nm (Figure 3.2). The emission is detected in two polarization channels, parallel and perpendicular to the long axis of the wires, with signals $I_{\parallel}$ and $I_{\perp}$, respectively. The polarization of the emission depends on the mode of the antenna, evolving from linear polarization along the antenna to unpolarized emission for increasing order resonances. For quantitative analysis, we define the degree of linear polarization $DOLP = (I_{\parallel}\text{-}I_{\perp})/(I_{\parallel}+I_{\perp})$. By taking statistics over approximately 200 antennas per length, we observe clear oscillations in polarization degree as a function of antenna length, on and off resonance (Figure 3.3).

Yet, linearly polarized emission along the antenna, with constant $DOLP \approx 1$, is expected for an oscillating current on a line and predicted by our resonator model even off resonance (Figure 3.3c). The observed oscillations in polarization are due to partial coupling of the QDs to the antennas, namely, a fraction of the emission does not interact with the antenna mode. This fraction of the radiation results in depolarization. The relative weight of the contributions of antenna emission and uncoupled background to the total polarization varies as the antenna is tuned to resonance with the QD emission. The resonances in polarization are thus attributed to the resonant modes j, and indicate the best overlap between antenna mode and the luminescence spectrum of the QD, centered around 800 nm.

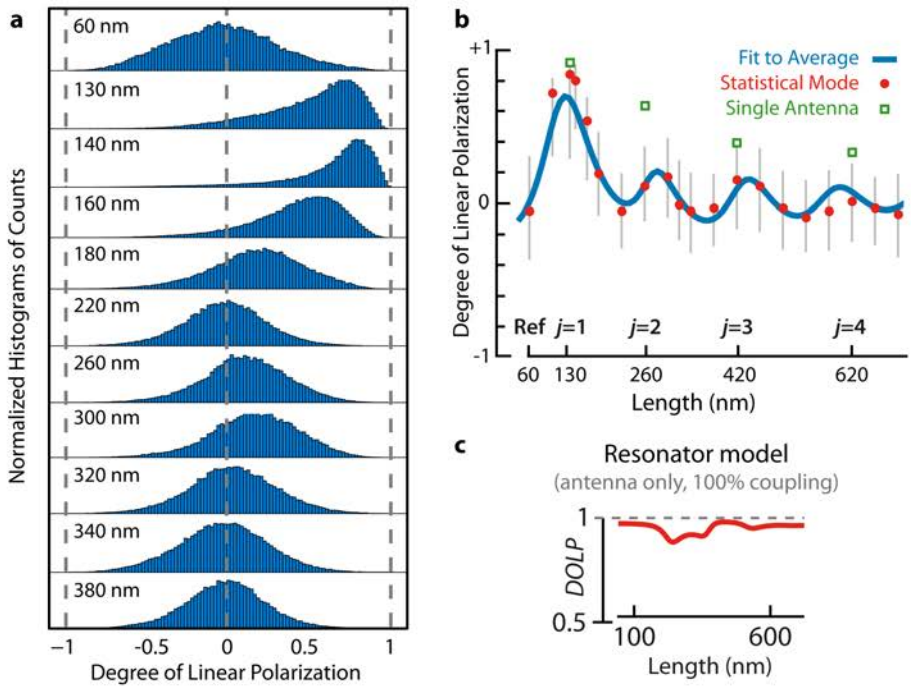

Figure 3.3 **Polarization oscillations map the resonant modes of antennas of increasing length. a, b,** Histograms and statistical analysis of linear polarization measurements taken over approximately 200 antennas per length shows oscillations of the polarization on and off resonance. Vertical gray lines in **b** indicate the standard deviation around the average polarization. Green squares identify the individual antennas studied in detail in the next figures. **c,** The 1D-resonator model predicts a linear polarization close to unity and, consequently, unpolarized contributions were added to the model to describe the oscillations with a fit to the average polarization (blue line in **b**).

λ_{SP} (nm)	$k_i\,/k_0$	$\phi\,\lambda_{SP}/2\pi$ (nm)	$\lvert r\rvert$
313±3	0.150±0.025	34±2	0.7±0.03

Table 3.1 **Antenna parameters retrieved by fitting the polarization measurements with a 1D-resonator model.** These values, that reproduce the results as a blue line in Figure 3.3b, represent an equivalent average antenna, with losses (k_i) and reflectivity ($|r|$), that is inhomogeneously broadened and does not represent the quality of individual antennas. The wavelength in vacuum of the emission is λ_0=800 nm.

After taking into account this partial coupling of QDs to the antenna mode, our one-dimensional cavity model reproduces the observed oscillations in average polarization with a fit (Figure 3.3b, blue line) based on a superposition of the theoretical antenna emission plus an incoherent sum of two perpendicular polarizations describing uncoupled emission. The antenna parameters retrieved by fitting to the average polarization are presented in Table 3.1.

The average polarization decreases for increasing order of modes because the resonances are damped due to dissipation, resulting in a lower coupling efficiency. This average represents the inhomogeneously broadened distribution of antennas in the arrays, similarly to the broadened spectrum of an ensemble of molecules. Individual antennas exhibiting higher degrees of polarization are singled out from this ensemble (squares in Figure 3.3b). We focus next on these individual cases, where the emitter-antenna coupling is stronger.

3.3. Multipolar radiation of a quantum dot

Polarization alone does not allow identification of the resonance order or multipolar character of the emission. For a detailed understanding of resonant antenna modes and their coupling to QDs, we turn to angular radiation patterns [70, 73] for selected QD-antenna systems, which will ultimately lead us to a quantitative demonstration of multipolar radiation.

Angular radiation patterns of nanowire antennas

The antennas lie on a glass substrate, which affects the angular radiation patterns by funneling and projecting most of the emission into the substrate half-space, especially above the critical angle of the air-glass interface. As a result, the radiation pattern of a point multipole on a substrate (Figures 3.1c and d) differs from what is expected in free space (Figures 3.1e). Fourier images of single antennas contain the directions of emission of the coupled system into the substrate.

For off-resonance lengths, similarly to the absence of polarization, the quantum dot angular emission is hardly affected by the antenna and the pattern is rotationally symmetric (Figure 3.4a).

At resonance, the angular pattern becomes dominated by the antenna mode. For the j=1 resonance, the emission represents a linear dipole along the antenna (Figure 3.4c); the planar degeneracy in transition dipole moment of our semiconductor nanocrystals (Figure 3.4a) [47, 51] is lifted by coupling to the antenna mode. The antenna pattern is almost identical to a point electric dipole, inasmuch as conventional half-wave dipole antennas are almost point Hertz dipoles.

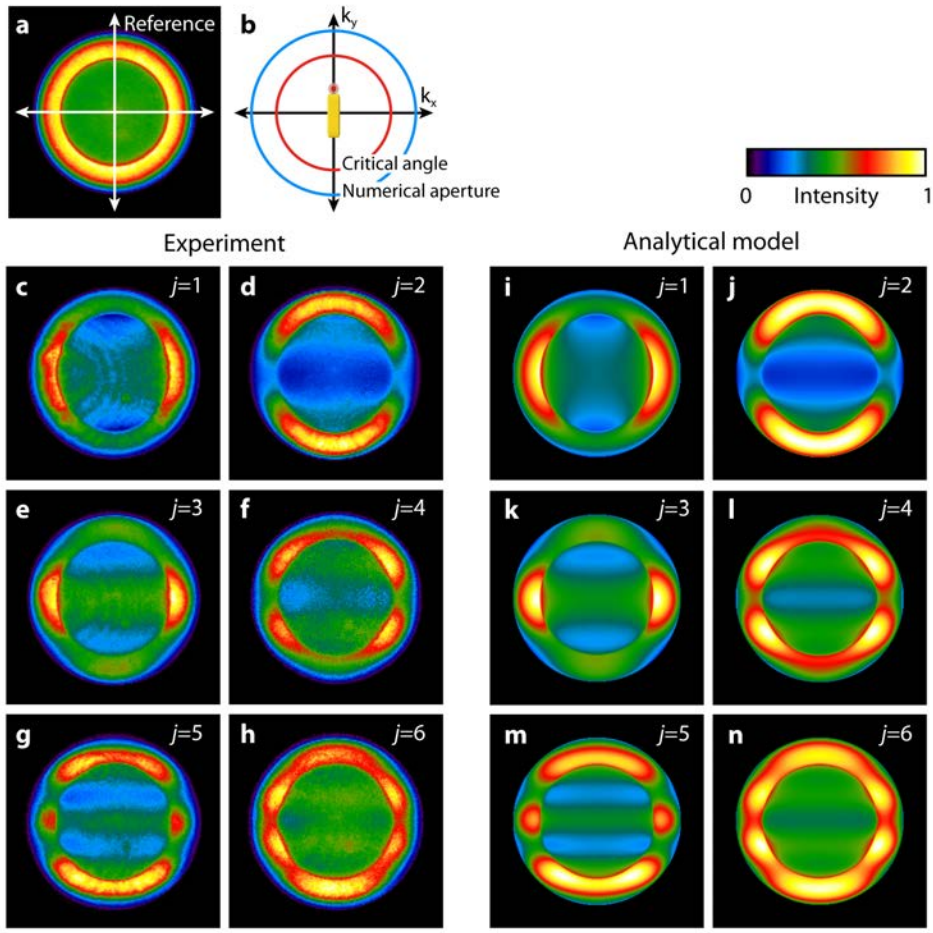

Figure 3.4 **Multipolar angular radiation patterns of quantum dots coupled to antennas of increasing resonance order.** Fourier-space images recorded in the back focal plane of the microscope objective. **b,** Schematic of an angular pattern highlighting the critical angle of the glass-air interface and the numerical aperture of the objective (maximum collection angle). The orientation of the antenna and the relative position of the quantum dot are superimposed. **a,** Reference structure: quantum dot on an off-resonance 60-nm square. **c-h,** Experimental patterns of the first 6 resonant antenna modes. The first four antennas are the individual antennas marked in Figure 3.3. **i-n,** The patterns are reproduced with the analytical resonator model, including a rotationally symmetric background. The left and right columns group together odd and even modes respectively, with opposite angular symmetries.

The j=2 resonance has even charge symmetry and its radiation pattern is oriented perpendicular to the first mode (Figure 3.4d), corresponding to a linear or longitudinal quadrupole. Due to their opposite symmetry, the central horizontal maximum in the emission of the dipole becomes a minimum in the emission of the quadrupole, despite their equally parallel polarization along the antenna. This is a clear illustration of the non-equivalence of polarization and angular measurements; in general, the observation of a polarization cannot be attributed to a single antenna mode with a characteristic angular pattern.

The third order resonance has the symmetry of the half-wave dipole antenna but its lobes are now narrower (Figure 3.4e), a characteristic of higher multipoles. For increasing order modes additional lobes appear, with alternating symmetry and positions of minima and maxima. Related patterns have been measured recently in the electroluminescence, cathodoluminescence and far-field scattering of antennas of different resonant orders [21, 65, 74] and in the emission of photonic crystal cavities [75]. The sharp features of our patterns gradually wash out for higher order resonances due to a lower coupling, which results in a rotationally symmetric background added to the pure antenna modes. For longer wires [55, 57, 71], several resonances start overlapping within the luminescence spectrum of the QD, and a band pass filter was used to select the central part of the emission spectrum for j=5 and j=6 to improve the contrast (Figures 3.4g-h).

The j=2 resonance illustrates the physics involved. This antenna efficiently converts the emission of a dipolar transition (QD) into quadrupolar radiation by coupling to the optical antenna. Its angular pattern consists of two broad lobes directed along the antenna and resembles the pattern of a point quadrupole on glass (Figure 3.1d). The coupling of a dipole transition to a quadrupolar mode is possible because the placement of the QD at the end of the antenna breaks the inversion symmetry of the QD-antenna system. Because the total antenna length (260 nm) is on the order of half the wavelength, the j=2 mode radiates effectively [70]. It is therefore neither sub-radiant nor dark, despite its even charge symmetry. For antennas, multipolar moments are not necessarily small and, for antenna dimensions on the order of the wavelength, the radiant character of the mode is independent of its multipolar nature.

Multipolar and dipolar antenna modes radiate with a comparable rate, in contrast to multipolar transitions in small quantum emitters such as molecules, quantum dots or ions, which are usually several orders of magnitude slower in radiative rates than dipolar transitions. Indeed, the ratios of average detected luminescence per antenna for the different modes are $I_{j=1}$: $I_{j=2}$: $I_{j=3}$: $I_{j=4}$ = 1: 0.4: 0.25: 0.3, with oscillations in radiated power following those of the polarization response in Figure 3.3b. In absolute terms, the average count rate for the dipolar

resonance ($I_{j=1}$) is 135 kCounts per ms for an excitation power density of 1.08 kW cm^2. A QD coupled to the j=2 mode thus provides a novel nanoscale system: a bright single quantum emitter that interacts with light as a quadrupole.

1D-resonator model of angular radiation patterns

To assess the strength of the coupling of the QDs to the antennas, we compare the experimental angular patterns to our 1D analytical model in Figures 3.4i to 3.4n. The experimental results fit accurately to a sum of the theoretical antenna emission pattern, *i.e.* pure antenna mode, plus an incoherent background consisting of two equal in-plane dipoles. The relative weights of the antenna mode and the uncoupled background give a measure for the effectiveness of the coupling of the QD to the antenna mode. We find through such a fitting that the fraction of the emitted power corresponding to the antenna mode is 90% and 60% for the first two resonances j=1 and j=2, respectively, denoting high coupling efficiencies between the QD and the plasmon mode of the antenna. The coupling is stronger than for longer nanowires [56, 57] due to enhancement by the antenna resonances.

For an electric dipole at one of the ends of the antenna (position y=-L/2), with the origin chosen at the center of the antenna and the antenna axis oriented along y, the current distribution along the antenna is related to the plasmon wavevector k by [70]:

$$J(y) \propto \frac{e^{ikL/2}(r+1)}{1-r^2e^{2ikL}}(e^{iky} - re^{ikL}e^{-iky}).$$

From this current distribution, we obtain the emitted field as:

$$\mathbf{E}(k_x, k_y) = \mathbf{E}_0(k_x, k_y) \int_{-L/2}^{L/2} J(y)e^{-ik_y y}dy,$$

where k_x and k_y are the projections of the wave vector (of magnitude k_0) of the emitted radiation along the in-plane x and y coordinates, and $\mathbf{E}_0(k_x, k_y)$ is the electric field emitted by a y-oriented electric dipole above an air-glass interface [76]. This dipole is situated 15 nm away from the interface on the air side, at half the experimental antenna height of 30 nm.

The radiation pattern of each individual antenna was reproduced using a least-squares linear fit to find the optimal weights of the antenna mode and the uncoupled background for different sets of antenna parameters (see Section 3.1 for definitions). We found the best fit to the individual antennas for the values of antenna parameters summarized in Table 3.2. The parameters related to the losses and the reflectivity of these individual antennas have a better quality than the inhomogeneously broadened average antenna obtained from polarization measurements in Table 3.1.

j (mode)	λ_{SP} (nm)	$k_i\,/k_0$	$\phi\,\lambda_{SP}/2\pi$ (nm)	$\lvert r\rvert$	R^2 (fit quality)
1	280±10	0.01±0.03	32±2	1±0.05	0.980
2	250±10	0.04±0.03	32±2	1±0.05	0.987
3	280±10	0.04±0.03	32±2	1±0.05	0.982
4	330±10	0.01±0.03	32±2	1±0.05	0.967
5	330±10	0.08±0.02	32±2	1±0.05	0.976
6	310±10	0.08±0.02	32±2	1±0.05	0.971

Table 3.2 **Antenna parameters retrieved by fitting the angular patterns of individual antennas with a 1D-resonator model.** To ease the computational burden of the calculation, antenna radiation patterns were calculated only once for a set of combinations of antenna parameters. A linear fit was calculated for each set, and the best fit is shown in this Table. The uncertainties in the antenna parameters are given by the spacing between consecutive steps in the exploration of antenna parameter space.

Multipolar expansion of angular radiation patterns

To describe the nature of these radiating modes, we reproduce their angular patterns with a point multipolar expansion [77], conclusively demonstrating multipolar radiation of otherwise dipolar quantum emitters (Figure 3.5). An oscillating distribution of charge on a wire generates propagating electromagnetic fields that can be decomposed in axial multipoles oriented along the antenna. Since magnetic multipoles vanish for line sources, we fit our experimental results of individual antennas with a coherent superposition of electric multipoles (ℓ) near a dielectric interface with complex coefficients a_ℓ. In our calculations we use the angular spectrum representation based on vector spherical harmonics, as formulated by Inoue and Hori [77]. Both propagating and evanescent fields are refracted and reflected using the Fresnel coefficients of the air-glass interface. We add, again, two equal and incoherent in-plane dipoles with emission constant in the azimuth angle to account for the emission of uncoupled QDs and autoluminescence of the antenna.

The expansion coefficients (a_ℓ) for the first two resonant modes confirm our previous assignments of their prominently dipolar and quadrupolar characters. They also confirm an efficient coupling to both antennas, with the majority of the photons emitted through the corresponding antenna multipole channels. Although it is tempting to assign one multipole order to each resonant mode, for instance ℓ=3 multipole to j=3 mode, this is generally not the case beyond the two lowest

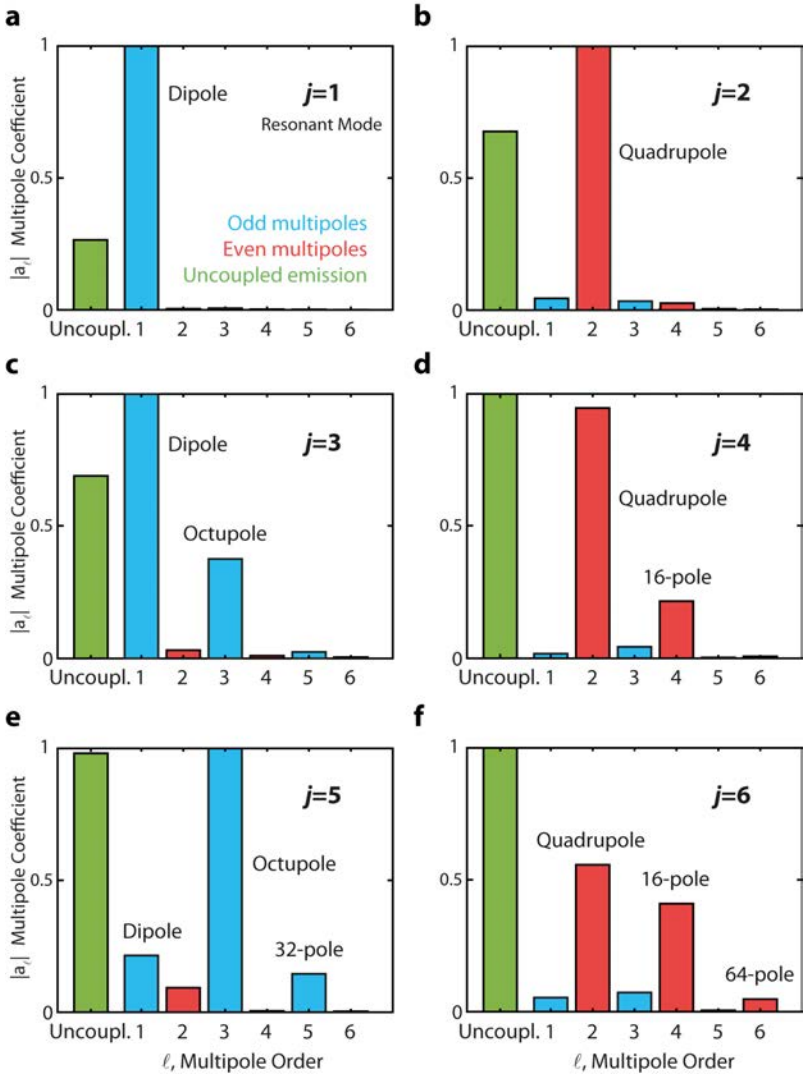

Figure 3.5 **The multipolar nature of the emission is described by a multipolar expansion of the angular radiation patterns. a-f,** The experimental radiation patterns of the individual resonant antennas of Figures 3.4c-h were fit to a superposition of even (red) and odd (blue) multipoles oriented along the antenna plus an incoherent rotationally symmetric background consisting of two in-plane dipoles (uncoupled emission, green). Superpositions of even and odd multipoles dominate the even (right) and odd (left) modes, respectively. The complex multipole coefficients $|a_\ell|$ are normalized to the amplitude of the maximum coefficient. Note that for equal coefficient amplitudes $|a_\ell|$, each isolated term in the expansion radiates the same power in free space but not on a substrate.

modes. For higher order resonances, even modes are composed of a coherent superposition of predominantly even multipoles; complementarily, odd modes are dominated by odd multipoles. This expansion also demonstrates that the background contribution (green bars in Figure 3.5) increases and starts dominating for higher order modes as expected for a decreasing coupling efficiency.

3.4. Other signatures of antenna resonances

The antennas control the emission of the QD not only in polarization and angular patterns but also in other properties. For completeness, we explore next the modifications of the emission spectrum and the lifetime that result from resonant coupling.

Modification of the emission spectrum

Due to the coupling of two oscillators (QD and antenna), a spectral shift or modification is expected in the emission of our hybrid systems [13, 14]. These spectral changes are a possible method to monitor antenna resonances. When the broad spectrum of the quantum dot and the resonance of the antenna overlap exactly, this effect is barely visible when the coupling occurs in the weak coupling regime, as in our case. The shifts are, however, most evident when the antenna is slightly detuned with respect to the natural QD wavelength.

We argue that a small detuning between antenna and QD spectral maxima is convenient to discern the antenna mode of interest from uncoupled emitters, because the antenna acts as a spectral filter enhancing only coupled QDs. As a result, we find that in the identification of antenna resonances in polarization and angular measurements, the resonant antennas are slightly red-shifted with respect to the QD.

We show two such modified emission spectra of QDs coupled to antennas of first and second resonant modes detuned to the red of the QD emission (Figures 3.6b and c). They are compared to the average spectrum of QDs on a nonresonant metal structure of 60 nm (shaded black line), which is basically identical to the spectrum of an isolated QD. From the observed spectral shifts in emission, a spectral enhancement can be calculated (in green, defined as the antenna divided by the reference). Comparing both resonances, a weaker modulation of emission spectrum is observed for the second order mode, corresponding to a lower coupling efficiency. Dark-field scattering spectra acquired under far-field unpolarized illumination are shown for comparison in Figure 3.6c.

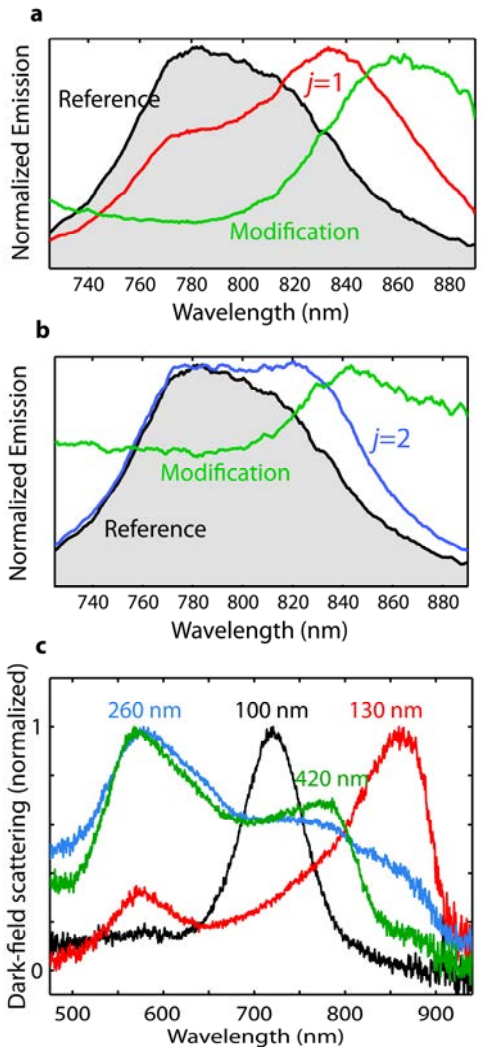

Figure 3.6 **Modification of the quantum-dot emission spectrum by antenna resonances. a-b,** Spectra of QDs coupled to antennas at the first (red) and second (blue) resonant modes. The average spectrum of such quantum dots on a non-resonant metal structure of 60 nm (black line) is very similar to an isolated QD. A spectral modification is calculated (green) defined as the antenna signal divided by the reference, revealing the modulation of the spectrum of emission by the antenna. **c,** Dark-field scattering spectra of antennas of different lengths. Under this configuration, excitation from the far field does not allow access to the quadrupolar mode for L=260 nm and no peak is observed around λ=800 nm.

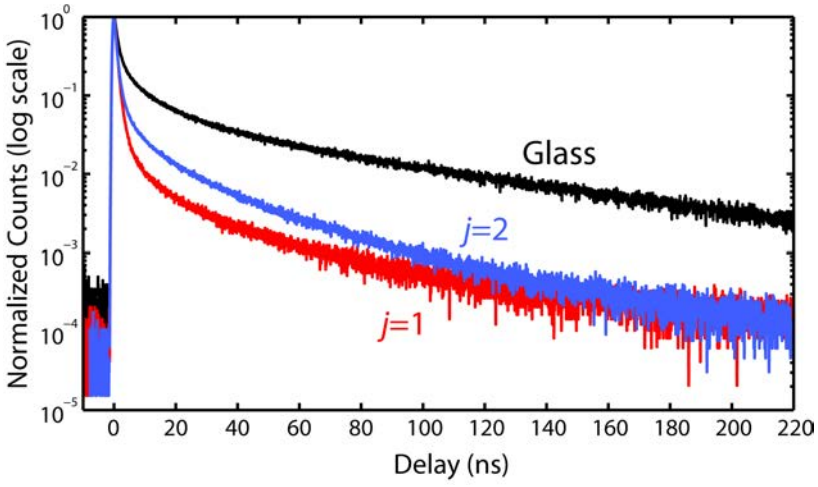

Figure 3.7 **The emission lifetime is shortened by coupling to resonant antennas.** Lifetime of the emission for the first and second resonant modes and for quantum dots directly on the glass substrate without antennas. Measurements were performed under ps-pulsed excitation with a 640 nm diode laser. The decay is bi-exponential in all three situations.

Modification of the emission lifetime

The enhancement of decay rates was one of the first applications of optical antennas [6-8]. To achieve this goal, specific designs like the gap antenna were investigated for emission [8, 9, 78, 79] and excitation [80, 81]. Although the increase of transition rates is not the primary goal of a nanowire antenna, it is interesting to observe the effect of a resonant antenna on the lifetime of a QD.

To this end, we measure the emission lifetime of emitter-antenna systems under pulsed excitation, with a pulse length of several ps, and compare it to QDs on the same glass substrate (Figure 3.7). The decay is bi-exponential; we can identify two components in the lifetime with different time scales of a few ns and more than 100 ns, respectively. Comparatively, the lifetime is reduced more by coupling to the dipolar mode than to the quadrupolar mode.

A quantitative study of this effect requires the disentanglement of excitation, emission and non-radiative rates. Such a separation of transition rate contributions would be possible with QDs thanks to the photophysics of bi-excitons (two excitons that coexist in the QD and decay faster than a single exciton). The generation rate of bi-excitons is excitation power dependent [80], resulting in a faster decay rate for higher laser powers because of an increased probability of creating two excitons. Since nanowire antennas are not an optimal

design for lifetime modification, we do not pursue this methodology in this Chapter, and conclude that coupling to a resonant antenna has a clear effect on the transition rates as well.

3.5. Discussion and conclusions

In a broader context of plasmonic modes, angular measurements are a powerful tool for understanding how the unit cells of metamaterials interact with light [74, 82, 83]. Additionally, multipoles provide a natural basis to study both metamaterials and multi-antenna devices because semi-analytical methods can be employed to describe the collective response if the multipolar expansion of the unit cell is known [84-86].

In metamaterials, the near-field coupling between elements supporting different modes, *e.g.*, dipole-quadrupole, leads to interesting polarization [87] and spectral effects such as electromagnetically induced transparency [88, 89], a situation that resembles the coupling of dipolar QDs to quadrupolar antennas. Similar spectral effects could be explored in our hybrid systems, formed by the combination of quantum-mechanical transitions and other plasmon modes.

On the other hand, the multipolar character of an emitter is intimately related to the angular momentum of light [90-93]. In addition to the angular intensity distributions, the antenna also controls the underlying phase of each lobe. Hence, the ideas presented here can be extended to design systems that could serve as nanoscale integrated sources and detectors of optical orbital angular momentum [94, 95]. Furthermore, a multipole moment is mostly sensitive to certain components of the electromagnetic field. With a QD coupled to the quadrupolar mode, for example, a nanoscale probe that is sensitive to the electric field gradient can be envisioned.

In conclusion, we presented a systematic study of nanowire modes and their interaction with quantum emitters. The use of optical antennas allowed us to convert the radiation of electric dipole transitions efficiently into novel multipolar photon sources. These results provide a wealth of new opportunities for the nanoscale control and engineering of the usually inefficient interaction of single quantum emitters with well-defined modes of the light field.

4.

Nanoslot Antennas at Magnetic Resonance

In this Chapter, we address the emission of light through a nanoaperture in a metal film as an antenna problem. We demonstrate, explicitly, that resonant nanoslots display a predominantly magnetic dipole response. We observe clear differences in the angular radiation patterns of resonant and non-resonant antennas, and compare our results to calculations with magnetic and electric dipole sources, respectively. At resonance, angular radiation patterns evidence the dominant magnetic dipole character, accompanied by a more efficient launching of surface plasmons. Off resonance, angular patterns are divergent beams, as for electric dipoles. The resonant magnetic mode is preserved even when plasmons are suppressed by a chromium layer. Through simulations, we draw a parallel with an electric dipole nanowire antenna, in agreement with Babinet's principle. Our results highlight the potential of resonant nanoslot antennas as interfaces between photons, emitters, and propagating surface plasmons.

4.1. From nanowire to nanoslot antennas

The control of nanoscale magnetic fields at optical frequencies provides new opportunities for enhancing the interaction of light with matter. While the optical response is usually determined by electric dipole moments, certain nanostructures do also possess a magnetic dipole moment, most notably split-ring resonators [96] and dielectric resonators (wires and spheres) [97-99]. At longer wavelengths, Bethe and Bouwkamp showed that an aperture in a perfectly conducting screen behaves as a superposition of electric and magnetic dipoles [100, 101]. From their models, it was expected that nanoapertures in real metals would exhibit magnetism at optical frequencies, a relevant fact to explain light transmission through nanohole arrays [102], to understand near-field microscopy aperture probes or to excite surface plasmon polaritons (SPPs) [43].

To understand the interaction of a sub-wavelength hole with light, both the responses to electric and magnetic fields need to be considered [103-107]. Recent detailed studies have focused on non-resonant circular apertures [105, 108, 109]. For non-circular apertures, both the shape of the hole and the polarization of the incident light influence transmission [110-112]. Such nanoapertures can be exploited to develop optical antennas for various applications [18, 113-115] and, more fundamentally, to selectively image, focus, and interact with optical magnetic fields [109, 116-121]. Recently, rectangular apertures have been investigated with an electron beam as local source [122-124]. As these studies only mapped the normal component of the electric field, they could not expose the magnetic dipole character of the fundamental resonance.

In this Chapter, we address the emission of light through a nanoaperture as an antenna problem to demonstrate experimentally that resonant nanoslots emit predominantly as magnetic dipoles.

Babinet's principle for complementary antennas

To gain intuition, we start by invoking Babinet's principle for complementary structures as used in antenna engineering to obtain magnetic antennas [90, 125, 126]. Rigorously valid for perfectly conducting, infinitely thin plane screens, it relates the $\boldsymbol{E}$ and $\boldsymbol{B}$ fields radiated by wire and slot antennas through the interchanges $\boldsymbol{E}_{\text{slot}}=c\boldsymbol{B}_{\text{wire}}$ and $\boldsymbol{B}_{\text{slot}}=-\boldsymbol{E}_{\text{wire}}/c$ [90], as illustrated in Fig. 4.1a. This extension by Booker of Babinet's principle accounts for polarization, unlike the original principle based on the diffraction of scalar fields. The principle still holds qualitatively true for real metals at optical frequencies [127-129]. In this respect, nanoslot antennas are spatially extended implementations of a point (Fitzgerald) magnetic dipole, just as nanowires are of a point (Hertz) electric dipole.

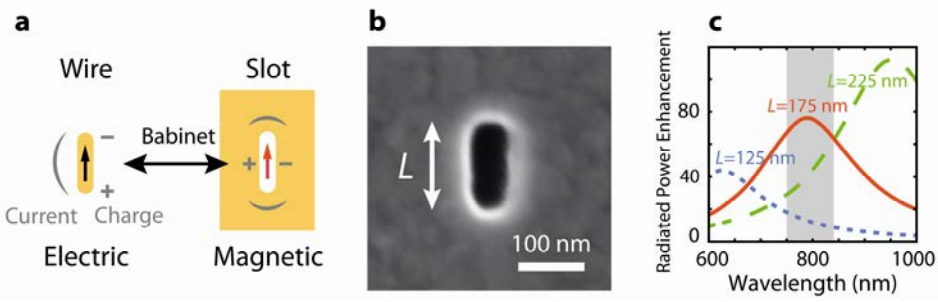

Figure 4.1 **Nanoslot antennas as resonant magnetic dipole antennas. (a)** Schematic of Babinet's principle for complementary wire and slot antennas, dual antennas for electric and magnetic fields, respectively. Electric current magnitude and charge signs are sketched in gray. **(b)** Scanning electron microscopy image of a single nanoslot antenna in a gold film. **(c)** Resonant matching through numerical simulations of the slot length to the emission spectrum of our quantum dots. The shadowed area indicates the full-width at half-maximum of the luminescence spectrum.

4.2. Probing nanoslot modes

In our experiments, we probe the emission of a nanoaperture antenna in the far field by feeding it with electric dipoles from its near field, similarly to the generator in a conventional slot antenna (Fig. 4.1a). Arrays of antennas were fabricated by focused ion beam milling into a thermally-evaporated, 60-nm-thick gold film on a glass substrate. The width of the slots is 60 nm and their length varies from 100 to 250 nm in steps of 25 nm, encompassing the first resonant length of 175 nm (Fig. 4.1c). The separation between neighboring slots was kept to distances larger than 8 μm to avoid mutual interference.

The nanoslots are excited by the photoluminescence of quantum dots (QDs) with emission wavelengths around 800 nm. A colloidal QD solution (Invitrogen, Qdot ITK 800 Organic) was dissolved with volume ratio [1:4.5] in a PMMA:Trichlorobenzene solution [1:2] and spin-cast at 8000 r.p.m. to form a thin film covering the nanostructured metal film. Photoluminescence of the QDs was excited with a circularly-polarized, continuous-wave laser at 633 nm. The excitation and emission wavelengths were separated using a dichroic mirror and a long-pass filter. Although the QDs are deposited all over the sample, they are preferentially excited and detected inside the nanoslots because the metal film is otherwise opaque, as observed in confocal microscopy images (Fig. 4.2a).

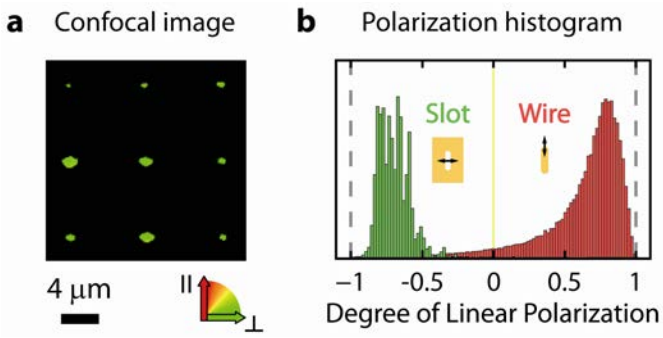

Figure 4.2 **Imaging and polarization of resonant nanoslots. (a)** Confocal photoluminescence microscopy image of an array of resonant nanoslots covered with quantum dots. The red-yellow-green color scale represents degrees of linear polarization of the electric field. **(b)** Histograms of the degree of linear polarization (weighted with counts per pixel) of the emission of arrays of resonant nanoslots (green) and nanowire (red) antennas.

To distinguish between electric and magnetic dipole emission, we analyze angular radiation patterns of individual slots. Electric and magnetic dipoles emit electromagnetic fields with interchanged symmetries and polarizations [90]. Thus both types of emitters can be identified by using a metal film acting as a mirror, thanks to an angle-dependent self-interference of direct and reflected waves. A related technique has been used in the past to determine the magnetic dipole nature of rare-earth ion luminescence [130, 131]. We record angular radiation patterns by imaging the back focal plane of a microscope objective. The use of a high numerical aperture objective (NA=1.46) allows us to collect emission into the glass substrate, including SPP leakage radiation at 42°.

Resonant and non-resonant nanoslots

We investigate slots of different lengths around L=175 nm, where we expect overlap between the quantum dot emission spectrum and the antenna resonance. Off resonance, we find that angular radiation patterns are divergent beams with a maximum value at an angle normal to the metal film. The trend is similar for both blue- and red-detuned slots of lengths L=125 and L=225 nm, respectively (Figures 4.3a and c). Surface plasmons are inefficiently launched and are hardly observable. When a linear polarizer is used to analyze an angular pattern, we observe that the beam is slightly elongated along the polarization direction. A comparison with the radiation patterns of in-plane electric dipoles in the vicinity of a metal film [45, 132] leads us to attribute these patterns to inefficient off-resonance coupling of the QDs to the antenna mode, emitting almost as if the

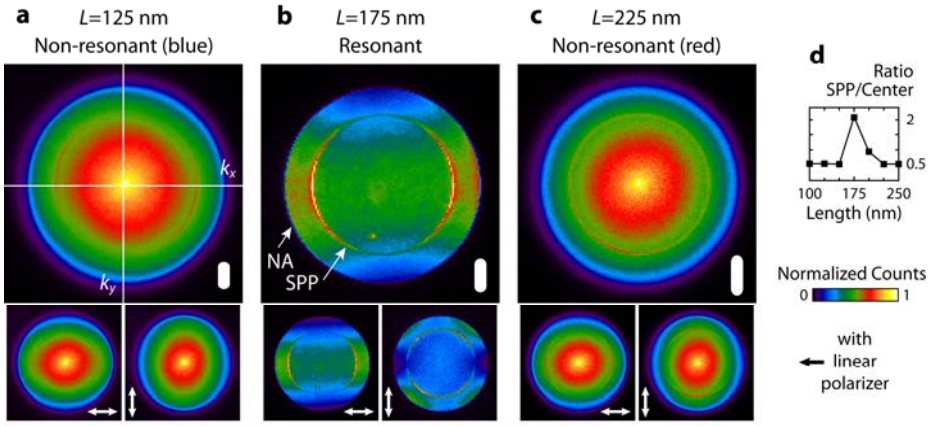

Figure 4.3 **Experimental angular radiation patterns of individual slot nanoantennas show clear differences on and off resonance.** The images, recorded in the back focal plane of the microscope objective, contain the Fourier-space photoluminescence emission into the glass substrate of quantum dots coupled to antennas. **(a, c)** Off-resonant antennas of lengths L=125 and L=225 nm, respectively, possess diverging angular radiation patterns. **(b)** Resonant antennas with L=175 nm emit both into free space and into surface plasmons. The nanoslots are oriented vertically along the y-direction. The images in the bottom row decompose the radiation pattern in two polarization components, parallel and perpendicular to the antenna, by means of a linear polarizer. **(d)** Length dependence of the ratio SPP/center of intensities at the SPP angle in the x-direction and at the center of the back focal plane. At resonance, the emission into high angles is higher than off resonance. Statistics were taken over several antennas of the same length. Standard deviations are smaller than the points (average).

antenna were not present. The situation is thus similar to the inefficient coupling to non-resonant nanowires seen in the previous Chapter. The results are therefore consistent with two perpendicular electric dipoles of QDs close to a mirror (Fig. 4.4c), not coupled to any antenna mode. The angular patterns are in agreement with recent results on non-resonant apertures as the basis of more complex antenna designs [18, 113], and are qualitatively similar to diffraction through near-field aperture probes [133, 134].

At resonance, the angular pattern is strikingly different due to efficient coupling of the emitters to the antenna mode, now dominating in Fig. 4.3b. The emission is linearly polarized across the slot, with a 7:1 intensity ratio between perpendicular polarizations (Fig. 4.2b). With the two lobes characteristic of

dipolar emission and transverse-magnetic polarization, in free space it would constitute an unequivocal signature of a magnetic dipole oriented along the slot. The situation is, however, more complicated because of the presence of a metal film that supports SPPs. Indeed, the most prominent feature in Fig. 4.3b is the emission of SPPs in a narrow angular range [43].

The role of surface plasmons

Because of boundary conditions at the interface between a metal and a dielectric, an in-plane magnetic dipole excites SPPs more efficiently than an in-plane electric dipole. The ratio of SPP intensity emitted at a given angle by a magnetic dipole and an electric dipole can be estimated by the relation $|\boldsymbol{E}_{\mathrm{MD\ y}}|^2/|\boldsymbol{E}_{\mathrm{ED\ x}}|^2 \propto |1+\varepsilon|$ [105]. For an Au film and a wavelength of 800 nm, a magnetic dipole excites approximately 25 times more SPPs. This significant difference in excitation efficiency, observed in our measurements by comparing the visibility of SPPs on and off resonance (Fig. 4.3d), is an indirect proof of the dominance of a magnetic dipole at the antenna resonance. Nanoslot antennas at magnetic resonance are thus a more efficient interface between free-space photons, emitters, and propagating surface plasmons.

To assess the role of SPPs in sustaining the magnetic mode, we deposit a 10-nm Cr layer in order to suppress the propagation of SPPs on the air-metal interface. Off resonance, the angular pattern in Fig. 4.4a remains the same. At resonance, the magnetic mode is preserved as well in the absence of surface plasmons, which are now damped out in the Cr film resulting in a small dip at the SPP angle (Fig. 4.4b).

The suppression of SPPs allows us also to disentangle them from free-space radiation of the slot, making it possible to compare with a simple model based on point dipoles. For simulations, we use the Finite-Difference Time-Domain method (FDTD Solutions, Lumerical). We calculate the emission patterns of electric and magnetic dipoles close to a perfect electric conductor mirror, which retain the characteristics of the measured angular patterns on and off resonance, respectively (Figures 4.4c and d). We conclude that the emission of nanoslots at high angles is due to magnetic dipole radiation, whereas the convex curvature of the radiation pattern at low angles indicates the residual contribution of electric dipoles.

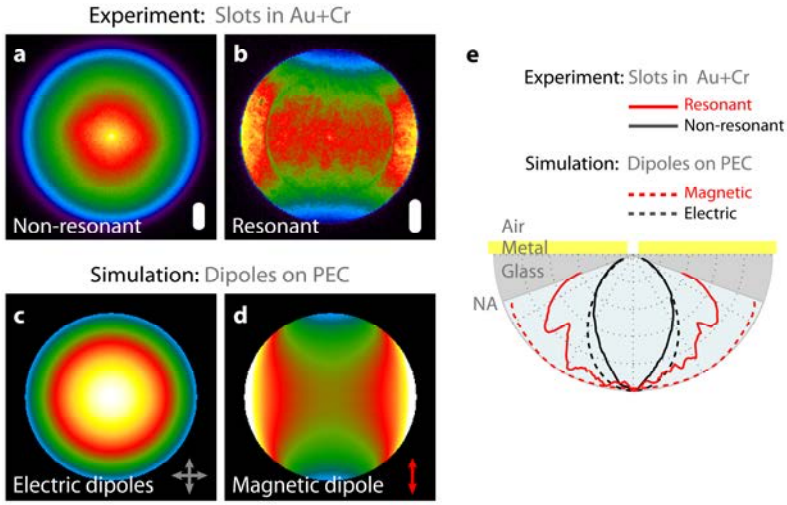

Figure 4.4 **The suppresion of surface plasmons allows a direct comparison to a point-dipole model. (a, b)** Angular radiation patterns on and off resonance of nanoslot antennas covered with a 10-nm Cr film, as obtained in the back focal plane of a collection objective. By suppressing SPP contributions to the emission, the magnetic mode is still preserved and a two-lobe pattern is more clearly observed. **(c, d)** FDTD calculations of the angular emission of point electric and magnetic dipoles, respectively, in front of a perfect electric conductor (PEC) mirror, as it would be recorded in the back focal plane. The electric dipoles are oriented randomly on the plane whereas the magnetic dipole is oriented along the slot long axis. Both are placed at a distance to the metal of 1 nm, much smaller than the wavelength. **(e)** Comparison of angular patterns for experimental slot antennas (solid lines) and simulated point dipoles on PEC (dashed), converted to angular space with the apodization factor $1/\cos\theta$, where θ is the inclination angle. A linear polarizer across the slot was used to increase the contrast of angular features.

4.3. Characteristics of resonant nanoslot modes

The perimeter of the slot is the key geometrical parameter controlling the antenna resonance by establishing standing-wave currents [135, 136]. Previous studies have shown that the resonance of an aperture could potentially stem from other sources, namely, waveguide modes resonantly excited at cut-off [137-140] or vertical cavity resonances [135, 140].

We performed additional simulations with a mode solver, integrated in Lumerical FDTD Solutions, that showed that the fundamental TE_{10} waveguide

mode is clearly beyond cut-off, with a small effective refractive index of 0.02 and high losses on the order of 100 dB/μm. No sharp variations of waveguide propagation constants were observed around the resonance and, hence, we discard the waveguide resonance found for larger apertures at the lowest order mode cut-off [137, 140].

On the other hand, vertical Fabry-Pérot cavity resonances require thicker metal films [135] and they are roughly independent of the perimeter. They can thus be disregarded as the origin of our resonances. Note that, for thicker films, Babinet's principle will eventually break down even qualitatively due to the appearance of vertical modes.

Duality between nanoslots and nanowires

Simulations of energy densities and currents establish a duality between a resonant nanoslot and a nanowire antenna (half-wave electric dipole, j=1 mode in Chapter 3, also introduced in Section 1.3). For numerical simulations, we take the optimal situation of an electric dipole source at the slot center and oriented across its short gap. The magnetic energy density U_B accumulates at the ends of the nanoslot (Fig. 4.5a), just as the electric energy density would concentrate at the ends of a nanowire (Fig. 1.3e). Equally, the maximum of electric energy density U_E at the center of the nanoslot (Fig. 4.5b) follows the distribution of the magnetic field in nanowires. The magnetic field of a slot enters at one end of the antenna and exits at the other, with a substantial magnetic field perpendicular to the slot, just as perpendicular electric fields dominate the near field of an electric dipole antenna at a close distance. $\boldsymbol{B}$ and $\boldsymbol{E}$ are essentially exchanged.

The origin of this optical magnetism can be understood in terms of a magnetic current inside the slot. The equivalence principle allows the substitution of an aperture by its equivalent electric and magnetic surface currents. They are defined as $\boldsymbol{J}_E=\boldsymbol{n}\times\boldsymbol{H}$ and $\boldsymbol{J}_M=-\boldsymbol{n}\times\boldsymbol{E}$, where $\boldsymbol{n}$ is the unit vector normal to the metal film [141]. Following Babinet's principle, the electric current in a nanowire becomes a magnetic current in a nanoslot; a sinusoidal, standing-wave magnetic current inside the aperture (Fig. 4.5c) acts as a source of magnetic dipole moment along the slot [100, 101, 142, 143]. The magnetic current mimics the electric current of a half-wave electric dipole antenna (Figures 1.3d and 4.1a).

Although it is possible to determine the radiated fields of a slot entirely in terms of electric currents, the use of fictitious magnetic currents is advantageous because of simplicity. The electric surface currents curving around a nanoslot point both in the same direction (Fig. 4.5d) inducing magnetic dipoles perpendicular to the film that cancel each other out; to obtain a magnetic moment from the electric currents alone (without the use of the equivalence

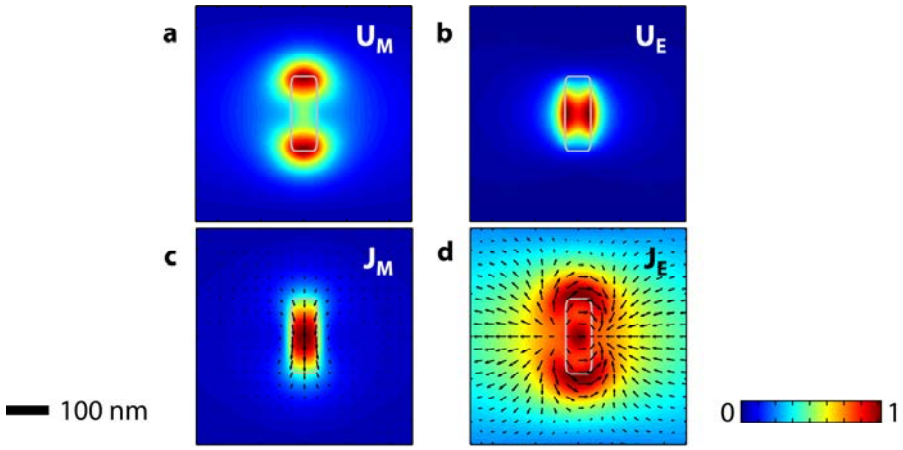

Figure 4.5 **Nanoslot and nanowire antennas as dual antennas.** Energy densities (U) and surface currents (J) in a nanoslot show the complementarity to an electric dipole nanowire antenna. FDTD simulations of magnetic energy density **(a)**, electric energy density **(b)**, magnetic surface current **(c)**, and electric surface current **(d)** of a resonant nanoslot antenna on a gold film. The quantities are evaluated on a plane monitor 20 nm below the metal film (substrate side) at a wavelength of 800 nm. The nanoslot is dual to a nanowire antenna when magnetic and electric quantities are exchanged. The absolute value of both currents is represented in color, while arrows indicate the imaginary part of the magnetic current and the real part of the electric current, respectively.

principle), a three-dimensional integration would be necessary to include currents on the inner walls of the slots [144].

4.4. Discussion and conclusions

Comparing our results to previous experiments on light transmission through non-resonant circular apertures [108, 109, 133, 134], two main differences arise. First, both for apertures at the end of a tip illuminated through a tapered probe [134] and for apertures on a metal film illuminated by a plane wave [108], a higher divergence in the diffraction patterns was observed for smaller holes. This trend is not present in our observations due to the resonant and non-resonant character of the excitation mechanism with local electric dipoles. Second, for transmission through aperture probes, a simple model of dipoles in free space was able to describe the experiments [134]. In our case, the presence of an extended metal film must be taken into account to explain the angular patterns.

Furthermore, according to conventional antenna theory [126], the size of the ground plane is expected to affect both the radiation pattern and the efficiency of a slot antenna, and at least one wavelength of surrounding metal is necessary not to alter its response (compare, for example, apertures at the end of sub-wavelength probes [116] and apertures on extended films [109]). Although the size of the surrounding metal film controls in part the radiation characteristics, the magnetic resonance is still governed by the perimeter, with only the metal closest to the aperture contributing to its dispersion.

The basic features of the angular emission of our nanoslots were reproduced with a model consisting of point dipoles in front of a mirror. This configuration, however, poses a limit for further quantification of the weight of electric and magnetic dipole contributions to the emission, because of the necessity to choose a distance of the equivalent dipolar sources to the metal film and of the effective medium seen by the emitters inside the slots. Finally, we remark that plane wave excitation of a hole under oblique incidence has been recently exploited as a magnetic field polarization analyzer [109], in clear reciprocity to our observation of higher radiation at high angles of a magnetic dipole near a ground plane.

In summary, we have explicitly demonstrated that resonant nanoslot apertures radiate as magnetic dipole antennas. Our results provide a new entry on the classical topic of how light interacts with nanoapertures in metal films, in particular for resonant apertures. The demonstrated role of the antenna resonance will be of direct use to control and enhance light emission, to increase the efficiency of interfaces between plasmons and free-space radiation, and as the basis of more complex antenna designs. We have also shown that Babinet's principle is valid to a certain extent for real metals. Theoretical efforts to quantify its validity for optics will result in simpler design rules for nanoaperture-based antennas, adding a full complementary set of building blocks for nanophotonic devices and materials.

5.

Directional Nanoantennas

Nanoscale quantum emitters are key elements in quantum optics and constitute the ultimate limit in sensing. However, efficient optical excitation and detection of such emitters involves large solid angles because their interaction with freely-propagating light is omnidirectional. In this Chapter, we present unidirectional antennas for controlling the emission of single quantum emitters. By coupling quantum dots to the near field of an antenna, the emission is determined by the antenna mode in polarization and radiation pattern. We demonstrate experimentally the operation of a Yagi-Uda antenna driven by a single emitter. Next, we explore through simulations the optimization of such multi-element antennas with a log-periodic design. Finally, we show both with experiments and theory that a single split-ring resonator is a particularly suitable directional design that harnesses the interference of magnetic and electric components. These results open new possibilities for effective communication of light to, from and between nano-emitters.

5.1. Directing light on the nanoscale

One of the most recognizable characteristics of antennas is their directed emission and reception. At optical frequencies, the control of directionality with micrometric devices has mainly been pursued in the past by means of photonic crystal structures [145] and surface-plasmon-based devices [146-149]. For structures approaching the nanometer scale, diffraction poses a limit to the collimated beaming of light.

On the other hand, the interaction of quantum emitters with light can be enhanced with microcavities [150, 151]. Photon extraction and the control of angular patterns are then an issue. Tapered semiconductor nanowires have also been engineered to improve the extraction efficiency of enclosed emitters [152]. Compared to these approaches, plasmonic nanoantennas offer a much smaller footprint in an open and accessible geometry, combining strong sub-wavelength fields and increased transition rates together with directionality. Earlier, variations in the angular emission of molecules by the presence of metallic objects in their near field were observed [11, 153, 154].

From electric dipoles to plane waves

Single quantum emitters such as molecules, ions or quantum dots usually interact with light as electric dipoles. The excitation and emission patterns are thus dipolar, with isotropic emission in free space in the plane perpendicular to the dipole moment axis. Because of the wide range of angles involved, it is difficult to interact with a single emitter efficiently from the far field. At macroscopic scales, light is preferably manipulated on the basis of plane waves, be it experimentally with beams of low divergence or theoretically with plane-wave expansions. In the near field, however, dipoles are dominant and provide a simple description of the emission, absorption and scattering of light by nanoscale objects.

Given the mismatch between far-field and near-field optics, obtaining a directional antenna to convert efficiently between localized fields (or excitons) and collimated propating light is a canonical problem in nano-optics. In this Chapter, we demonstrate that unidirectional nanoantennas can determine the electromagnetic mode of light emission, greatly reducing the solid angle necessary to interact with quantum emitters.

Unidirectional optical antennas thus provide an effective interface to address nano-emitters from the far field, for use in directed, bright single-photon sources for quantum optical technologies, in planar biochemical sensors, or in light-harvesting and emission devices.

Types of directional antennas

First, we briefly evaluate design strategies of conventional directional antennas [3, 155] and analyze their feasibility at optical frequencies. The principles of operation can be identified as follows, with possible overlap between categories:

Antenna arrays: directionality is obtained by interference of the scattering of multiple elements. The phase and separation between elements are chosen to create a directed wave and suppress radiation in the opposite direction. Yagi-Uda antennas (with as few as two elements [156, 157]), log-periodic antennas, and phased array antennas fall under this category. Micrometric antenna concepts based on diffraction gratings are close to this principle [158], including bull's eye apertures [18] and slit-based antennas [113].

Traveling-wave or leaky-wave antennas: their operation is based on the propagation of a bound wave leaking to radiation along its length. Examples include long wires [159] and slot waveguides [160] fed locally at one end. Directionality can also be achieved by removing reflection of the wave at the distal end of a long antenna (or waveguide) either by means of a load (Beverage antenna) or by tapering/flaring the antenna end. At optical frequencies, they are inherently broadband but lossy and large.

Patch or microstrip antennas: a resonant metallic patch is backed by a reflecting ground plane, separated by a thin dielectric film [161-163]. For small patches the emission lobe may be broad, while for larger patches the radiation efficiency may decrease.

Aperture antennas: directional radiation may occur at the end of an open-ended waveguide. Examples include horn antennas and cavity-backed slot antennas.

Reflector antennas: they act as small mirrors. An example is the parabolic antenna [164]. Radiation patterns are inherently sensitive to the position of the sources and losses as surface plasmons may not be negligible. A corner reflector is also commonly used for enhancing the performance of Yagi-Uda antennas for TV reception.

Multipolar interference antennas: they exploit the different symmetries of the electromagnetic fields radiated by electric dipoles, magnetic dipoles, and electric quadrupoles. Their interference can produce directivity from a single, compact element [165, 166].

In all cases, directionality is ultimately limited by diffraction, and larger structures display higher directivities. The smallest nanoantennas provide thus asymmetric dipolar patterns, with minimal reduction of beam width of the main lobe. In this Chapter, we will study directional optical antennas of the *Antenna*

Array (Yagi-Uda and log-periodic antennas) and *Multipolar Interference* (split-ring resonator) types.

5.2. Yagi-Uda nanoantennas

At radio and microwave frequencies, highly directed beams are commonly obtained with Yagi-Uda antennas [167]. A Yagi-Uda antenna consists of an array of mutually detuned dipoles; an actively driven feed element is surrounded by a set of parasitic elements, acting as reflectors and directors (Fig. 5.1a). The reflectors and directors are detuned in length with respect to the dipolar resonance of the feed, and the spacing between elements is chosen such that a travelling wave pointing towards the directors is created.

In the optical regime, directional far-field scattering of a polarized laser beam from arrays of Yagi-Uda antennas was demonstrated [168, 169]. A Yagi-Uda antenna operating in reception mode has been also demonstrated by mapping its near-field for opposite incident directions [170]. A nanoparticle array consisting of identical elements, akin to a Yagi-Uda antenna, was also shown to concentrate light at different positions along the chain for different wavelengths [171]. Complete control of the direction of light emission from a single dipolar emitter using an optical Yagi-Uda antenna was theoretically proposed by several authors [172-174].

In this Section, we realize unidirectional nanoscale photon sources by coupling single quantum systems to a Yagi-Uda design. The realization of such a source requires the precise near-field coupling of an emitter to a nanoscale antenna that is tuned to the emission spectrum. We place a quantum dot (QD) at the resonant feed element of a nanofabricated Yagi-Uda antenna. Next we confirm the coupling by characterizing the modification of the emission polarization. Finally, we demonstrate that the QD emission is indeed highly directed, and that the directionality can be tuned by varying the antenna dimensions.

Driving a Yagi-Uda antenna only through its feed element

To obtain a strong near-field coupling of a quantum dot to the antenna mode, it is critical to place the emitter at a position of high electric mode density, i.e. at one of the ends of the feed element. Optimal performance will be obtained when only the feed element is driven, similarly to the presence of a single source wire in conventional Yagi-Uda antennas. To achieve this, we use again a two-step electron beam lithography process combined with chemical functionalization. The first lithography step defines the antenna structures on a glass substrate, followed by thermal evaporation of a 30 nm layer of gold. The second lithography step sets the boundaries for the formation of a self-assembled monolayer of

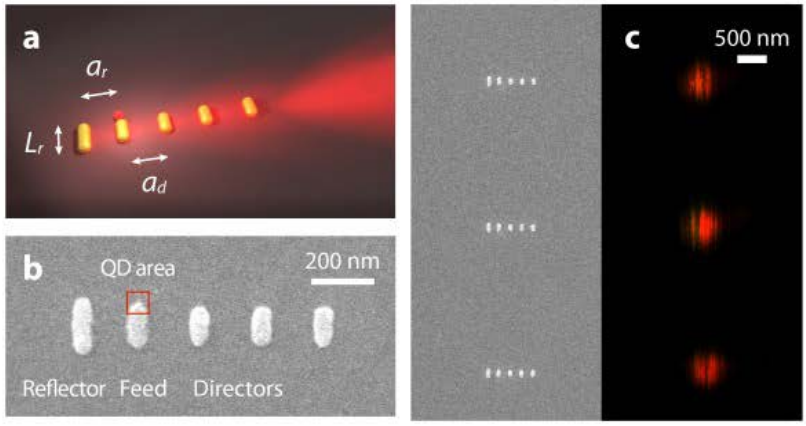

Figure 5.1 **Optical Yagi-Uda antennas driven by quantum dots. (a)** Schematic of a Yagi-Uda antenna consisting of a feed element, one reflector and three directors, with different distances between reflector and feeed, and between feed and director. **(b)** Scanning electron microscopy (SEM) image of fabricated 5-element Yagi-Uda antenna. A quantum dot (QD) is attached to one end of the feed element inside the marked area. **(c)** Comparison of SEM and scanning confocal luminescence microscopy images of three antennas driven by QDs. The image is color-coded for degree of linear polarization (see inset).

mercaptoundecanoic acid exclusively on the predefined exposed areas. Core-shell QDs (Invitrogen, Qdot 800 ITK Amino) are immobilized on the functionalized areas (70 nm squares) and the remaining resist is removed.

We used numerical simulations (CST, Microwave Studio, transient solver) to design 5-element gold Yagi-Uda antennas for operation wavelengths around 800 nm [175]. A typical fabricated antenna is shown in Fig. 5.1b, with feed length L_f =145 nm, spacing a_r=175 nm between reflector and feed, and a_d=200 nm between directors. The total length is 830 nm, approximately one emission wavelength.

Emission polarization by coupling to the antenna

We characterize the emission of QDs on antennas with a confocal microscope with three dedicated detection branches; for luminescence imaging, angular detection, and spectroscopy, respectively. The use of a high-numerical-aperture objective (1.46 NA) is essential for the angular detection. The sample is excited by a circularly polarized He-Ne laser beam (λ=633 nm), which is focused to address a single antenna at a time. The resulting luminescence is separated from the excitation wavelength with a dichroic mirror and a long-pass filter. For confocal detection, the use of a polarizing beam-splitter and two detection channels ($I_\parallel$ and

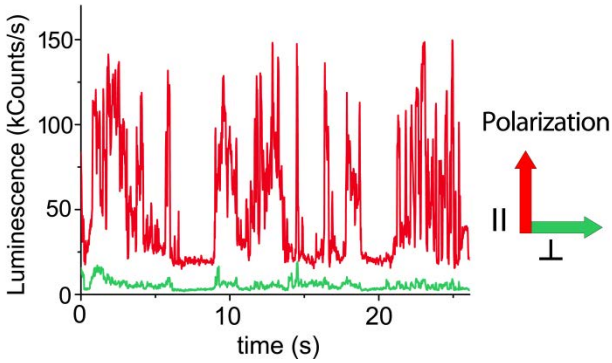

Figure 5.2 **Blinking of the emission evidences the presence of single quantum dots.** Intensity time-trace of luminescence in both polarization channels for one of the antennas in Fig. 5.2c, where blinking has a visible effect in the scanning luminescence images as vertical stripes. The signal is telegraphic, with on and off periods.

$I_\perp$) with avalanche photodiodes allows us to determine polarization anisotropies. For detection of the angular emission, we record images of the intensity distribution on the back focal plane of the high-NA objective (conoscopy) [42] on an EMCCD camera. These Fourier-plane images (momentum space) contain the directions of emission towards the substrate.

All presented confocal luminescence images are color-coded (red-yellow-green) for the degree of linear polarization, $DOLP = (I_\parallel\text{-}I_\perp)/(I_\parallel+I_\perp)$, with red being linear polarization parallel to the feed longitudinal axis. All antenna-QD systems in Fig. 5.1c show red, *i.e.* linearly polarized, confirming that the QD drives the linear dipole of the feed element [11, 176]. The QDs are cleanly positioned on the antennas and the emission arises from quantum emitters, since discrete blinking events interrupt the signal as the sample is raster-scanned. This blinking is better seen in the luminescence time-trace displayed in Fig. 5.2, where clear on and off states can be identified, characteristic of a single emitter. From many such time-traces, we conclude that single QDs occur frequently, while the typical number is 1, 2 or 3; a number that can be controlled by both the size of the functionalized area and the concentration of the deposited QD solution.

To gain direct insight into the changes in the QD emission upon coupling to the antenna, we compare three types of nanostructures (Fig. 5.3): small 60-nm gold squares, $\lambda/2$ dipole antennas, and the Yagi-Uda antennas. The small, off-resonant squares are taken as a reference for QDs on metal, while the dipole antennas are essentially the feed element of a Yagi-Uda antenna. In the reference case, the polarization of the luminescence varies with a *DOLP* ranging from -0.5

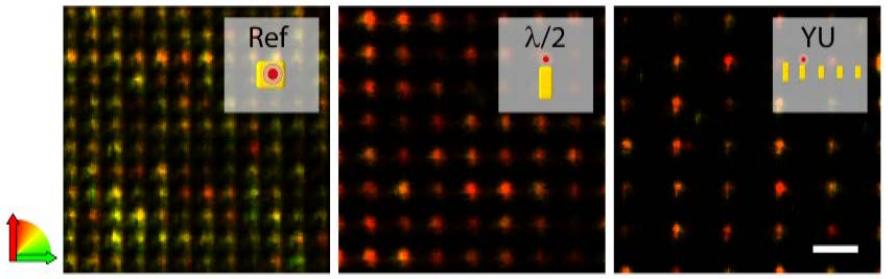

Figure 5.3 **The polarization of the emission is controlled by coupling to the antenna mode.** Scanning confocal luminescence images of QDs on reference 60 nm gold squares (Ref), half-wave dipole antennas ($\lambda/2$) and Yagi-Uda antennas (YU), respectively. Different colors represent changes in the degree of linear polarization. YU corresponds to YU145 in the text. The schematics in the insets are not to scale. Scale bar is 2 μm.

to 0.5 (Fig. 5.3, left) because the QDs have different orientations and the gold squares induce no preferential direction. The corresponding angular emission pattern is shown in Fig. 5.4a. All ensuing momentum-space images contain two distinct circles in the polar angle θ: the outer circle is the maximum collection angle of our objective (θ_{NA}=72.8°), while the inner circle is the critical angle for the glass-air interface (θ_c=41.1°). A dipole close to an interface emits primarily into the high index medium, with sharply peaked maxima at the critical angle. Moreover, our QDs exhibit a degenerate transition dipole moment contained on a "bright" plane [47, 48]. As a result, the radiation pattern of a QD is nearly isotropic in the azimuthal angle φ.

When coupled to a $\lambda/2$ dipole resonant nanoantenna (Fig. 5.3, center), the picture changes dramatically: the QD luminescence turns into a clear linear polarization parallel to the long axis of the antenna ($DOLP \approx 0.8$) and the radiation pattern transforms to that of a linear dipole close to an interface [42]. These are two clear signatures of the near-field coupling [11]. Remarkably, the QD emission becomes fully determined by the antenna mode, both in polarization and direction, despite the degeneracy of the QD dipole moment.

A Yagi-Uda antenna directs the emission

Now, we can also control the emission direction. To this end, we position QDs at one end of the $\lambda/2$ feed element of Yagi-Uda antennas (Fig. 5.3, right). The luminescence remains strongly linearly polarized ($DOLP \approx 0.8$), but the radiation pattern now shows a single lobe, demonstrating the unidirectional emission of a QD due to coupling to an optical antenna.

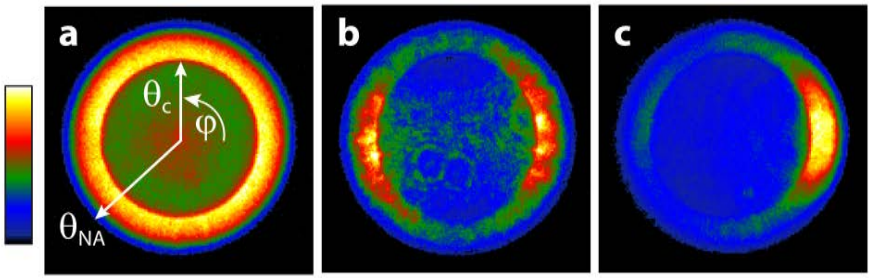

Figure 5.4 **Unidirectional emission of an optical Yagi-Uda antenna and comparison to other metal nanostructures.** Radiation patterns (intensity distribution at the back focal plane of the objective) from single structures in Fig. 5.4: **(a)** Non-resonant square; **(b)** Half-wave dipole antenna; **(c)** Yagi-Uda antenna. Critical (θ_C) and Numerical Aperture (θ_{NA}) angles are indicated. For the YU antenna, a 830 nm long-pass filter was used, as in Fig. 5.7.

The directional performance can be quantified by a front-to-back ratio (*F/B*), defined as the intensity ratio between the point with maximum emitted power and the point diametrically opposite in the radiation pattern. The *F/B* value is essentially 0 dB for the reference squares and the dipole antennas, as expected for symmetrical structures. For the Yagi-Uda antenna in Fig. 5.4, *F/B* is 6.0 dB (or alternatively, an intensity ratio of 4). The directed emission is centered at θ=49.4°, with a beam half width at half maximum of 12.5° in θ and 37.0° in φ.

The experimental angular radiation pattern, calculated from the Fourier-plane image, agrees well with the theoretical prediction (Fig. 5.5). The simulations quantify that as much as 83.2% of the QD emission is directed into the high-index glass substrate. The emission is thus truly unidirectional, unlike configurations with a low index contrast interface, which results in two separate emission lobes into both half spaces [168]. In this context, other authors have shown that a planar dielectric multilayer structure allows collection efficiencies close to unity [177], at the expense of isotropic emission in φ and still requiring the use of a high numerical aperture (solid immersion) objective. It should be noted that the brightness of the QDs coupled to Yagi-Uda antennas is comparable to that of dipole antennas, indicating that, despite the parasitic antenna elements, the radiation efficiency is similar.

The maximum experimental *F/B* values tend to be lower than the numerically calculated values because part of the signal stems from autoluminescence of the gold nanoparticles and a fraction of the QD emission is not coupled to the antenna, both contributing to an isotropic background, as it was shown in Chapter 3.

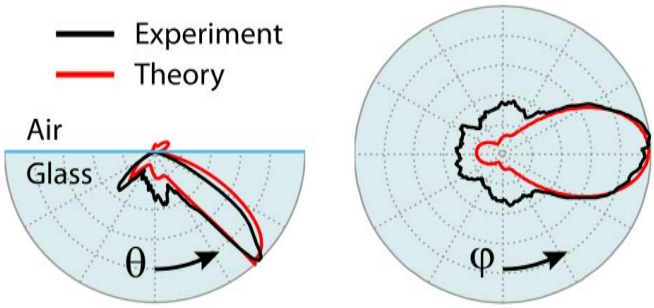

Figure 5.5 **Unidirectional emission in angular space**. Angular radiation patterns in the polar (θ) and azimuthal (φ) angles for a Yagi-Uda antenna (black), in good agreement with the theoretical prediction (red). The emission pattern was converted to angular space from the back focal plane of Fig. 5.5c.

Parameter tuning and spectral dependence

Any Yagi-Uda antenna is designed to operate at a certain frequency and bandwidth. To assess the frequency dependence of the directionality, we fabricated Yagi-Uda antennas tuned to four different resonant frequencies (Fig. 5.6, top row), identified with their feed element lengths L_f: 110 to 160 nm (complete parameter set in the inset table). Increasing the antenna length creates a red-shift of the resonance. The shortest antennas (YU110 and YU125) emit clearly directionally. These antennas are tuned close to the QD emission, and their bandwidth contains the complete luminescence spectrum. These observations are in agreement with the calculated bandwidth of 150 nm for end-fire operation, defined as $F/B > 3$ dB. On the other hand, for longer antennas (YU145 and YU160), the antenna resonance is more detuned from the QD emission, and directivity is hindered by short wavelength components of the spectrum. This spectral dependence does also occur for radio frequency Yagi-Uda antennas [178] and was in fact predicted for the optical regime [172, 179].

To corroborate the analysis above, we evaluate the dependence of the directionality on the wavelength of the emitted photons for antennas of different sizes (Fig. 5.6). We focus our attention on the antennas labeled as YU145, that illustrate the spectral trends also observed for other sizes. These antennas are red-detuned from the QD emission. As a result, the QD emission spectrum is modified by the near-field coupling to the antenna (see Section 3.3). We divide the emission spectrum of YU145 in three parts by using three different filters.

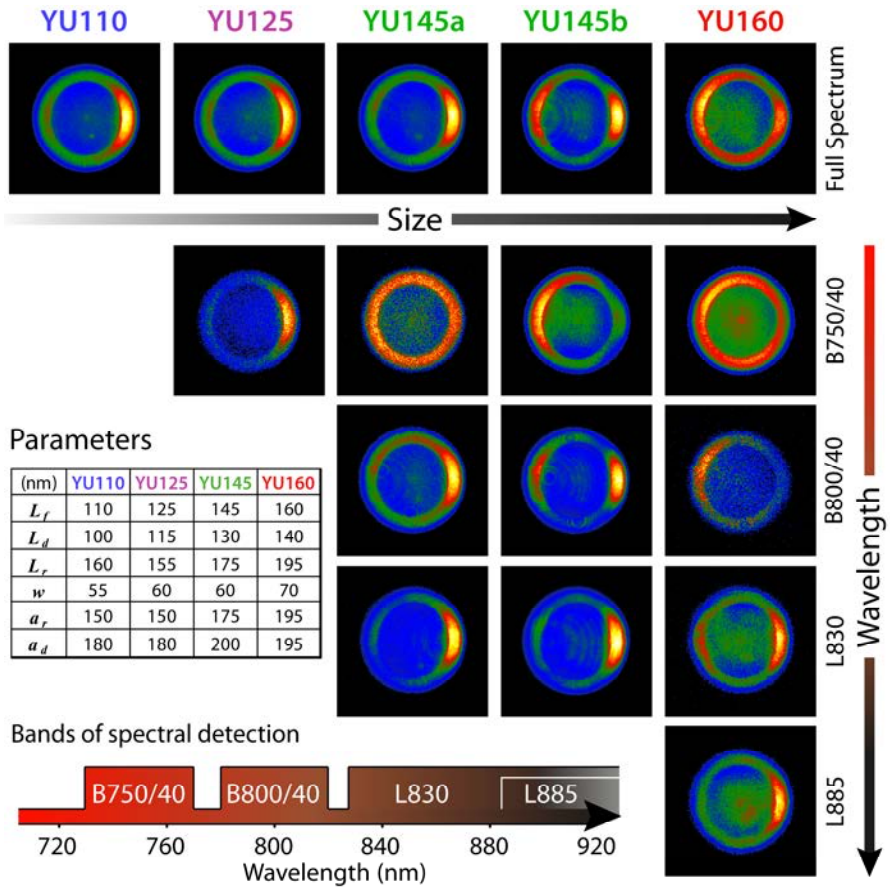

Figure 5.6 **Tuning of optical Yagi-Uda antennas in size and in wavelength**. Top row: radiation patterns in the back focal plane of the objective for five different individual Yagi-Uda antennas of increasing overall size, characterized by the length of the feed element L_f, from 110 to 190 nm. Two antennas with L_f =145 nm are shown (YU145a and YU145b). The full emission spectrum was recorded. Below each length, the angular radiation patterns of that specific antenna is decomposed in different spectral detection windows. The patterns show that performance is best for wavelengths to the red of the feed resonance. The inset table contains the fabricated Yagi-Uda antenna parameter sets for different feed element lengths and spacings, as measured by Scanning Electron Microscopy. L_f is the length of the feed element, L_d the length of the three directors, L_r the length of the reflector, w the width of the elements, a_r the spacing between the centers of the reflector and the feed, a_d the spacing between the centers of the feed element and the first director, and the spacing between the directors. The height of all the elements is 30 nm for all antennas.

Although hardly any directed emission is observed for the complete spectrum (Fig. 5.6, top row), a high directivity is recovered when only the long wavelength part of the spectrum is selected (Fig. 5.6, second row from the bottom). For short wavelengths, below a cut-off value, the emission is even reversed with the main lobe pointing backwards, a fact also present in our numerical simulations. We observe a similar behavior for the longer antenna YU160, with all characteristic wavelengths shifted to longer wavelengths. For shorter antennas, YU110 and YU125, the antennas are blue-detuned with respect to the quantum dot spectrum and a lower directivity is observed for the full spectrum.

In summary, by tuning the antenna or selecting certain emission bands, we have proved the frequency dependence of the directivity of an optical Yagi-Uda antenna.

Conclusions

We have demonstrated the unidirectional emission of quantum-dot–Yagi-Uda systems; the antenna transforms the non-directional quantum-dot luminescence into a directed light source which can now be efficiently collected with lower numerical aperture optics. By reciprocity, we anticipate that the antennas work both in emission and absorption. Most remarkably, all this control over photon emission is obtained from an antenna that is only a single wavelength long.

Further optimization of the many Yagi-Uda design parameters, including the addition of more director elements, might sharpen up the unidirectional cone. This trend will eventually saturate when metal losses start to dominate the multi-element scattering. The operation bandwidth can be increased through the use of a Log-Periodic design [3], which we study in the next Section. An inherent problem of the Yagi-Uda design for optical frequencies is the need to position the source to drive locally one individual element, which might not be compatible with some of the potential applications. We will explore in the next Sections designs that alleviate this requirement.

5.3. Log-Periodic nanoantennas

Yagi-Uda antennas are the archetypal directional antennas. However, at radio frequencies the original design has been improved by other geometries which, based on the same principle of operation, offer higher directivities and wider bandwidths of operation.

In this Section, we study log-periodic optical antennas, one of the evolutions of the classical Yagi-Uda design. We show through numerical simulations that the family of log-periodic designs has a considerable potential for improving both the directivity and the operation bandwidth as a result of the self-similar relation

between the lengths, separations and widths of the elements. Moreover, the source can be located at the end of different antenna elements, distributing the role of the feed element. We systematically study the influence of geometrical parameters on angular performance and local field enhancement to find optimum values. Next, we demonstrate that introducing a gap in the dipole array architecture can provide at least a ten-fold enhancement of the emitted power. Finally we present an optical zigzag antenna capable of both broader spectral response and even higher directivity.

Introduction to Log-Periodic antennas

A variety of RF antennas rely on self-similar designs. Fractal antennas are important representatives of this category, providing a remarkable combination of compactness, broadband (or multiband) behavior and highly isotropic angular patterns. Fractal designs have been found to be especially suitable for compact microwave communication devices, such as mobile phones [3, 155]. Their omnidirectional response can be a desirable property for certain applications of optical antennas, such as light-harvesting. However, for others such as biochemical sensors and single-photon sources, directivity is essential for efficient excitation and detection.

Most theoretical studies on directional optical antennas have focused on the classical Yagi-Uda design [172-174] , which is one of the few that have been realized experimentally [54, 168, 169]. It provides directivity for a specific design frequency with a limited bandwidth [3], as we have demonstrated in the previous Section. Both bandwidth and directivity could be improved by adopting a more general geometry, opening new degrees of freedom for further optimization. Antenna designs with self-similarity along a single dimension are a promising approach to combine directivity and broadband behavior. Indeed, a number of such designs have been extensively studied and used in the RF regime, receiving the name of log-periodic (LP) antennas because they exhibit a series of resonance frequencies which are equally spaced when plotted in logarithmic scale [3, 155]. The common denominator of this family of antennas is a geometrical condition: the size of their elements and the mutual separation scales as a geometric progression.

Chains of metallic particles have been proposed for sub-wavelength light localization and guiding. For example, nanofocusing with self-similar chains of metal nanoparticles [180] or ultrafast, controlled changes in localization [181] were proposed. Graded-size particle chains were predicted to show localization at different positions for different excitation wavelengths [182], an effect that had also been observed experimentally for arrays of identical particles [171]. More

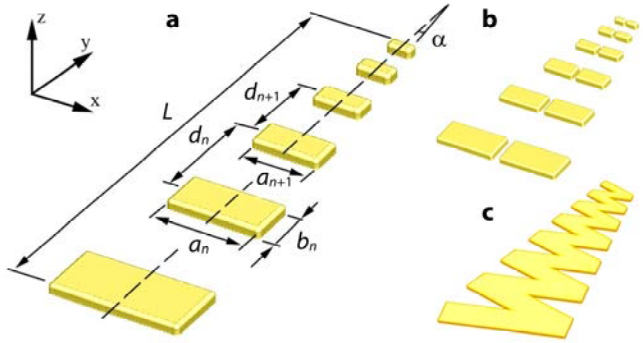

Figure 5.7 **Log-periodic optical antennas**. Geometrical configuration of three types of log-periodic antennas: **(a)** dipole array, **(b)** gap-dipole array and **(c)** zigzag antennas.

recent simulations [183, 184] for antenna designs based on tapered dipole arrays revealed directional and multiband characteristics. In the present study, we report on the performance of strictly self-similar LP antennas, accounting for the effects of the different parameters.

Three flavors of LP antennas will be studied based on arrays of different unit elements: dipole nanowire antennas, gap antennas, and nanowires connected in zigzag. The geometrical parameters defining a dipole-array LP antenna are illustrated in Fig. 5.7a. The scaling factor r (or its reciprocal value τ) is the ratio between the lengths (a_n and a_{n+1}) of two consecutive elements, as well as between two consecutive widths (b_n and b_{n+1}) and between inter-element distances (d_n and d_{n+1}): $r=1/\tau=a_n/a_{n+1}=b_n/b_{n+1}=d_n/d_{n+1}$. Hence, only one of the element lengths a_n suffices to define all the other lengths, once the scaling factor r is fixed. The distance d_n between adjacent elements with numbers n and $n+1$ can be expressed normalized to the element length [3], thus defining an inter-element distance factor: $\sigma=d_n/2a_n$. The parameters τ and σ are also related to the antenna apex half angle by $\alpha=tan^{-1}(1-\tau)/4\sigma$. The geometrical description of the antenna is completed with the definition of the aspect ratio of the elements $AR = a_n/b_n$, the element thickness and the edge rounding. The number of elements (N), the length of one given element (a_n), the scaling factor (r) and the inter-element distance (σ) were systematically varied for dipole-array antennas in order to investigate their effect on the directivity, local field enhancement and radiated power.

Although analytical methods can be applied for the study of relatively simple multi-element nanoantenna architectures [172, 174, 185, 186], we will employ the Finite-Difference Time-Domain (FDTD) method because it is an approach suitable for our complex three-dimensional objects. All FDTD simulations were

carried out using commercially available software (FDTD Solutions by Lumerical Solutions, Inc.). The values of the antenna parameters were selected in such a way that the resulting dipolar resonances of their elements were in the visible and near infrared.

Antennas can operate either in reception or in emission mode. In the case of optical Yagi-Uda antennas, operation in emission can be achieved by placing an emitter at a position of maximum modal field, where coupling is most efficient. For a Yagi-Uda antenna to be directional, this source must best be positioned at the end of the resonant feed element, usually next to the largest element or reflector. This requirement can be relaxed by making use of a LP design, where the roles of feed and directors are distributed over all the elements of the antenna. As a result, in the case of optical LP antennas, the optimal position for the emitter is not known *a priori*.

In the reception configuration, antennas were illuminated with a plane wave directed along the y-axis either in the positive (forward) or negative (backward) direction. The local spectrum of the electric field around the antenna elements was recorded. On the other hand, in emission configuration, the antennas were driven by placing an electric dipole source in the antenna near field and the resulting angular far field power distribution was analyzed. In both configurations, the effect of changing the position of the point field monitors (or dipoles) was investigated. The directionality in both operation modes was assessed by calculating the forward-to-backward ratio, F/B=10 $log(|E|^2_{fw}/|E|^2_{bw})$, and the full-width at half-maximum (FWHM) beam width.

Dipole array Log-Periodic antennas in receiving mode

First, we consider a 6-element dipole array antenna made of gold under plane-wave illumination and surrounded by air. Its parameters are a_3=120 nm, r=1.14, σ=0.4, and AR=2.1. We define two directions of incidence: backward and forward incidence, for a plane wave impinging from the smallest and largest element, respectively. The antenna is thus expected to perform satisfactorily in reception mode for illumination the in the backward direction.

The electric field enhancement in the vicinity of the antenna elements is shown in Figure 5.8, with near-field patterns that resemble those found for Yagi-Uda antennas both theoretically [173] and experimentally [170]. The field shifts from the shortest (a_6=92 nm) to the longest element (a_1=178 nm) with increasing wavelength of the backward-incident plane wave and reaches values of over 500 (normalized to the incident plane wave).

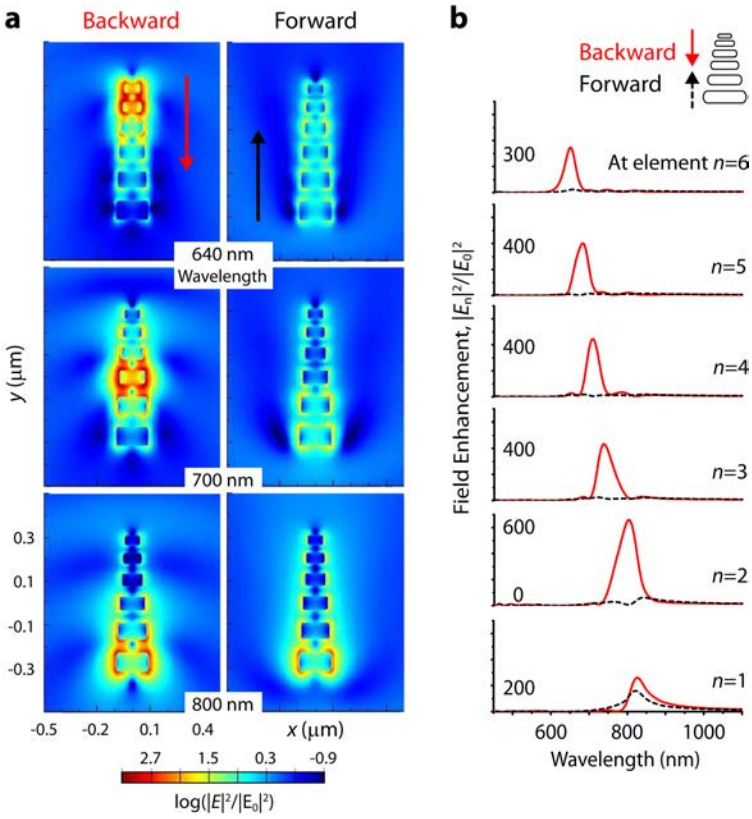

Figure 5.8 **Dipole array Log-Periodic antennas in reception**. **(a)** Electric field enhancement depending on the direction of incidence and the wavelength of the excitation plane wave. **(b)** Spectra of electric field at the end of each antenna element n. The maximum field concentration is achieved for backward illumination at the second largest element. The field shifts to shorter elements with shorter excitation wavelength. The electric field is normalized to the incident plane wave. Antenna parameters are N=6, r=1.14, σ=0.4, AR=2.1, a_3=*120 nm*.

For sufficiently small inter-element distance (σ) or scaling factor (r) the field enhancement is expected to occur simultaneously at different elements because adjacent resonances have overlapping bandwidths. At resonance, the field enhancement for forward illumination is generally an order of magnitude smaller, except at the longest element n=1, which is similar to the reflector in a Yagi-Uda antenna. Away from the resonance, the forward intensity can be similar or even higher than the backward intensity at particular wavelengths. Therefore, by reciprocity, bi-directionality or even backward directivity should be expected in emission configuration for a source at that position.

The log-periodicity of our antennas was confirmed by analyzing the ratio of the resonant wavelength on each consecutive element; the ratio $\lambda_n/\lambda_{n+1} = r$ is constant. A clear linear scaling relation for the resonance with length was found, in agreement with previous reports on the dependence of the resonance wavelength with the length of single gold nanorods [16, 17].

Next, we investigate the variation of directivity and field enhancement as a function of antenna geometry by changing the parameters N, r and σ for backward incidence (Fig. 5.9). In general, no clear relationship can be established between the directional figure-of-merit, F/B, and the element selected as a detector (n, the "feed"), except for the "reflector" ($n=1$) which consistently presents F/B values below 2.5 dB because it is the only element without a longer neighbor. For a fair comparison between different antennas, therefore, we obtained the F/B and the backward incidence field enhancement for each antenna element and calculated the maximum, minimum and average values over the resonances of all the elements excluding the "reflector". Each point in Fig. 5.9 corresponds thus to different positions on the antenna and different wavelengths.

Regarding the number of elements, while the directionality reaches a maximum for N=10 elements, the optimum value of $|E|^2_{bw}$ is obtained between $N=6$ and $N=10$ depending on whether we consider its maximum or minimum value. The decrease of the field enhancement values with increasing number of elements is associated to increasing losses by the addition of parasitic elements. These losses, however, do not directly decrease our measure of directionality (F/B, a self-normalized quantity).

Both $|F/B|$ and $|E|^2_{bw}$ reach a maximum for a scaling factor $1.1 \leq r \leq 1.14$ and the optimum inter-element distance is found to be $\sigma \approx 0.4$. The trends are similar for the average and minimum values, as well, indicating that the operation is similar across positions at different wavelengths. These optimal values of r and σ correspond to tapering angles $2° < \alpha < 3.2°$, close to the value of 3.3° reported for tapered antennas with constant element width and inter-element distance [183].

Combining the optimum values of all four parameters ($N=6$, $r=1.14$, $\sigma=0.4$, $AR=2.1$), the results for the F/B values at resonance for each element are 2.2, 20.6, 13.8, 19.5, 19.1 and 11.9 dB, for n = 1, …, 6, respectively. The applied approach consisting of varying the antenna geometrical parameters one-at-a-time does not guarantee reaching an absolute optimum but permits the evaluation of the influence of each parameter.

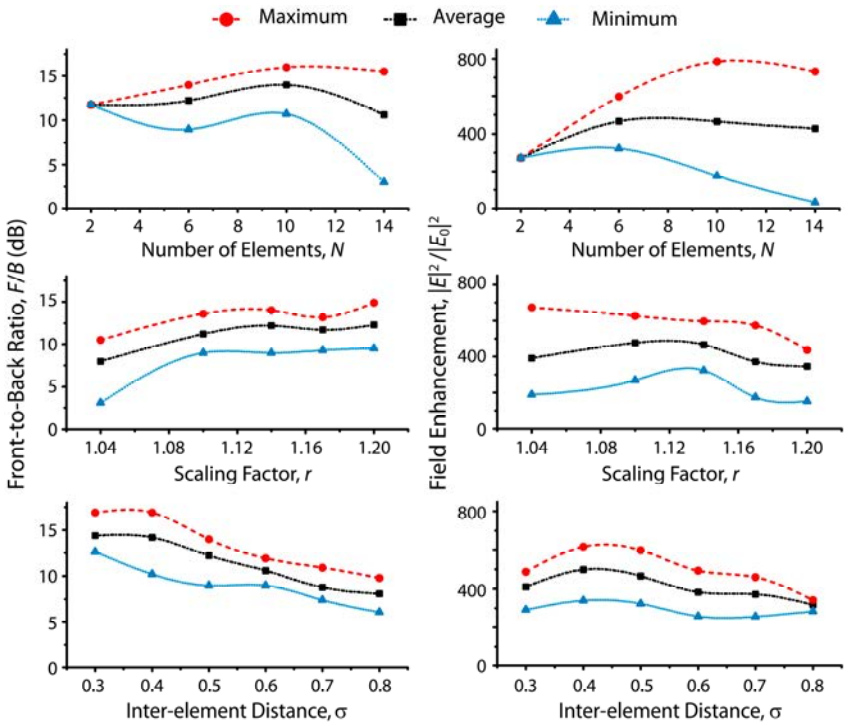

Figure 5.9 **Effect of geometric design parameters of dipole array log-periodic antennas on directionality and field enhancement**. The antennas operate in reception mode with plane wave illumination from front and back (to determine F/B ratios), or from the front end (to determine field enhancements). Since both quantities vary from one element to another within the same antenna, the spectral resonances of all the elements were identified and tabulated, and the maximum (red), minimum (blue) and average (black) values were calculated with all the element resonances. Thus, different points correspond to different wavelengths.

Dipole array Log-Periodic antennas in emission mode

In order to assess the emission performance of the dipole array log-periodic antennas driven with a point dipole source, we placed the antennas on a glass substrate (n=1.52), a common experimental configuration. Simulations allowed us to obtain far-field angular radiation patterns (Fig. 5.10). The width of the angular emission pattern decreases with the number of antenna elements (N), as expected for diffraction by a larger antenna. When the source spectrum does not overlap with the resonance of the element used as a feed, lower intensity antenna modes can be excited emitting in the backward (curves with scaled up intensities in Fig.

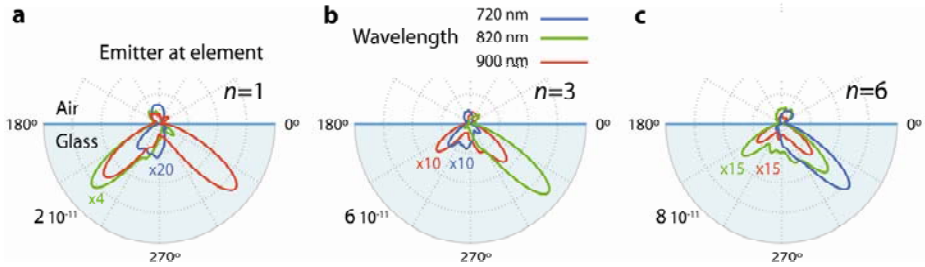

Figure 5.10 **Wavelength dependence of angular patterns in emission mode. (a, c)** Far-field radiation patterns (yz plane) of a 6-element dipole-array antenna with parameters as in Figure 5.9 but placed on a glass substrate. The antenna is driven by a point dipole source placed at element 1, 3 and 6, respectively. Due to the smaller radiated power of off-resonance emission patterns, multiplying factors were applied (see tags).

5.10) and even in a lateral direction rather than in forward direction (not shown). Backward emission was already demonstrated experimentally for detuned Yagi-Uda antennas in Section 5.2, while lateral emission can be associated with the asymmetric position of the source with respect to the antenna axis (y).

Gap-antenna Log-Periodic arrays

An improved LP antenna design makes use of the field enhancement in the gap between two nanowires. We investigate next a log-periodic gap-antenna array (Fig. 5.7b), as opposed to a simple dipole array (Fig. 5.7a). Adding a gap has been suggested for improved performance in other directional antennas [179, 187]. We construct such an antenna by shifting laterally two identical dipole arrays to leave a narrow gap between them. When fed by a dipole at the center of one gap, the angular patterns are very similar to the ones corresponding to simple dipole array LP antennas with regard to beam direction, width and shape. However, both the forward and backward beam intensities present a strong enhancement with respect to those of the corresponding simple dipole array. For an antenna with 15 nm wide gaps driven by a dipole at n=2, an enhancement of about one order of magnitude is obtained (Fig. 5.11). The resonant wavelength of this element pair in the gap-antenna array is slightly red-shifted with respect to the simple dipole array (910 and 885 nm, respectively), as in other gap antennas [15].

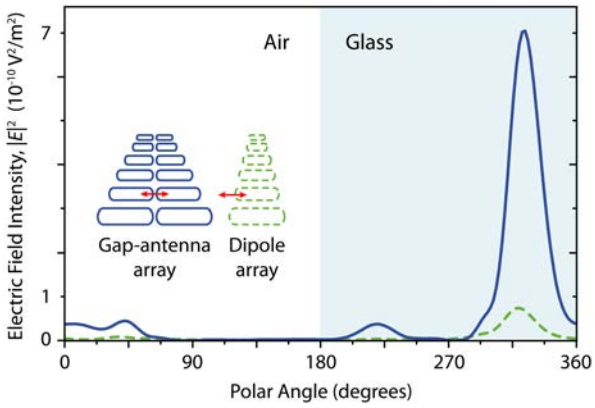

Figure 5.11 **Adding a gap enhances the power radiated by a log-periodic nanoantenna**. Far-field radiation patterns of a gap-antenna array (blue) and a single-dipole array (green, dashed) on a glass substrate. The parameters of both antennas are the same as in Figures 5.9 and 5.11, with a gap is 15 nm. The antennas are driven by an electric dipole in the gap or at the end of the second element, at their resonant wavelengths (910 nm and 885 nm, respectively).

Zigzag Log-Periodic antennas

To conclude our study of self-similar directional antennas, we consider another log-periodic architecture: the zigzag antenna (Fig. 5.7c), known in RF technology for its strong directivity and broad bandwidth [155]. At optical frequencies, we find indeed that this design increases both directionality and bandwidth compared to dipole arrays. These antennas are obtained by tilting the elements of a dipole-array LP antenna until its ends join.

The local spectrum of a 14-element zigzag antenna, operating in reception mode, displays a more complex band structure than its equivalent 14-element dipole-array antenna (compare Figures 5.12a and b) as a consequence of the overlap between the fields of adjacent elements. Furthermore, under forward incidence, the zigzag antenna presents lower intensities at the resonant wavelengths for backward incidence, resulting in very high F/B values (Fig. 5.13a). The F/B ratio of the zigzag antenna increases with element number n, reaching values as high as 32 dB, whereas for the corresponding dipole-array antenna it diminishes. At the same time, the smallest elements present a relatively high field enhancement under backward incidence, and a smaller dependence of field enhancement on n is also found (Fig. 5.13b), suggesting that surface plasmons instead of multiple scattering play a determining role in the collective response of its elements.

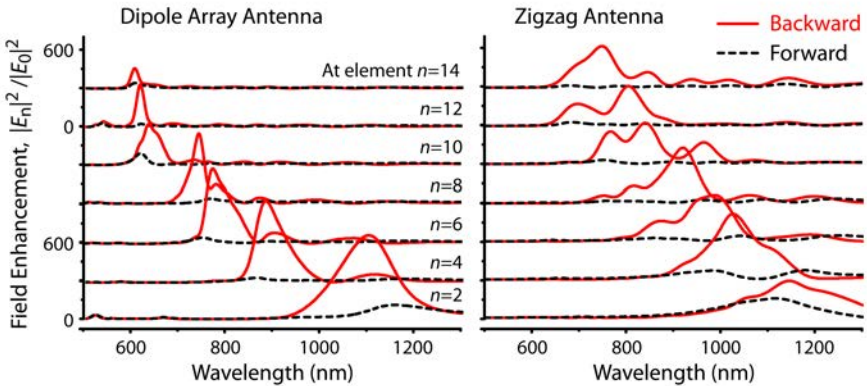

Figure 5.12 **Zigzag Log-Periodic antennas in reception**. Comparison of the local spectra of a dipole-array antenna (left) and a zigzag antenna (right) with N=14 elements, illustrating the larger bandwidth of the zigzag with respect to the dipole array. The antennas operate in air under plane wave illumination.

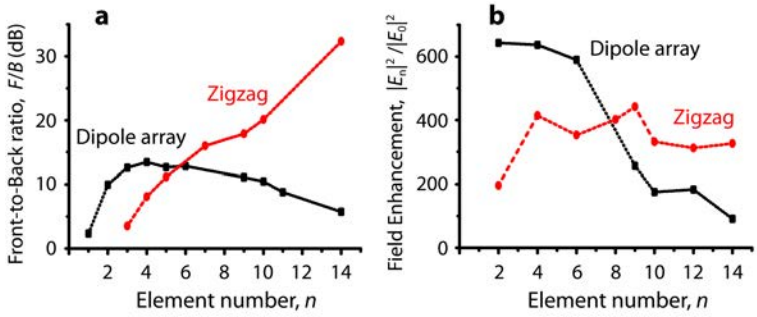

Figure 5.13 **Zigzag log-periodic antennas can outperform dipole array antennas**. **(a)** Dependence of the maximum F/B ratio and **(b)** the maximum field enhancement ontained at the end of different elements for the dipole array (black) and the zigzag (red) antennas in Figure 5.13. The zigzag can be more directional and less sensitive to the position of the point detector.

In summary, zigzag antennas present certain advantages compared to simple dipole arrays: potentially higher directivity, broader bandwidth and a more robust field enhancement in reception mode. By reciprocity, it is expected for emission that performance is less sensitive to the source position.

Conclusions

We have presented systematic simulations of several types of log-periodic optical antennas. The dipole array design was investigated in detail with focus on

directivity and field enhancement as a function of geometrical design parameters. Directionality is found for dipolar sources (or point detectors) near most antenna elements at different wavelengths. The use of resonant gap antennas in log-periodic arrays allows achieving stronger beam intensity enhancement. Zigzag antennas present an increased directivity towards the smallest elements while the radiated power is relatively independent on the position of the source/detector.

The proposed set of self-similar designs offers a basis for improving the basic Yagi-Uda design, which consists of identical director elements. By opening up the parameter space and tapering element sizes, log-periodic antennas can outperform simpler Yagi-Uda antennas. Effectively, the number of possible "feed"elements is increased, with the feed role distributed among all elements. However, the important practical drawback of multi-element antennas, positioning the emitters at the ends of the elements, has not been removed by this optimization.

Indeed, we tested experimentally the performance of log-periodic designs in experiments similar to Section 5.2 (results not shown in this Thesis), but now for emitters randomly attached to the surface of the antennas (no lithographic positioning). We found that, due to the narrow gaps between the antenna elements, the emission was dominated by radiation towards lateral directions, with polarization across the gaps between elements. When the emitters are not selectively positioned, they couple more strongly to the transversal mode of the gap than to the longitudinal nanowire mode. Log-periodic antennas are still expected to outperform Yagi-Uda antennas if the emitters are selectively positioned at the ends of the elements. In the next Section, we will shift the design paradigm from multi-element to single-element antennas in order to overcome this limitation.

5.4. Magneto-Electric nanoantennas

Because of their reliance on the interference between dephased dipoles, multi-element antennas have relatively narrow bandwidths. Directivity is gained at the expense of bandwidth, as different phase profiles are added to obtain directionality. In Section 5.2, we have seen that a Yagi-Uda nanoantenna offered directivity only in part of the spectrum of emission, partially improved in Section 5.3 by the introduction of a Log-Periodic design. The performance was also sensitive to the position of the emitters and the antennas needed to be driven from specific feed elements for operation at a given wavelength. These two requirements limit the applicability of directional nanoantennas in many practical devices. In this Section, we experimentally realize a compact and robust optical antenna that outperforms the previously studied multi-element antennas in both bandwidth and directionality. Interestingly, this single-element design is more

robust against changes in the position of the local source, bringing directional optical antennas closer to practical applications.

Magneto-electric interference

A magneto-electric antenna exploits the interference between magnetic and electric modes as a principle of operation. The fields radiated by alternating electric and magnetic multipoles have opposite symmetries, which can be used for the design of optical antennas with a target radiation pattern. The interference of both a magnetic dipole (MD) and an electric quadrupole (EQ) with an electric dipole (ED) can lead to directional radiation. The concept of magneto-electric interference is schematically explained in Fig. 5.14c for a MD perpendicular to an ED. For an antenna, if both dipoles are excited simultaneously, the emission can be directed to the forward or backward directions depending on the relative phase between both dipoles.

For implementation of this principle at optical frequencies, nanostructures with coexisting multipolar resonances are required. The directional scattering of dielectric nanospheres supporting magnetic dipole Mie resonances has been demonstrated recently both theoretically and experimentally [99, 165, 188-191]. Other particles that exhibit directionality as a result of multipolar interference are metal-dielectric nanoshells and nanocups [166, 192].

Specifically, we will employ a split-ring resonator architecture (SRR), known for its optical magnetic response. The resonances of SRRs have been studied extensively within the context of metamaterials [96, 193-195]. A U-shaped SRR design with a carefully chosen geometry (Fig. 5.14a) allows us to optimize the directionality through the balance between different multipolar components. Similarly to a gap antenna, the width and the separation between the SRR arms can be used for improving the coupling of ED emitters to the antenna mode thanks to local electric field enhancement. The two arms are connected by a bridge, whose width controls how much the antenna differs from two parallel, unconnected wires.

Directionality from a split-ring resonator

We fabricate Au nanoantennas by standard electron-beam lithography on a glass substrate with 10 nm of ITO. The antennas, 40-nm high, are covered completely with a molecular monolayer (MUA) for attachment of QDs at random positions on the metal surface. We obtained arrays of SRRs with a square aspect ratio (equal length and total width, L) covered with QDs. We fixed the gap and bridge sizes (g and b, respectively) to g= 35 nm and b=50 nm after a systematic exploration of the parameter space. The photoluminescence of the QDs is excited

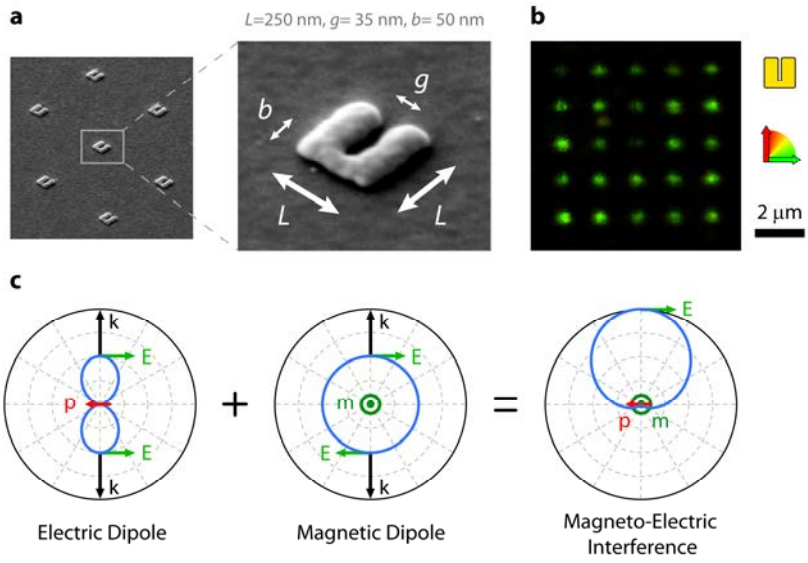

Figure 5.14 **Split-ring resonators as magneto-electric antennas. (a)** Scanning electron microscopy images of split-ring resonators. The base is a square of length L. Two arms are separated by a gap (g) and connected by a bridge (b). **(b)** Confocal photoluminescence microscopy image of quantum dots coupled to SRR antennas, showing linearly polarized emission. **(c)** Principle of magneto-electric interference of multipoles with different symmetries of the emitted field. As an example, a magnetic dipole and a crossed electric dipole interfere resulting in an asymmetric radiation pattern.

by a focused circularly-polarized laser, as in previous Chapters, for the study of one antenna at a time. Confocal microscopy shows that the emission of a SRR is linearly polarized across the gap (green color in Fig. 5.14b, $DOLP$= -0.7), indicating efficient coupling of the emitters to the antennas even without nano-positioning the QDs at optimal points.

For angular measurements, the light collected in the back focal plane images spans the entire QD emission spectrum ($FWHM$ = 80 nm). For a non-optimized SRR of size 220 nm, the radiation pattern is almost symmetric (inset of Fig. 5.15b). For an optimal size of 250 nm, the angular pattern of the magneto-electric antenna is directional with F/B = 8.5 dB (equivalent to a linear ratio of 7, Fig. 5.15a and b). Such a high directionality is obtained for most antennas on an array, as exemplified by another nominally identical antenna (SRR 250 #2 in Fig. 5.15b). Performance is robust and reproducible, even for emitters coupled to the antenna at random positions.

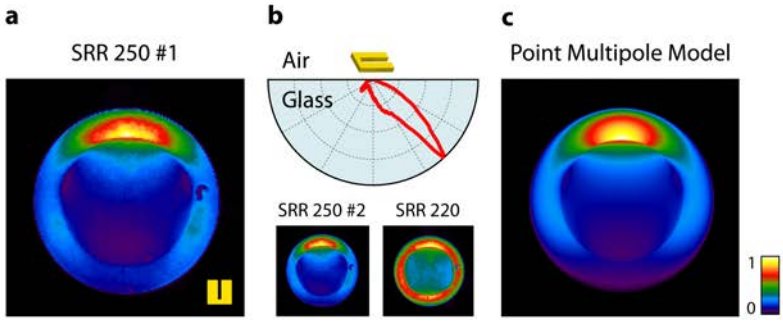

Figure 5.15 **Directed emission by a split-ring resonator. (a)** Angular radiation pattern as recorded in the back focal plane of the microscope objective for a SRR with parameters L=250, g=35, and b=50 nm. **(b)** Section of the same angular radiation pattern along the main lobe direction. For comparison, another directional antenna with the same nominal parameters (left bottom) and an antenna of another size with poor performance (right bottom, L=220, g=35, b=50 nm) are shown. **(c)** Calculated angular radiation pattern for a superposition of an electric dipole (p_x), a magnetic dipole (m_z), an electric quadrupole (Q_{xy}=Q_{yx}) and a small rotationally-symmetric uncoupled background ($|p_x|^2$+$|p_y|^2$). The main features of the pattern are reproduced with this simplified model, including the small side lobes.

Analysis of the antenna mode

To understand the excellent performance with respect to bandwidth and source position, we simulate numerically the characteristics of the antenna mode excited by a point electric dipole source. Using the FDTD method, we identify SRR sizes that are close to resonance for the central wavelength of the QD emission. For a size of L=250 nm, the QD emission spectrum overlaps well with an extended resonance (Fig. 5.16a, red line) when the emitter is placed at the vertical center of the antenna inside the gap, with an orientation perpendicular to the SRR arms.

By comparing simulated near fields with the higher-order resonances of SRRs [193-195], we assign the antenna mode to the 2nd and 3rd standing-wave resonances of a thin, U-shaped SRR. A plateau around λ=800 nm between the 2nd and 3rd order resonances provides the simultaneous magnetic dipole, electric quadrupole and electric dipole necessary for directional emission. Excitation of the antenna in-between resonances is confirmed by the position dependence of the radiated power (Fig. 5.16b). Emitters excite the antenna efficiently over a large area of the gap, covering a distance of more than 100 nm from the bridge. Furthermore, the spectral *FWHM* of the enhancement spans around 200 nm in wavelength. These

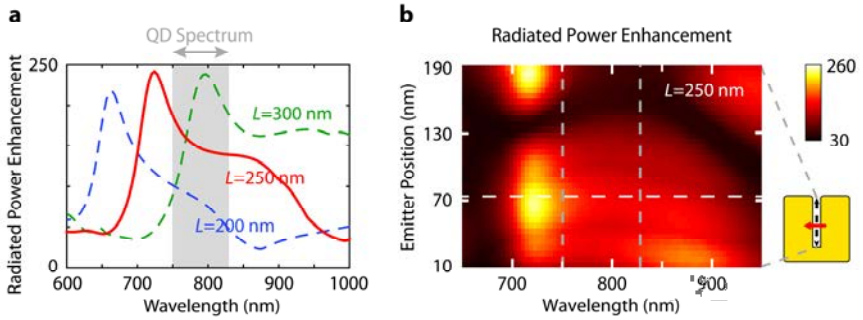

Figure 5.16 **Modal properties of a split-ring resonator antenna.** In simulations, a point electric dipole excites the antenna at a position along the gap with orientation across the gap. **(a)** Enhancement of radiated power (proportional to the radiative rate enhancement) normalized to the power radiated by the emitter in vacuum for SRRs of varying L with g=35 and b=50 nm. The source is placed at the vertical center of each antenna and 20 nm above the substrate, at half the height of the antenna. **(b)** Spectral and emitter position dependence of the radiated power enhancement for the SRR with L=250 nm. The horizontal white line indicates the position of the source for the spectrum in **a** (red line). The vertical gray lines show the *FWHM* spectrum of emission in the experiment.

two factors are responsible for the robustness of the directionality for broadband emitters randomly attached to the antennas. Importantly, the external quantum efficiency of the emitter-antenna system remains over 70% within the bandwidth of the QD as required for a good antenna design.

Angular radiation patterns are also obtained in simulations, confirming the experimentally observed directional emission with *F/B* ratios over 10 dB for wavelengths between 750 and 850 nm for a dipole inside the gap. When the dipole is at the top end of the gap, the antenna emits in the opposite direction but the radiated power is much lower for all wavelengths within the bandwidth of the QD (gray lines in Fig. 5.16b). The net result is that the SRR antenna emits directionally even for emitters randomly positioned on the antenna.

Point multipole interference

The directional radiation of a SRR can be explained with a point multipolar expansion. As in Chapter 3 (nanowire antennas), we use an expansion based on the angular spectrum representation including the presence of the glass substrate [77]. Whereas for 1D nanowires only longitudinal electric multipoles along the antenna were necessary, in the current case of a fully 2D SRR it is not known *a*

priori which magnetic and electric multipolar terms should be taken into account in the expansion.

For a preliminary assessment of the orders of magnitude of each electric ($a_{\ell,m}$) and magnetic ($b_{\ell,m}$) multipolar coefficient, where m= -ℓ, …, +ℓ, we first obtained a multipolar expansion of the antenna in free-space by direct numerical integration of the simulated FDTD fields [84]. The results indicated that the emission of the antenna is dominated by similar contributions by an electric dipole across the gap (p_x), a magnetic dipole perpendicular to the SRR (m_z) and two electric quadrupole terms (Q_{xy}= Q_{yx}) with the rest of Cartesian components of the quadrupole moment tensor equal to zero. Equivalently, this quadrupole is given in terms of multipolar coefficients by $a_{2,2}$= -$a_{2,-2}$ with $a_{2,0}$= $a_{2,1}$= $a_{2,-1}$= 0 [82].

With this simplification, it is now possible to reproduce the experimentally observed angular patterns. We find, indeed, that the electric dipole, the magnetic dipole and the electric quadrupole, all have a non-negligible contribution to the radiation pattern (Fig. 5.15c); although the interferences of EQ-ED or MD-ED alone already give directional patterns, only the combination of the three reproduce all the features of the experimental angular pattern in Fig. 5.15a.

Conclusions

With a more compact, more broadband and more robust single-element design, our magneto-electric antennas direct light emission comparably better than the multi-element antennas of Sections 5.2 and 5.3. The volume of the antenna is only $\lambda^3/200$, the directional bandwidth is at least 200 nm and there is no need to accurately position the emitters. Further tuning of the geometrical parameters may result in higher directional and radiative enhancements. Interestingly, split-ring resonators may be patterned by simpler nanofabrication methods such as shadow-mask lithography because they do not require the alignment of multiple elements. Therefore, these results are promising for the integration of directional nanoantennas in light-emitting and light-harvesting devices.

From a fundamental point of view, the directional response of a SRR may be a property to exploit in metamaterials. Understanding this directionality is necessary to explain transmittance and absorption spectra commonly found in experiments. For example, optical activity has been observed for achiral arrays of SRRs under oblique incidence [196, 197]. This is a direct consequence of the magneto-electric origin of the directionality of a single SRR.

6.

Antenna-Enhanced Forbidden Transition Spectroscopies

In previous Chapters, we have controlled the emission of electric dipole electronic transitions with multipolar electromagnetic antenna modes. Multipolar electronic transitions in the emitters themselves, although usually slow compared to electric dipoles, play a relevant role in various optical spectroscopies of several materials. In this Chapter, through numerical simulations, we evaluate and compare nanoantenna designs for the enhancement of magnetic dipole and electric quadrupole transitions, while simultaneously aiming to suppress electric dipole emission. We identify promising geometries and materials suitable for the experimental enhancement of *forbidden*-transition spectroscopies.

6.1. Multipolar transitions in spectroscopy

At short wavelengths of the electromagnetic spectrum (X- and gamma rays), multipolar transitions are common in atomic spectra due to the comparable size of atom and wavelength. At much longer wavelengths, in the microwave and radio-frequency domains, magnetic resonance spectroscopy relies on magnetic dipole transitions, which can be enhanced by cavities and antennas.

In the optical regime, on the other hand, non-electric-dipole electronic transitions are often neglected because their transitions rates are usually several orders of magnitude slower than electric dipole (ED) transitions. However, magnetic dipole (MD) and electric quadrupole (EQ) transitions do occur, particularly in cases where ED transitions are forbidden [1]. Examples of such *forbidden* transitions with very slow transitions rates that are yet visible include the green and red emission lines of atomic oxygen present in the *aurora borealis*.

Enabling optical *forbidden* spectroscopies through the selective enhancement of non-electric-dipole transitions would constitute a valuable resource for a variety of spectroscopic techniques, potentially providing more chemical specificity and new structural information compared to ED spectroscopic methods.

Electric-dipole-forbidden optical transitions

Electronic transitions of non-ED origin have been demonstrated or expected to be present in a variety of materials for different types of optical spectroscopies. First, we briefly summarize some relevant examples that could benefit from the enhancement of MD and EQ transitions:

Circular dichroism. The different response of chiral molecules to circularly polarized optical fields is due to the interference between an ED and either a MD or an EQ [198]. For the effect to be visible, both types of transitions involved must have fixed relative orientations and phases [199]. Dissymmetry factors are usually very small because of the lower strength of the non-ED contribution to the product of both moments.

Luminescence of rare earth ions. The electronic structure of the lanthanide elements favors MD moments that can be comparable or higher than ED transitions [200].

Second harmonic generation in centrosymmetric materials. SHG is forbidden in the ED approximation in centrosymmetric materials. Yet, certain centrosymmetric molecules and crystals display a significant amount of SHG (*e.g.,* several phthalocyanines and C_{60} [201-203]). When surface effects are discarded, MD and EQ transitions explain the origin of the bulk SHG signal [204, 205].

Oxides. Certain spectral lines of oxides such as Cu_2O and Cr_2O_3 are attributed to electric-dipole-forbidden transitions [206, 207].

Atoms. The enhancement of an EQ transition in a vapor of atomic cesium was reported under evanescent wave illumination of total internal reflection on a dielectric interface [208].

Quantum dots and wires. In some semiconductor nanostructures, particularly of larger sizes, non-ED effects have been measured for emission near a mirror [209] and were also investigated theoretically [210, 211].

Molecular aggregates (J- and H-aggregates). Coherent coupling between aligned molecular units can lead to non-dipolar contributions to excitation, emission and energy transfer, because of the extended nature of the excitonic wave function.

Raman and hyper-Raman spectroscopy. Raman vibration modes with symmetries that have dipole-forbidden emission can potentially be activated through EQ radiation by strong electric field gradients. This electromagnetic mechanism has been suggested for the appearance of certain Raman lines near metal nanoparticles [212, 213].

As in previous Chapters, angular measurements offer great potential to study the multipolar nature of the interaction of light with matter, both in absorption and in emission [214, 215]. In particular, back focal plane imaging can uncover non-ED contributions in emission [130].

6.2. Enhancing forbidden transitions

The interaction strength of an electric dipole, a magnetic dipole, and an electric quadrupole with an electromagnetic field is proportional to the local electric field, the magnetic field and the gradient of the electric field, respectively. It is possible to control their transition rates by changing their electromagnetic environment [216]. Far-field approaches based on mirrors and dielectric interfaces allow enhancement factors below an order of magnitude for MD [217-220] and EQ transitions [208, 209]. Bringing into light more *forbidden* transitions requires, however, larger enhancements.

Optical nanoantennas have the potential to modify the selection rules thanks to their strongly confined evanescent fields. Each antenna design concentrates particular components of the electromagnetic field at specific locations. Antennas can thus be devised to favor a given quantum-mechanical multipolar transition in an emitter through an enhanced local field of interest.

To completely break the selection rules, ED transitions should ideally be suppressed as well. Competition between different transition channels in an

emitter may result in deletion of the excited state through another ED decay channel. For an emitter at a given position on an antenna, a high branching ratio between non-ED/ED transition rates is in principle desirable. Additionally, from a practical point of view, it is preferable to have such a high enhancement and ratio at all accessible points near the antenna.

Several nanostructures have been proposed recently for enhancing MD or EQ optical transitions. Separate works evaluated the possibility of MD emission control with metal nanowires [70], metal-insulator-metal resonators [221] and semiconductor spheres [222-224]. For EQ transitions, independent theoretical works predict enhancement by slits [225], metal spheres [213], dielectric spheres [226], and gap antennas [227, 228].

In this Chapter, we provide a systematic evaluation and comparison of different resonant antenna designs for MD and EQ enhancement: metal nanospheres, metal nanowires, semiconductor disks, and split-ring resonators. We identify geometries suitable for experimental realization, incorporating the effect of surrounding media such as a dielectric substrate, and evaluating the possible enhancement of ED transitions at the same or other emitter positions. The presented simulations can therefore guide realistic experiments to manipulate *forbidden* transitions.

Simulation method

We model the enhancement of non-ED transitions with classical electrodynamics. Using the Finite-Difference Time-Domain method (FDTD Solutions, Lumerical Inc.), we solve Maxwell's equations numerically for MD and EQ sources. Our approach is essentially similar to the study of ED enhancement by optical antennas with the FDTD method [229]. By solving the full electromagnetic problem in 3D, this method offers flexibility to study any nanoantenna design.

We compute the power radiated by an emitter coupled to an antenna, P_{rad}, by integrating the Poynting vector over a surface enclosing the emitter-antenna system. The same emitter alone, without antenna and in vacuum, would radiate a power $P_{\mathrm{rad},0}$. We define the radiated power enhancement as the ratio $P_{\mathrm{rad}}/P_{\mathrm{rad},0}$. The radiated power enhancement relates directly to the radiative rate enhancement: $P_{\mathrm{rad}}/P_{\mathrm{rad},0} = \Gamma_{\mathrm{rad}}/\Gamma_{\mathrm{rad},0}$. We will evaluate the performance of our antennas in terms of this quantity.

We use mesh sizes of 1-3 nm and employ perfectly-matched layers at the boundaries of the simulation volume. Temporal propagation is terminated when the total power decays to 10^{-6} times the injected power for MD sources. For EQ sources, the fields excited by a 20-fs pulse are propagated during a total of 200 fs to ensure decay and convergence.

For maximum accuracy, we place the electric and magnetic dipolar sources at the positions of the mesh Yee cells where the respective fields are numerically evaluated [230]. We construct EQ sources by adding two ED sources with the same orientation 180° out of phase, separated by 1 nm. A finer refinement mesh of 0.1 nm is used surrounding the EQ. The relative positions of the EDs determine the resulting EQ, which can be of longitudinal or lateral character for collinear or parallel dipoles, respectively. They correspond to the diagonal and off-diagonal terms of the Cartesian quadrupole moment tensor (Q_{ij} with i, j= x, y, z).

As a general methodology, we simulate the emission of ED, MD or EQ sources with different orientations and at different positions, normally 5 nm away from the antenna surface. The resonance of each antenna is tuned by sweeping its dimensions. In our results, we highlight the three most relevant situations: a non-ED transition at its optimal position; an ED transition at the same position; and an ED transition at its optimal position. For clarity, only dipole orientations with maximum enhancement at each position are shown.

6.3. Magnetic dipole emission enhancement

A MD transition is optimally enhanced at points of maximum magnetic field. Although a useful starting point is the investigation of antenna designs with magnetic resonances, antennas with either electric or magnetic modes may be used for MD emission enhancement.

In this Section, we show that nanowire antennas, metal-insulator-metal resonators and silicon disks offer realistic possibilities for MD enhancement. We also evaluate the use of split-ring resonators. For a fair comparison between different materials and geometries, we focus our attention to wavelengths in the range 900-1100 nm.

Metal nanowire antennas

Magnetic fields are enhanced at positions where electric currents are maximal. For a half-wave nanowire antenna, the current peaks at the center of the resonator (Fig. 1.3d). A MD with orientation following the magnetic field lines around the wire can be enhanced around 60 times (green line in Fig. 6.1, top).

Compared to the emission of an ED at the same position, the ratio MD/ED is relatively poor, a factor of only 4 (see red line). Moreover, the emission of an ED placed at the end of the nanowire is around 3 times more strongly enhanced (dashed red line) than a MD at its optimal position. Therefore, if ED transitions compete with MD transitions in the emitter, MD enhancement might only be observed if the emitters are selectively placed at the center of the antenna.

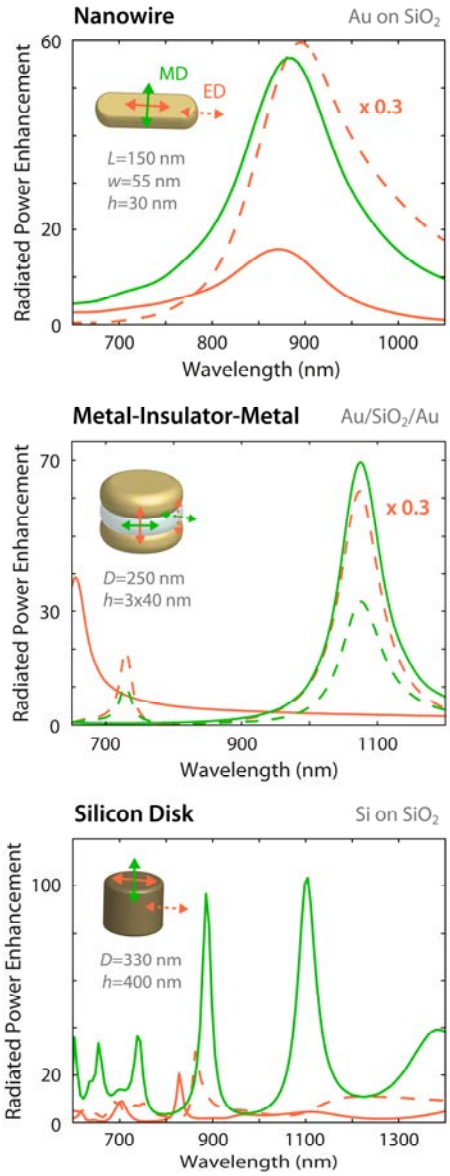

Figure 6.1 **Antennas for magnetic dipole transitions.** Radiated power enhancement, equivalent to radiative rate enhancement, for three antenna designs: a gold nanowire; a gold-silica-gold resonator; and a silicon disk. Magnetic (electric) dipoles are shown in green (red). Continuous (dashed) lines indicate that the source position is optimal for magnetic (electric) dipole enhancement. For EDs at positions with larger enhancenent than the maximum MD enhancement, a multiplying factor of 0.3 is applied for representation. Sources are 5, 20 and 5 nm away from the antenna surface. All antennas lie on a glass substrate Parameters are length (L), diameter (D), height (h), and width (w).

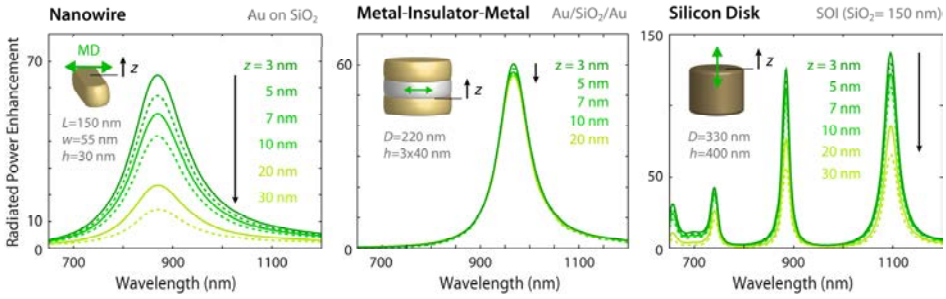

Figure 6.2 **Distance dependence of magnetic dipole enhancement.** The spatial dependence of magnetic enhancement is different for the three proposed resonators. It decays rapidly within 15 nm for a nanowire, it remains approximately constant within a MIM resonator, and it is confined to 30 nm for silicon disk, when half-maximum values are considered. The nanowire and the MIM resonator are on a glass substrate, whereas the silicon resonator lies on a silicon-on-insulator wafer with a 150-nm SiO_2 layer.

Metal-insulator-metal resonators

Another source of strong magnetic fields is the circulation of electric currents between two parallel metal plates. Metal-insulator-metal (MIM) resonators composed of cylindrical disks possess magnetic resonances that can be used for ED emission enhancement [231]. For MD transitions, we obtain results that are comparable in absolute value to a nanowire antenna (Fig. 6.1, center).

There are, however, important advantages. First, for an emitter placed at the center of the resonator, where magnetic fields are maximal, the ratio of MD/ED emission is significantly higher than for a nanowire (compare green and red continuous lines). Second, the maximum MD enhancement is obtained for orientations within the plane of the dielectric layer instead of a single direction. As a result, the average enhancement will be higher for emitters with random orientations. Third, although ED transitions display higher enhancement than MD transitions at the rims of the resonator, the emitters may be contained only inside the dielectric layer, making it easier in practice to position them towards the center of the resonator. This might be accomplished, for example, by means of radial chemical etching of the dielectric host material. MD enhancement is almost constant with respect to the height of the emitter inside the resonator, providing an extended volume for emission enhancement (Fig. 6.2, center).

Semiconductor resonators

Semiconductor and dielectric nanospheres and nanowires exhibit magnetic resonances [97-99] that may be used for the enhancement of MD transitions. They support low-order Mie resonances whose local magnetic field distribution is maximal at its center. Here, we evaluate a related antenna geometry that might be more controllably used in experiments; a cylindrical silicon disk on a substrate.

Enhancement factors can be above 100 at near-infrared wavelengths for MD dipoles centered and perpendicular to the top surface of the silicon disks (Fig. 6.1 for a disk on a glass substrate; Fig. 6.2 for a disk on a silicon-on-insulator substrate). At that position, the contrast of MD/ED enhancement can exceed 20 times. Importantly, an ED is only weakly enhanced at other positions around the resonator, *e.g.*, at the side or at the edges.

Although other dielectric materials with a lower —yet relatively high— refractive index still support similar magnetic resonances, the enhancement is smaller [222]. By simulating disks made of diamond ($n \approx 2.4$) and TiO_2 ($n \approx 2.7$), we found enhancements of MD transitions below 30 at the studied wavelengths. The higher refractive index of semiconductors such as Si ($n \approx 3.6$) contributes to a stronger resonant enhancement.

Split-ring resonators

The curvature of the electric current in a resonant split-ring resonator produces strong magnetic fields, especially near its curved section. We evaluate next MD enhancement with a U-shaped resonator (SRR), similar in geometry to a tuning fork, whose arms can be tuned into resonance by varying their length.

The first resonant mode of a SRR in air offers a high enhancement of both ED and MD transitions (Fig. 6.3, left). However, the antenna dimensions are small even when surrounded only by air, and even smaller geometries would be required for antennas on a realistic glass substrate. Larger split-ring resonators exhibiting higher-order resonances may be considered for ease of fabrication, including a glass substrate. We find, however, that the MD enhancements achievable with higher-order modes on a substrate are considerably lower and provide a lower contrast of MD/ED enhancement (Fig. 6.3, right).

Finally, we also simulated other structures known to support magnetic resonant modes —including nanoslot antennas, parallel wire pairs, and metal/dielectric core-shell resonators— and found no evidence of performance superior to, for example, a nanowire antenna.

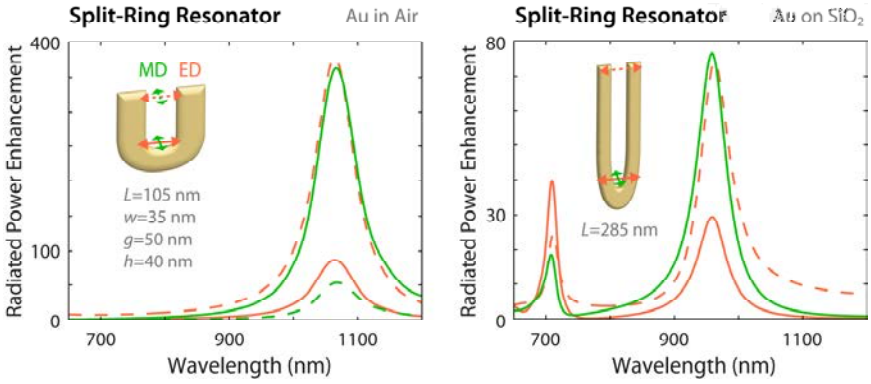

Figure 6.3 **Split-ring resonators for magnetic dipole transitions.** Power radiated by U-shaped gold resonators operating at the fundamental (left) and high order resonances (right), in air and on a glass substrate, respectively. Line colors and styles represent the different dipole types and positions sketched in the insets. The antenna parameters are vertical length (L), arm width (w), gap between arms (g), and height (h).

6.4. Electric quadrupole emission enhancement

An EQ transition is best enhanced at points with strong electric field gradients. The evanescent fields of surface plasmons in noble metals naturally enhance EQ transitions because the electric field is normal to the metal surface and decays exponentially away from it. They produce mainly field gradients of the form $\nabla_i E_i$, where i is the direction normal to the metal surface.

Resonant antennas further contribute to the observation of EQ transitions through electric field enhancement, because the emission of the individual EDs constituting the EQ is also enhanced separately. We assess here the performance of resonant nanospheres and nanowire antennas for EQ transitions.

Metal spheres

A noble metal sphere with a nanoscale radius provides a basic combination of field gradients and resonant emission. Although the resonance of the antenna can still be identified, our simulations show that there is a relatively constant level of non-resonant enhancement throughout the spectrum (Fig, 6.4, left).

A longitudinal quadrupole with dipoles oriented along the radius of the sphere can be enhanced by more than 3 orders of magnitude as a result of field gradients of the form $\nabla_x E_x$. The different local fields seen by each dipole break the symmetry of the emitter producing more radiation.

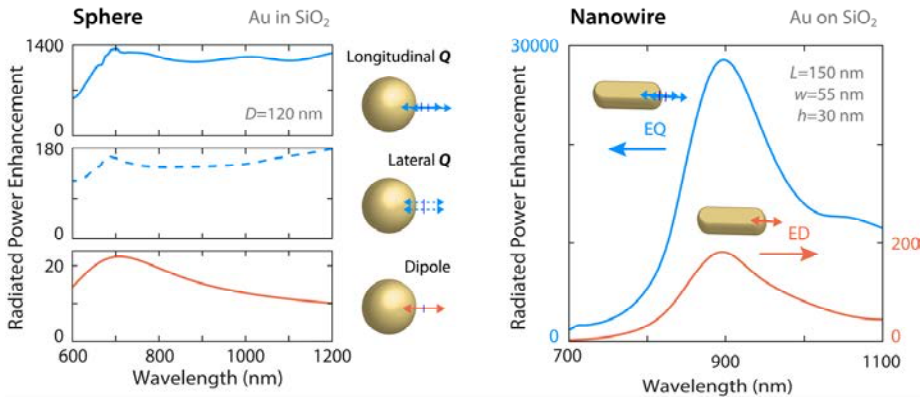

Figure 6.4 **Antennas for electric quadrupole transitions.** The field gradients near a gold sphere and a nanowire can enhance the radiative rates of quadrupolar transitions by several orders of magnitude. In both cases, the enhancement is much higher than for ED sources. Two types of quadrupoles are compared, lateral and longitudinal, with constituting dipoles at different relative positions. All sources are 5 nm away from the antenna surface.

A lateral quadrupole, on the other hand, is less enhanced because quadrupole moment components like Q_{xy} interact with crossed field-gradients, $\nabla_x E_y$, which are not particularly enhanced by the geometry of a sphere.

Metal nanowires

A nanowire antenna may have sharper edges than a sphere, producing steeper field gradients as well as higher resonant local fields. The result is that an EQ transition is enhanced by more than 4 orders of magnitude. The resonance of the antenna is clearly visible in the spectrum of Figure 6.4, with similar shapes for ED and EQ sources. Interestingly, ED emission is enhanced by at least 2 orders of magnitude less than EQ transitions.

Radius of curvature and symmetry breaking

The simple cases of sphere and wire antennas allow us to identify two general principles for further optimization of EQ transitions.

When the radius of a sphere is decreased from 80 to 20 nm, we observe an overall increase of EQ emission (Fig. 6.5, left). Similarly to the lightning-rod effect, sharp edges and tips with small radius of curvature further enhance EQ transitions. Displacing the EQ towards points with a lower symmetry such as the edges of a nanowire favors EQ transitions (Fig. 6.6, right). This spatial effect has been reported for gap antennas made of pairs of spheres [227] or nanowires [228],

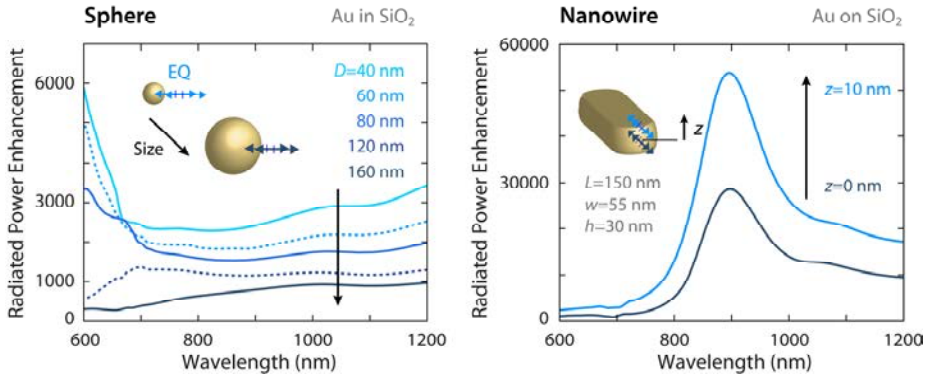

Figure 6.5 **Field gradients near edges for quadrupolar transitions.** The power radiated by a quadrupole transition increases near antennas features of small radius of curvature, such as smaller spheres (diameter, D) or the sharper edges of a nanowire (position of the emitter with respect to the center height of the nanowire, z).

and enhancements of up to 6 orders of magnitude have been predicted just out of the center of a very narrow gap.

To conclude, we propose the use of gap antennas with sharp ends (*e.g.*, bow-tie geometry) to obtain even higher enhancements. Breaking the lateral symmetry of a gap antenna by slightly misaligning its two arms may lead to higher enhancements of lateral quadrupoles as well. Finally, since the extent of the decay of evanescent fields depends on material parameters, other metals may additionally increase EQ transition rates.

6.5. Conclusions

We have demonstrated through numerical simulations the feasibility of enhancing magnetic dipole and electric quadrupole transitions with resonant optical antennas. The antenna mode does not need to have the same multipolar character as the transition, as illustrated with nanowire ED antennas and both MD and EQ sources. With realistic configurations and potentially working at other wavelengths, our results can serve as a guide to a range of spectroscopic experiments.

The observable effects of the activation of *forbidden* transitions by optical antennas will depend on the enhanced optical process. Experimental signatures of such enhancement could be the spectral modification of an emitter through the appearance or suppression of spectral lines, the shortening of a decay lifetime, or a signal intensity enhancement.

By altering the hierarchy of the selection rules, light-matter interaction can be radically modified. Enhancing *forbidden* transitions with optical antennas would open a new degree of freedom for optical spectroscopies. Some of the possibilities that would be enabled include new electronic structure or conformational information in complex materials, strong second-harmonic generation from otherwise weak centrosymmetric materials, or the use of the specificity of *forbidden* transitions in a dipole-dominated environment as a sensing or contrast mechanism.

Conclusion

In this Thesis, we have demonstrated the control of light emission with optical antennas. The near-field coupling of an emitter to a tailored nanoantenna resulted in controlled directions of emission, polarization, decay rate or wavelength spectrum. Each antenna design conferred its properties on the emitter, dominating the emission.

Nanowire antennas produced multipolar radiation from dipolar transitions, acting as converters between fundamental electromagnetic modes with different symmetries. Nanoslot antennas were shown to possess a dominant magnetic dipole response at resonance, even when driven by electric dipole sources. Yagi-Uda and log-periodic antennas directed light emission through the interference of dephased electric dipoles. Judiciously tuned split-ring resonators made unidirectional emission possible with a single, compact element through interfering multipolar moments. Finally, we explored the possibility of enhancing multipolar transitions in the emitters themselves with optical antennas of arbitrary multipolar character.

Our antennas were mainly inspired by conventional antenna designs. There is still plenty of room for ideas and improvement to be drawn by the optical antenna engineer from that vast body of knowledge. Yet, designs exclusive to optical frequencies might be found that outperform classical ones, as illustrated in our example of magneto-electric antenna (split-ring resonator). Those potential designs might be more suited to the peculiarities and applications of optical antennas.

Research in optical antennas is full of opportunities for integration in photonic devices. For example, directional antennas can couple light into dielectric, semiconductor or plasmonic waveguides. A coherent communication link between two independent emitters with optical antennas has yet to be demonstrated; it could boost the prospects for nanophotonic wireless networks. The combination of nanoantennas with micro/nano-fluidics has the potential to revolutionize biochemical sensors. The control of the electromagnetic modes of emission and absorption enabled by optical antennas provides interesting opportunities to

manipulate the orbital angular momentum of light with sub-wavelength sources and detectors, ideal for integration in more complex devices.

Light emission can still be more radically manipulated with optical antennas. Breaking the selection rules through the enhancement of multipolar transitions with optical antennas seems certainly within experimental reach, as shown in the simulations in this Thesis. For dipolar transitions, our work always took place in the weak-coupling regime. Access to the strong-coupling regime would allow the use of quantum electrodynamics effects as a resource for optoelectronics. Also for dipolar emitters, emission and excitation enhancements reported in the experimental literature are still far from the values predicted by theory. If the enhancements expected for gap antennas are obtained, they would enable the detection of very slow emitters such as single rare-earth ions. Such emitters would constitute virtually unbleachable solid-state sources of single photons for quantum information technologies. The enhancement of these and other emitters could be combined with spin manipulation.

This Thesis provided part of the necessary groundwork for these and other exciting experiments by establishing the fundamental methods and the Optical Physics of antennas as nano-optical elements.

Bibliography

[1] C. Cohen-Tannoudji, B. Diu, F. Laloe, *Quantum Mechanics*. (Wiley VCH, 2006), vol. 2.

[2] K. J. Vahala, "Optical microcavities". *Nature* **424**, 839 (2003).

[3] C. A. Balanis, *Antenna Theory: Analysis and Design*. (John Wiley and Sons, Inc., ed. 3, 2005).

[4] P. Biagioni, J.-S. Huang, B. Hecht, "Nanoantennas for visible and infrared radiation". *Rep. Prog. Phys.* **75**, 024402 (2012).

[5] P. Bharadwaj, B. Deutsch, L. Novotny, "Optical antennas". *Adv. Opt. Photon.* **1**, 438 (2009).

[6] S. Kühn, U. Hakanson, L. Rogobete, V. Sandoghdar, "Enhancement of single-molecule fluorescence using a gold nanoparticle as an optical nanoantenna". *Phys. Rev. Lett.* **97**, 017402 (2006).

[7] P. Anger, P. Bharadwaj, L. Novotny, "Enhancement and quenching of single molecule fluorescence". *Phys. Rev. Lett.* **96**, 113002 (2006).

[8] J. N. Farahani, D. W. Pohl, H. J. Eisler, B. Hecht, "Single quantum dot coupled to a scanning optical antenna: A tunable superemitter". *Phys. Rev. Lett.* **95**, 017402 (2005).

[9] A. Kinkhabwala *et al.*, "Large single-molecule fluorescence enhancements produced by a bowtie nanoantenna". *Nature Photon.* **3**, 654 (2009).

[10] T. H. Taminiau, R. J. Moerland, F. B. Segerink, L. Kuipers, N. F. van Hulst, "$\lambda/4$ resonance of an optical monopole antenna probed by single molecule fluorescence". *Nano Lett.* **7**, 28 (2007).

[11] T. H. Taminiau, F. D. Stefani, F. B. Segerink, N. F. van Hulst, "Optical antennas direct single-molecule emission". *Nature Photon.* **2**, 234 (2008).

[12] H. Mertens, J. S. Biteen, H. A. Atwater, A. Polman, "Polarization-Selective Plasmon-Enhanced Silicon Quantum-Dot Luminescence". *Nano Lett.* **6**, 2622 (2006).

[13] M. Ringler *et al.*, "Shaping emission spectra of fluorescent molecules with single plasmonic nanoresonators". *Phys. Rev. Lett.* **100**, 203002 (2008).

[14] J. S. Biteen, N. S. Lewis, H. A. Atwater, H. Mertens, A. Polman, "Spectral tuning of plasmon-enhanced silicon quantum dot luminescence". *Appl. Phys. Lett.* **88**, 131109 (2006).

[15] J. Aizpurua *et al.*, "Optical properties of coupled metallic nanorods for field-enhanced spectroscopy". *Phys. Rev. B* **71**, 235420 (2005).

[16] L. Novotny, "Effective wavelength scaling for optical antennas". *Phys. Rev. Lett.* **98**, 266802 (2007).

[17] G. W. Bryant, F. J. García de Abajo, J. Aizpurúa, "Mapping the plasmon resonances of metallic nanoantennas". *Nano Lett.* **8**, 631 (2008).

[18] H. Aouani *et al.*, "Bright Unidirectional Fluorescence Emission of Molecules in a Nanoaperture with Plasmonic Corrugations". *Nano Lett.* **11**, 637 (2011).

[19] S. Schietinger, M. Barth, T. Aichele, O. Benson, "Plasmon-Enhanced Single Photon Emission from a Nanoassembled Metal−Diamond Hybrid Structure at Room Temperature". *Nano Lett.* **9**, 1694 (2009).

[20] L. Tang *et al.*, "Nanometre-scale germanium photodetector enhanced by a near-infrared dipole antenna". *Nature Photon.* **2**, 226 (2008).

[21] K. C. Y. Huang *et al.*, "Antenna electrodes for controlling electroluminescence". *Nat. Commun.* **3**, 1005 (2012).

[22] P. Ghenuche, S. Cherukulappurath, T. H. Taminiau, N. F. van Hulst, R. Quidant, "Spectroscopic Mode Mapping of Resonant Plasmon Nanoantennas". *Phys. Rev. Lett.* **101**, 116805 (2008).

[23] M. Frimmer, Y. Chen, A. F. Koenderink, "Scanning Emitter Lifetime Imaging Microscopy for Spontaneous Emission Control". *Phys. Rev. Lett.* **107**, 123602 (2011).

[24] M. Pfeiffer *et al.*, "Positioning plasmonic nanostructures on single quantum emitters". *Phys. Status Solidi B* **249**, 678 (2012).

[25] C. Gruber, P. Kusar, A. Hohenau, J. R. Krenn, "Controlled addressing of quantum dots by nanowire plasmons". *Appl. Phys. Lett.* **100**, 231102 (2012).

[26] Q. Zhang *et al.*, "Large ordered arrays of single photon sources based on II-VI semiconductor colloidal quantum dot". *Opt. Express* **16**, 19592 (2008).

[27] R. M. Vitor *et al.*, "Controlled placement of colloidal quantum dots in sub-15 nm clusters". *Nanotech.* **24**, 125302 (2013).

[28] D. M. O'Carroll, C. E. Hofmann, H. A. Atwater, "Conjugated Polymer/Metal Nanowire Heterostructure Plasmonic Antennas". *Adv. Mat.* **22**, 1223 (2009).

[29] K. Rivoire *et al.*, "Lithographic positioning of fluorescent molecules on high-Q photonic crystal cavities". *Appl. Phys. Lett.* **95**, 123113 (2009).

[30] L. Martiradonna, T. Stomeo, M. D. Giorgi, R. Cingolani, M. D. Vittorio, "Nanopatterning of colloidal nanocrystals emitters dispersed in a PMMA matrix by e-beam lithography". *Microelectron. Eng.* **83**, 1478 (2006).

[31] E. Wolf, "Electromagnetic diffraction in optical systems. I. An integral representation of the image field". *Proc. Roy. Soc. London A* **253**, 349 (1959).

[32] B. Richards, E. Wolf, "Electromagnetic diffraction in optical systems II. Structure of the image field in an aplanatic system". *Proc. Roy. Soc. London A* **253**, 358 (1959).

[33] F. D. Stefani, J. P. Hoogenboom, E. Barkai, "Beyond quantum jumps: Blinking nanoscale light emitters". *Phys. Today* **62**, 34 (2009).

[34] M. Nirmal *et al.*, "Fluorescence intermittency in single cadmium selenide nanocrystals". *Nature* **383**, 802 (1996).

[35] P. Bharadwaj, L. Novotny, "Robustness of Quantum Dot Power-Law Blinking". *Nano Lett.* **11**, 2137 (2011).

[36] E. Shafran, B. D. Mangum, J. M. Gerton, "Using the Near-Field Coupling of a Sharp Tip to Tune Fluorescence-Emission Fluctuations during Quantum-Dot Blinking". *Phys. Rev. Lett.* **107**, 037403 (2011).

[37] S. Jin, N. Song, T. Lian, "Suppressed Blinking Dynamics of Single QDs on ITO". *ACS Nano* **4**, 1545 (2010).

[38] S. Hohng, T. Ha, "Near-Complete Suppression of Quantum Dot Blinking in Ambient Conditions". *J. Am. Chem. Soc.* **126**, 1324 (2004).

[39] P. Michler *et al.*, "Quantum correlation among photons from a single quantum dot at room temperature". *Nature* **406**, 968 (2000).

[40] G. Messin, J. P. Hermier, E. Giacobino, P. Desbiolles, M. Dahan, "Bunching and antibunching in the fluorescence of semiconductor nanocrystals". *Opt. Lett.* **26**, 1891 (2001).

[41] B. Lounis, H. A. Bechtel, D. Gerion, P. Alivisatos, W. E. Moerner, "Photon antibunching in single CdSe/ZnS quantum dot fluorescence". *Chem. Phys. Lett.* **329**, 399 (2000).

[42] M. A. Lieb, J. M. Zavislan, L. Novotny, "Single-molecule orientations determined by direct emission pattern imaging". *J. Opt. Soc. Am. B* **21**, 1210 (2004).

[43] B. Hecht, H. Bielefeldt, L. Novotny, Y. Inouye, D. W. Pohl, "Local Excitation, Scattering, and Interference of Surface Plasmons". *Phys. Rev. Lett.* **77**, 1889 (1996).

[44] A. Drezet *et al.*, "Leakage radiation microscopy of surface plasmon polaritons". *Mat. Sci. Eng. B* **149**, 220 (2008).

[45] A. L. Mattheyses, D. Axelrod, "Fluorescence emission patterns near glass and metal-coated surfaces investigated with back focal plane imaging". *J. Biomed. Opt.* **10**, 054007 (2005).

[46] C. J. R. Sheppard, M. Gu, "Imaging by a High Aperture Optical System". *J. Mod. Opt.* **40**, 1631 (1993).

[47] F. Koberling *et al.*, "Fluorescence anisotropy and crystal structure of individual semiconductor nanocrystals". *J. Phys. Chem. B* **107**, 7463 (2003).

[48] X. Brokmann, L. Coolen, J. P. Hermier, M. Dahan, "Emission properties of single CdSe/ZnS quantum dots close to a dielectric interface". *Chem. Phys.* **318**, 91 (2005).

[49] D. Patra, I. Gregor, J. Enderlein, M. Sauer, "Defocused imaging of quantum-dot angular distribution of radiation". *Appl. Phys. Lett.* **87**, 101103 (2005).

[50] K. T. Early *et al.*, "Linear dipole behavior in single CdSe-Oligo(phenylene vinylene) nanostructures". *ACS Nano* **3**, 453 (2009).

[51] S. A. Empedocles, R. Neuhauser, M. G. Bawendi, "Three-dimensional orientation measurements of symmetric single chromophores using polarization microscopy". *Nature* **399**, 126 (1999).

[52] L. Novotny, "Allowed and forbidden light in near-field optics. I. A single dipolar light source". *J. Opt. Soc. Am. A* **14**, 91 (1997).

[53] L. Novotny, N. F. van Hulst, "Antennas for light". *Nature Photon.* **5**, 83 (2011).

[54] A. G. Curto *et al.*, "Unidirectional Emission of a Quantum Dot Coupled to a Nanoantenna". *Science* **329**, 930 (2010).

[55] H. Ditlbacher *et al.*, "Silver nanowires as surface plasmon resonators". *Phys. Rev. Lett.* **95**, 257403 (2005).

[56] A. V. Akimov *et al.*, "Generation of single optical plasmons in metallic nanowires coupled to quantum dots". *Nature* **450**, 402 (2007).

[57] R. Kolesov *et al.*, "Wave-particle duality of single surface plasmon polaritons". *Nature Phys.* **5**, 470 (2009).

[58] K. Imura, T. Nagahara, H. Okamoto, "Plasmon Mode Imaging of Single Gold Nanorods". *J. Am. Chem. Soc.* **126**, 12730 (2004).

[59] J. Dorfmüller *et al.*, "Fabry-Pérot Resonances in One-Dimensional Plasmonic Nanostructures". *Nano Lett.* **9**, 2372 (2009).

[60] R. Esteban *et al.*, "Direct Near-Field Optical Imaging of Higher Order Plasmonic Resonances". *Nano Lett.* **8**, 3155 (2008).

[61] M. Schnell *et al.*, "Controlling the near-field oscillations of loaded plasmonic nanoantennas". *Nature Photon.* **3**, 287 (2009).

[62] C. Fumeaux *et al.*, "Measurement of the resonant lengths of infrared dipole antennas". *Infrared Phys. Technol.* **41**, 271 (2000).

[63] E. S. Barnard, R. A. Pala, M. L. Brongersma, "Photocurrent mapping of near-field optical antenna resonances". *Nature Nanotech.* **6**, 588 (2011).

[64] E. J. R. Vesseur, R. de Waele, M. Kuttge, A. Polman, "Direct Observation of Plasmonic Modes in Au Nanowires Using High-Resolution Cathodoluminescence Spectroscopy". *Nano Lett.* **7**, 2843 (2007).

[65] T. Coenen, E. J. R. Vesseur, A. Polman, "Deep Subwavelength Spatial Characterization of Angular Emission from Single-Crystal Au Plasmonic Ridge Nanoantennas". *ACS Nano* **6**, 1742 (2012).

[66] L. Douillard *et al.*, "Short Range Plasmon Resonators Probed by Photoemission Electron Microscopy". *Nano Lett.* **8**, 935 (2008).

[67] J. Nelayah *et al.*, "Mapping surface plasmons on a single metallic nanoparticle". *Nature Phys.* **3**, 348 (2007).

[68] E. S. Barnard, T. Coenen, E. J. R. Vesseur, A. Polman, M. L. Brongersma, "Imaging the Hidden Modes of Ultrathin Plasmonic Strip Antennas by Cathodoluminescence". *Nano Lett.* **11**, 4265 (2011).

[69] E. S. Barnard, J. S. White, A. Chandran, M. L. Brongersma, "Spectral properties of plasmonic resonator antennas". *Opt. Express* **16**, 16529 (2008).

[70] T. H. Taminiau, F. D. Stefani, N. F. van Hulst, "Optical Nanorod Antennas Modeled as Cavities for Dipolar Emitters: Evolution of Sub- and Super-Radiant Modes". *Nano Lett.* **11**, 1020 (2011).

[71] G. Della Valle, T. Sondergaard, S. I. Bozhevolnyi, "Plasmon-polariton nano-strip resonators: from visible to infra-red". *Opt. Express* **16**, 6867 (2008).

[72] M. K. Schmidt, S. Mackowski, J. Aizpurua, "Control of single emitter radiation by polarization- and position-dependent activation of dark antenna modes". *Opt. Lett.* **37**, 1017 (2012).

[73] E. R. Encina, E. A. Coronado, "Plasmonic Nanoantennas: Angular Scattering Properties of Multipole Resonances in Noble Metal Nanorods". *J. Phys. Chem. C* **112**, 9586 (2008).

[74] I. Sersic, C. Tuambilangana, A. F. Koenderink, "Fourier microscopy of single plasmonic scatterers". *New J. Phys.* **13**, 083025 (2011).

[75] F. Intonti *et al.*, "Young's Type Interference for Probing the Mode Symmetry in Photonic Structures". *Phys. Rev. Lett.* **106**, 143901 (2011).

[76] L. Novotny, B. Hecht, *Principles of Nano-Optics*. (Cambridge University Press, 2006).

[77] T. Inoue, H. Hori, "Theoretical Treatment of Electric and Magnetic Multipole Radiation Near a Planar Dielectric Surface Based on Angular Spectrum Representation of Vector Field". *Opt. Rev.* **5**, 295 (1998).

[78] O. L. Muskens, V. Giannini, J. A. Sánchez-Gil, J. Gómez Rivas, "Strong enhancement of the radiative decay rate of emitters by single plasmonic nanoantennas". *Nano Lett.* **7**, 2871 (2007).

[79] Y. C. Jun, R. Pala, M. L. Brongersma, "Strong Modification of Quantum Dot Spontaneous Emission via Gap Plasmon Coupling in Metal Nanoslits". *J. Phys. Chem. C* **114**, 7269 (2009).

[80] H. Aouani *et al.*, "Colloidal Quantum Dots as Probes of Excitation Field Enhancement in Photonic Antennas". *ACS Nano* **4**, 4571 (2010).

[81] M. Pfeiffer *et al.*, "Enhancing the Optical Excitation Efficiency of a Single Self-Assembled Quantum Dot with a Plasmonic Nanoantenna". *Nano Lett.* **10**, 4555 (2010).

[82] S. Mühlig, C. Menzel, C. Rockstuhl, F. Lederer, "Multipole analysis of meta-atoms". *Metamaterials* **5**, 64 (2011).

[83] D. J. Cho, F. Wang, X. Zhang, Y. R. Shen, "Contribution of the electric quadrupole resonance in optical metamaterials". *Phys. Rev. B* **78**, 121101 (2008).

[84] P. Grahn, A. Shevchenko, M. Kaivola, "Electromagnetic multipole theory for optical nanomaterials". *New J. Phys.* **14**, 093033 (2012).

[85] I. Sersic, C. Tuambilangana, T. Kampfrath, A. F. Koenderink, "Magnetoelectric point scattering theory for metamaterial scatterers". *Phys. Rev. B* **83**, 245102 (2011).

[86] N. Liu, H. Giessen, "Coupling Effects in Optical Metamaterials". *Angew. Chem. Int. Ed.* **49**, 9838 (2010).

[87] N. Tate *et al.*, "Quadrupole-Dipole Transform based on Optical Near-Field Interactions in Engineered Nanostructures". *Opt. Express* **17**, 11113 (2009).

[88] N. Liu *et al.*, "Plasmonic analogue of electromagnetically induced transparency at the Drude damping limit". *Nature Mater.* **8**, 758 (2009).

[89] S. Zhang, D. A. Genov, Y. Wang, M. Liu, X. Zhang, "Plasmon-Induced Transparency in Metamaterials". *Phys. Rev. Lett.* **101**, 047401 (2008).

[90] J. D. Jackson, *Classical Electrodynamics*. (Wiley, 1999).

[91] M. R. Foreman, P. Török, "Spin-orbit coupling and conservation of angular momentum flux in non-paraxial imaging of forbidden radiation". *New J. Phys.* **13**, 063041 (2011).

[92] G. Molina-Terriza, "Determination of the total angular momentum of a paraxial beam". *Phys. Rev. A* **78**, 053819 (2008).

[93] D. L. Andrews, "Optical angular momentum: Multipole transitions and photonics". *Phys. Rev. A* **81**, 033825 (2010).

[94] X. Cai *et al.*, "Integrated Compact Optical Vortex Beam Emitters". *Science* **338**, 363 (2012).

[95] N. Yu *et al.*, "Light Propagation with Phase Discontinuities: Generalized Laws of Reflection and Refraction". *Science* **334**, 333 (2011).

[96] C. Enkrich *et al.*, "Magnetic Metamaterials at Telecommunication and Visible Frequencies". *Phys. Rev. Lett.* **95**, 203901 (2005).

[97] N. Feth, C. Enkrich, M. Wegener, S. Linden, "Large-area magnetic metamaterials via compact interference lithography". *Opt. Express* **15**, 501 (2007).

[98] J. A. Schuller, R. Zia, T. Taubner, M. L. Brongersma, "Dielectric Metamaterials Based on Electric and Magnetic Resonances of Silicon Carbide Particles". *Phys. Rev. Lett.* **99**, 107401 (2007).

[99] A. García-Etxarri *et al.*, "Strong magnetic response of submicron Silicon particles in the infrared". *Opt. Express* **19**, 4815 (2011).

[100] H. A. Bethe, "Theory of Diffraction by Small Holes". *Phys. Rev.* **66**, 163 (1944).

[101] C. J. Bouwkamp, "On Bethe's theory of diffraction by small holes". *Philips Res. Rep.* **5**, 321 (1950).

[102] T. W. Ebbesen, H. J. Lezec, H. F. Ghaemi, T. Thio, P. A. Wolff, "Extraordinary optical transmission through sub-wavelength hole arrays". *Nature* **391**, 667 (1998).

[103] F. J. García de Abajo, "Colloquium: Light scattering by particle and hole arrays". *Rev. Mod. Phys.* **79**, 1267 (2007).

[104] F. J. García-Vidal, L. Martín-Moreno, T. W. Ebbesen, L. Kuipers, "Light passing through subwavelength apertures". *Rev. Mod. Phys.* **82**, 729 (2010).

[105] N. Rotenberg *et al.*, "Plasmon Scattering from Single Subwavelength Holes". *Phys. Rev. Lett.* **108**, 127402 (2012).

[106] A. Y. Nikitin, F. J. García-Vidal, L. Martín-Moreno, "Surface Electromagnetic Field Radiated by a Subwavelength Hole in a Metal Film". *Phys. Rev. Lett.* **105**, 073902 (2010).

[107] E. Popov *et al.*, "Surface plasmon excitation on a single subwavelength hole in a metallic sheet". *Appl. Opt.* **44**, 2332 (2005).

[108] J. M. Yi *et al.*, "Diffraction Regimes of Single Holes". *Phys. Rev. Lett.* **109**, 023901 (2012).

[109] H. W. Kihm *et al.*, "Bethe-hole polarization analyser for the magnetic vector of light". *Nature Commun.* **2**, 451 (2011).

[110] K. J. K. Koerkamp, S. Enoch, F. B. Segerink, N. F. van Hulst, L. Kuipers, "Strong Influence of Hole Shape on Extraordinary Transmission through Periodic Arrays of Subwavelength Holes". *Phys. Rev. Lett.* **92**, 183901 (2004).

[111] R. Gordon *et al.*, "Strong Polarization in the Optical Transmission through Elliptical Nanohole Arrays". *Phys. Rev. Lett.* **92**, 037401 (2004).

[112] A. Degiron, H. J. Lezec, N. Yamamoto, T. W. Ebbesen, "Optical transmission properties of a single subwavelength aperture in a real metal". *Opt. Commun.* **239**, 61 (2004).

[113] Y. C. Jun, K. C. Y. Huang, M. L. Brongersma, "Plasmonic beaming and active control over fluorescent emission". *Nature Commun.* **2**, 283 (2011).

[114] J. T. Choy *et al.*, "Enhanced single-photon emission from a diamond-silver aperture". *Nature Photon.* **5**, 738 (2011).

[115] Y. Alaverdyan, B. Sepúlveda, L. Eurenius, E. Olsson, M. Käll, "Optical antennas based on coupled nanoholes in thin metal films". *Nature Phys.* **3**, 884 (2007).

[116] M. Burresi *et al.*, "Probing the Magnetic Field of Light at Optical Frequencies". *Science* **326**, 550 (2009).

[117] R. L. Olmon *et al.*, "Determination of Electric-Field, Magnetic-Field, and Electric-Current Distributions of Infrared Optical Antennas: A Near-Field Optical Vector Network Analyzer". *Phys. Rev. Lett.* **105**, 167403 (2010).

[118] T. Grosjean, M. Mivelle, F. I. Baida, G. W. Burr, U. C. Fischer, "Diabolo Nanoantenna for Enhancing and Confining the Magnetic Optical Field". *Nano Lett.* **11**, 1009 (2011).

[119] D. Wang, T. Yang, K. B. Crozier, "Charge and current reservoirs for electric and magnetic field enhancement". *Opt. Express* **18**, 10388 (2010).

[120] M. Burresi *et al.*, "Magnetic Light-Matter Interactions in a Photonic Crystal Nanocavity". *Phys. Rev. Lett.* **105**, 123901 (2010).

[121] S. Vignolini *et al.*, "Magnetic Imaging in Photonic Crystal Microcavities". *Phys. Rev. Lett.* **105**, 123902 (2010).

[122] B. Ögüt *et al.*, "Hybridized Metal Slit Eigenmodes as an Illustration of Babinet's Principle". *ACS Nano* **5**, 6701 (2011).

[123] J. Zhang *et al.*, "Resonant slot nanoantennas for surface plasmon radiation in optical frequency range". *Appl. Phys. Lett.* **100**, 241115 (2012).

[124] J. C. Prangsma, D. van Oosten, L. Kuipers, "Local investigation of the optical properties of subwavelength rectangular holes with a focused beam of electrons". *Phil. Trans. R. Soc. A* **369**, 3456 (2011).

[125] H. G. Booker, “Slot aerials and their relation to complementary wire aerials (Babinet's principle)”. *J. Inst. Elect. Eng. - Part IIIA* **93**, 620 (1946).

[126] J. D. Kraus, R. J. Marhefka, *Antennas for all applications.* (McGraw-Hill, ed. Third, 2001).

[127] T. Zentgraf *et al.*, “Babinet’s principle for optical frequency metamaterials and nanoantennas”. *Phys. Rev. B* **76**, 033407 (2007).

[128] C. Rockstuhl, T. Zentgraf, T. P. Meyrath, H. Giessen, F. Lederer, “Resonances in complementary metamaterials and nanoapertures”. *Opt. Express* **16**, 2080 (2008).

[129] C. Rockstuhl, F. Lederer, “Negative-index metamaterials from nanoapertures”. *Phys. Rev. B* **76**, 125426 (2007).

[130] T. H. Taminiau, S. Karaveli, N. F. van Hulst, R. Zia, “Quantifying the magnetic nature of light emission”. *Nature Commun.* **3**, 979 (2012).

[131] P. Andrew, “Molecular fluorescence near metallic interfaces” PhD Thesis, University of Exeter (1998).

[132] E. H. Hellen, D. Axelrod, “Fluorescence emission at dielectric and metal-film interfaces”. *J. Opt. Soc. Am. B* **4**, 337 (1987).

[133] C. Obermuller, K. Karrai, “Far field characterization of diffracting circular apertures”. *Appl. Phys. Lett.* **67**, 3408 (1995).

[134] D. J. Shin, A. Chavez-Pirson, Y. H. Lee, “Multipole analysis of the radiation from near-field optical probes”. *Opt. Lett.* **25**, 171 (2000).

[135] H. Guo *et al.*, “Optical resonances of bowtie slot antennas and their geometry and material dependence”. *Opt. Express* **16**, 7756 (2008).

[136] B. Lee, I.-M. Lee, S. Kim, D.-H. Oh, L. Hesselink, “Review on subwavelength confinement of light with plasmonics”. *J. Mod. Opt.* **57**, 1479 (2010).

[137] R. Gordon, A. Brolo, “Increased cut-off wavelength for a subwavelength hole in a real metal”. *Opt. Express* **13**, 1933 (2005).

[138] F. J. García-Vidal, E. Moreno, J. A. Porto, L. Martín-Moreno, “Transmission of Light through a Single Rectangular Hole”. *Phys. Rev. Lett.* **95**, 103901 (2005).

[139] S. Collin, F. Pardo, J.-L. Pelouard, “Waveguiding in nanoscale metallic apertures”. *Opt. Express* **15**, 4310 (2007).

[140] I. A. Ibrahim *et al.*, “Bowtie-shaped nanoaperture: a modal study”. *Opt. Lett.* **35**, 2448 (2010).

[141] E. C. Jordan, K. G. Balmain, *Electromagnetic Waves and Radiating System.* (Prentice-Hall, ed. Second, 1968).

[142] F. J. García de Abajo, “Light transmission through a single cylindrical hole in a metallic film”. *Opt. Express* **10**, 1475 (2002).

[143] C. W. Chang, A. K. Sarychev, V. M. Shalaev, "Light diffraction by a subwavelength circular aperture". *Laser Phys. Lett.* **2**, 351 (2006).

[144] S.-Y. Lee *et al.*, "Role of Magnetic Induction Currents in Nanoslit Excitation of Surface Plasmon Polaritons". *Phys. Rev. Lett.* **108**, 213907 (2012).

[145] P. Kramper *et al.*, "Highly directional emission from photonic crystal waveguides of subwavelength width". *Phys. Rev. Lett.* **92**, 113903 (2004).

[146] H. J. Lezec *et al.*, "Beaming light from a subwavelength aperture". *Science* **297**, 820 (2002).

[147] N. F. Yu *et al.*, "Small-divergence semiconductor lasers by plasmonic collimation". *Nature Photon.* **2**, 564 (2008).

[148] F. López-Tejeira *et al.*, "Efficient unidirectional nanoslit couplers for surface plasmons". *Nat. Phys.* **3**, 324 (2007).

[149] Y. Alaverdyan, B. Sepúlveda, L. Eurenius, E. Olsson, M. Käll, "Optical antennas based on coupled nanoholes in thin metal films". *Nat. Phys.* **3**, 884 (2007).

[150] M. Pelton *et al.*, "Efficient source of single photons: A single quantum dot in a micropost microcavity". *Phys. Rev. Lett.* **89**, 233602 (2002).

[151] A. Badolato *et al.*, "Deterministic Coupling of Single Quantum Dots to Single Nanocavity Modes". *Science* **308**, 1158 (2005).

[152] J. Claudon *et al.*, "A highly efficient single-photon source based on a quantum dot in a photonic nanowire". *Nature Photon.* **4**, 174 (2010).

[153] H. Gersen *et al.*, "Influencing the angular emission of a single molecule". *Phys. Rev. Lett.* **85**, 5312 (2000).

[154] S. Kühn, G. Mori, M. Agio, V. Sandoghdar, "Modification of single molecule fluorescence close to a nanostructure: radiation pattern, spontaneous emission and quenching". *Mol. Phys.* **106**, 893 (2008).

[155] *Antenna Engineering Handbook*. J. L. Volakis, Ed., (McGraw-Hill, 2007).

[156] T. Pakizeh, M. Käll, "Unidirectional Ultracompact Optical Nanoantennas". *Nano Lett.* **9**, 2343 (2009).

[157] T. Shegai *et al.*, "A bimetallic nanoantenna for directional colour routing". *Nat. Commun.* **2**, 481 (2011).

[158] L. A. Blanco, F. J. García de Abajo, "Spontaneous light emission in complex nanostructures". *Phys. Rev. B* **69**, 205414 (2004).

[159] T. Shegai *et al.*, "Unidirectional Broadband Light Emission from Supported Plasmonic Nanowires". *Nano Lett.* **11**, 706 (2011).

[160] Y. Wang, A. S. Helmy, G. V. Eleftheriades, "Ultra-wideband optical leaky-wave slot antennas". *Opt. Express* **19**, 12392 (2011).

[161] P. Senellart *et al.*, "Controlling spontaneous emission with plasmonic optical patch antennas". *Nano Lett.*, (2013).

[162] A. Ahmed, R. Gordon, "Directivity Enhanced Raman Spectroscopy Using Nanoantennas". *Nano Lett.* **11**, 1800 (2011).

[163] O. Gazzano *et al.*, "Single photon source using confined Tamm plasmon modes". *Appl. Phys. Lett.* **100**, 232111 (2012).

[164] D. T. Schoen, T. Coenen, F. J. García de Abajo, M. L. Brongersma, A. Polman, "The Planar Parabolic Optical Antenna". *Nano Lett.* **13**, 188 (2012).

[165] S. Person *et al.*, "Demonstration of Zero Optical Backscattering from Single Nanoparticles". *Nano Lett.*, (2013).

[166] G. Pellegrini, P. Mazzoldi, G. Mattei, "Asymmetric Plasmonic Nanoshells as Subwavelength Directional Nanoantennas and Color Nanorouters: A Multipole Interference Approach". *J. Phys. Chem. C* **116**, 21536 (2012).

[167] H. Yagi, "Beam transmission of ultra-shortwaves". *Proc. IRE* **16**, 715 (1928).

[168] T. Kosako, Y. Kadoya, H. F. Hofmann, "Directional control of light by a nano-optical Yagi-Uda antenna". *Nature Photon.* **4**, 312 (2010).

[169] D. Dregely *et al.*, "3D optical Yagi-Uda nanoantenna array". *Nat Commun* **2**, 267 (2011).

[170] J. Dorfmüller *et al.*, "Near-Field Dynamics of Optical Yagi-Uda Nanoantennas". *Nano Lett.* **11**, 2819 (2011).

[171] R. de Waele, A. F. Koenderink, A. Polman, in *Nano Lett.* (2007), vol. 7, pp. 2004-2008.

[172] H. F. Hofmann, T. Kosako, Y. Kadoya, "Design parameters for a nano-optical Yagi-Uda antenna". *New J. Phys.* **9**, 12 (2007).

[173] T. H. Taminiau, F. D. Stefani, N. F. van Hulst, "Enhanced directional excitation and emission of single emitters by a nano-optical Yagi-Uda antenna". *Opt. Express* **16**, 10858 (2008).

[174] J. J. Li, A. Salandrino, N. Engheta, "Shaping light beams in the nanometer scale: A Yagi-Uda nanoantenna in the optical domain". *Phys. Rev. B* **76**, 245403 (2007).

[175] "Materials and methods are available as supporting material on *Science* Online".

[176] T. Shegai *et al.*, "Managing light polarization via plasmon-molecule interactions within an asymmetric metal nanoparticle trimer". *Proc. Natl. Acad. Sci. U. S. A.* **105**, 16448 (2008).

[177] K. G. Lee *et al.*, "A planar dielectric antenna for directional single-photon emission and near-unity collection efficiency". *Nature Photon.* **5**, 166 (2011).

[178] N. K. Takla, L. C. Shen, "Bandwidth of a Yagi Array with optimum Directivity". *IEEE Trans. on Antennas Propag.* **25**, 913 (1977).

[179] A. F. Koenderink, "Plasmon Nanoparticle Array Waveguides for Single Photon and Single Plasmon Sources". *Nano Lett.* **9**, 4228 (2009).

[180] K. Li, M. I. Stockman, D. J. Bergman, "Self-similar chain of metal nanospheres as an efficient nanolens". *Phys. Rev. Lett.* **91**, 227402 (2003).

[181] G. Leveque, O. J. F. Martin, "Narrow-band multiresonant plasmon nanostructure for the coherent control of light: An optical analog of the xylophone". *Phys. Rev. Lett.* **100**, 117402 (2008).

[182] A. V. Malyshev, V. A. Malyshev, J. Knoester, "Frequency-Controlled Localization of Optical Signals in Graded Plasmonic Chains". *Nano Lett.* **8**, 2369 (2008).

[183] I. S. Maksymov, A. R. Davoyan, Y. S. Kivshar, "Enhanced emission and light control with tapered plasmonic nanoantennas". *Appl. Phys. Lett.* **99**, 083304 (2011).

[184] A. E. Miroshnichenko *et al.*, "An arrayed nanoantenna for broadband light emission and detection". *Physica Status Solidi (RRL)* **5**, 347 (2011).

[185] A. G. Curto, F. J. García de Abajo, "Near-Field Optical Phase Antennas for Long-Range Plasmon Coupling". *Nano Lett.* **8**, 2479 (2008).

[186] A. G. Curto, A. Manjavacas, F. J. García de Abajo, "Near-Field Focusing with Optical Phase Antennas". *Opt. Express* **17**, 17801 (2009).

[187] A. Devilez, B. Stout, N. Bonod, "Compact Metallo-Dielectric Optical Antenna for Ultra Directional and Enhanced Radiative Emission". *ACS Nano* **4**, 3390 (2010).

[188] Y. H. Fu, A. I. Kuznetsov, A. E. Miroshnichenko, Y. F. Yu, B. Luk'yanchuk, "Directional visible light scattering by silicon nanoparticles". *Nature Commun.* **4**, 1527 (2013).

[189] A. E. Krasnok *et al.*, " Ultracompact all-dielectric superdirective antennas". *arXiv:1211.0230 [physics.optics]*, (2012).

[190] J. M. Geffrin *et al.*, "Magnetic and electric coherence in forward- and back-scattered electromagnetic waves by a single dielectric subwavelength sphere". *Nature Commun.* **3**, 1171 (2012).

[191] B. Rolly, B. Stout, N. Bonod, "Boosting the directivity of optical antennas with magnetic and electric dipolar resonant particles". *Opt. Express* **20**, 20376 (2012).

[192] W. Liu, A. E. Miroshnichenko, D. N. Neshev, Y. S. Kivshar, "Broadband Unidirectional Scattering by Magneto-Electric Core–Shell Nanoparticles". *ACS Nano* **6**, 5489 (2012).

[193] C. Rockstuhl *et al.*, "On the reinterpretation of resonances in split-ring-resonators at normal incidence". *Opt. Express* **14**, 8827 (2006).

[194] J. Zhou, T. Koschny, C. M. Soukoulis, "Magnetic and electric excitations in split ring resonators". *Opt. Express* **15**, 17881 (2007).

[195] G. Boudarham *et al.*, "Spectral Imaging of Individual Split-Ring Resonators". *Phys. Rev. Lett.* **105**, 255501 (2010).

[196] I. Sersic, M. A. van de Haar, F. B. Arango, A. F. Koenderink, "Ubiquity of Optical Activity in Planar Metamaterial Scatterers". *Phys. Rev. Lett.* **108**, 223903 (2012).

[197] E. Plum *et al.*, "Metamaterials: Optical Activity without Chirality". *Phys. Rev. Lett.* **102**, 113902 (2009).

[198] L. D. Barron, *Molecular Light Scattering and Optical Activity.* (Cambridge University Press, ed. Second, 2004).

[199] Y. Tang, A. E. Cohen, "Optical Chirality and Its Interaction with Matter". *Phys. Rev. Lett.* **104**, 163901 (2010).

[200] C. M. Dodson, R. Zia, "Magnetic dipole and electric quadrupole transitions in the trivalent lanthanide series: Calculated emission rates and oscillator strengths". *Phys. Rev. B* **86**, 125102 (2012).

[201] D. Wilk, D. Johannsmann, C. Stanners, Y. R. Shen, "Second-harmonic generation from C_{60} thin films at 1.064 μm". *Phys. Rev. B* **51**, 10057 (1995).

[202] B. Koopmans, A.-M. Janner, H. T. Jonkman, G. A. Sawatzky, F. van der Woude, "Strong bulk magnetic dipole induced second-harmonic generation from C_{60}". *Phys. Rev. Lett.* **71**, 3569 (1993).

[203] T. Yamada *et al.*, "Resonant enhancement of second-harmonic generation of electric quadrupole origin in phthalocyanine films". *Phys. Rev. B* **53**, R13314 (1996).

[204] P. Guyot-Sionnest, Y. R. Shen, "Local and nonlocal surface nonlinearities for surface optical second-harmonic generation". *Phys. Rev. B* **35**, 4420 (1987).

[205] S. Cattaneo, M. Kauranen, "Bulk versus surface contributions in nonlinear optics of isotropic centrosymmetric media". *Phys. Status Solidi B* **242**, 3007 (2005).

[206] M. Fiebig, D. Fröhlich, B. B. Krichevtsov, R. V. Pisarev, "Second Harmonic Generation and Magnetic-Dipole-Electric-Dipole Interference in Antiferromagnetic Cr_2O_3". *Phys. Rev. Lett.* **73**, 2127 (1994).

[207] A. Compaan, H. Z. Cummins, "Resonant Quadrupole-Dipole Raman Scattering at the 1S Yellow Exciton in Cu_2O". *Phys. Rev. Lett.* **31**, 41 (1973).

[208] S. Tojo, M. Hasuo, T. Fujimoto, "Absorption Enhancement of an Electric Quadrupole Transition of Cesium Atoms in an Evanescent Field". *Phys. Rev. Lett.* **92**, 053001 (2004).

[209] M. L. Andersen, S. Stobbe, A. S. Sørensen, P. Lodahl, "Strongly modified plasmon-matter interaction with mesoscopic quantum emitters". *Nature Phys.* **7**, 215 (2011).

[210] J. R. Zurita-Sánchez, L. Novotny, "Multipolar interband absorption in a semiconductor quantum dot. I. Electric quadrupole enhancement". *J. Opt. Soc. Am. B* **19**, 1355 (2002).

[211] P. K. Jain, D. Ghosh, R. Baer, E. Rabani, A. P. Alivisatos, "Near-field manipulation of spectroscopic selection rules on the nanoscale". *Proc. Natl. Acad. Sci. USA* **109**, 8016 (2012).

[212] M. Moskovits, D. P. DiLella, "Intense quadrupole transitions in the spectra of molecules near metal surfaces". *J. Chem. Phys.* **77**, 1655 (1982).

[213] P. G. Etchegoin, E. C. L. Ru, "Multipolar emission in the vicinity of metallic nanostructures". *J. Phys.: Cond. Matter* **18**, 1175 (2006).

[214] T. C. Damen, R. C. C. Leite, S. P. S. Porto, "Angular Dependence of the Raman Scattering from Benzene Excited by the He-Ne cw Laser". *Phys. Rev. Lett.* **14**, 9 (1965).

[215] J. A. Schuller *et al.*, "Orientation of luminescent excitons in layered nanomaterials". *Nature Nanotech.* **8**, 271 (2013).

[216] N. Yang, Y. Tang, A. E. Cohen, "Spectroscopy in sculpted fields". *Nano Today* **4**, 269 (2009).

[217] K. H. Drexhage, "Influence of a dielectric interface on fluorescence decay time". *J. Lumin.* **1–2**, 693 (1970).

[218] R. E. Kunz, W. Lukosz, "Changes in fluorescence lifetimes induced by variable optical environments". *Phys. Rev. B* **21**, 4814 (1980).

[219] S. Karaveli, R. Zia, "Strong enhancement of magnetic dipole emission in a multilevel electronic system". *Opt. Lett.* **35**, 3318 (2010).

[220] S. Karaveli, R. Zia, "Spectral Tuning by Selective Enhancement of Electric and Magnetic Dipole Emission". *Phys. Rev. Lett.* **106**, 193004 (2011).

[221] T. Feng, Y. Zhou, D. Liu, J. Li, "Controlling magnetic dipole transition with magnetic plasmonic structures". *Opt. Lett.* **36**, 2369 (2011).

[222] V. V. Klimov, V. S. Letokhov, " Electric and Magnetic Dipole Transitions of an Atom in the Presence of Spherical Dielectric Interface". *Laser Phys.* **15**, 61 (2005).

[223] B. Rolly, B. Bebey, S. Bidault, B. Stout, N. Bonod, "Promoting magnetic dipolar transition in trivalent lanthanide ions with lossless Mie resonances". *Phys. Rev. B* **85**, 245432 (2012).

[224] M. K. Schmidt *et al.*, "Dielectric antennas - a suitable platform for controlling magnetic dipolar emission". *Opt. Express* **20**, 13636 (2012).

[225] K. Deguchi *et al.*, "Simulation of Electric Quadrupole and Magnetic Dipole Transition Efficiencies in Optical Near Fields Generated by a Subwavelength Slit Array". *J. Phys. Soc. Jpn.* **78**, 024301 (2009).

[226] V. V. Klimov, V. S. Letokhov, "Quadrupole radiation of an atom in the vicinity of a dielectric microsphere". *Phys. Rev. A* **54**, 4408 (1996).

[227] R. Filter, S. Mühlig, T. Eichelkraut, C. Rockstuhl, F. Lederer, "Controlling the dynamics of quantum mechanical systems sustaining dipole-forbidden transitions via optical nanoantennas". *Phys. Rev. B* **86**, 035404 (2012).

[228] A. M. Kern, O. J. F. Martin, "Strong enhancement of forbidden atomic transitions using plasmonic nanostructures". *Phys. Rev. A* **85**, 022501 (2012).

[229] A. Mohammadi, V. Sandoghdar, M. Agio, "Gold nanorods and nanospheroids for enhancing spontaneous emission". *New J. Phys.* **10**, 105015 (2008).

[230] A. Taflove, S. C. Hagness, *Computational Electrodynamics: The Finite-Difference Time-Domain Method*. (Artech House, ed. 3rd, 2005).

[231] M. Kuttge, F. J. García de Abajo, A. Polman, "Ultrasmall Mode Volume Plasmonic Nanodisk Resonators". *Nano Lett.* **10**, 1537 (2009).

List of Publications

Book Chapter

"Directionality, polarization and enhancement by optical antennas"
N. F. van Hulst, T. H. Taminiau, and **A. G. Curto**,
Optical Antennas, Eds. M. Agio and A. Alù, Cambridge University Press (2013)

Journal Articles

"Antenna-Enhanced Forbidden Transition Spectroscopies"
A. G. Curto, M. Kuttge, and N. F. van Hulst,
In preparation

"Magneto-Electric Antennas for Directing Light Emission"
I. M. Hancu, **A. G. Curto**, M. Castro-Lopez, M. Kuttge, and N. F. van Hulst,
In preparation

"Probing the Magnetic Resonance of a Nanoslot Optical Antenna"
A. G. Curto, M. Kuttge, N. F. van Hulst
Under review in Physical Review Letters (2013)

"Multipolar Radiation of Quantum Emitters with Nanowire Optical Antennas"
A. G. Curto, T. Taminiau, G. Volpe, M. Kreuzer, R. Quidant, N. F. van Hulst,
Nature Communications **4**, 1750 (2013)

"Log-Periodic Optical Antennas with Broadband Directivity"
R. S. Pavlov, **A. G. Curto**, N. F. van Hulst,
Optics Communications **285**, 3334–3340 (2012)

"Unidirectional Emission of a Quantum Dot Coupled to a Nanoantenna"
A. G. Curto, T. Taminiau, G. Volpe, M. Kreuzer, R. Quidant, N. F. van Hulst,
Science **329**, 930-932 (2010)

"Near-Field Focusing with Optical Phase Antennas"
A. G. Curto, A. Manjavacas, and F. J. García de Abajo,
Optics Express **17** (20), 17801-17811 (2009)

"Near-Field Optical Phase Antennas for Long-Range Plasmon Coupling"
A. G. Curto and F. J. García de Abajo,
Nano Letters **8** (8), 2479-2484 (2008)

Other Publications

"Optical Antennas for Quantum Emitters"
A. G. Curto, M. Castro-Lopez, and N. F. van Hulst
Óptica Pura y Aplicada **44** (2) 325-331 (2011)